METHODOLOGIES TO PROMOTE MUSCLE DEVELOPMENT FOR ENGINEERING FUNCTIONAL SKELETAL MUSCLE TISSUE

BY

EUNKYUNG KO

DISSERTATION

Submitted in partial fulfillment of the requirements
for the degree of Doctor of Philosophy in Bioengineering
in the Graduate College of the
University of Illinois at Urbana-Champaign, 2019

Urbana, Illinois

Doctoral Committee:

Professor Hyunjoon Kong, Chair
Professor Rashid Bashir
Professor Martha L. Gillette
Professor M. Taher A. Saif

ABSTRACT

Skeletal muscle related diseases cause loss and weakness in the muscle and affect the quality of life of the patients. Although skeletal muscle tissue can regenerate when the damage is small, a patient must receive a surgery when the volumetric loss is too large. Skeletal muscle tissue engineering aims to recapitulate the physiology and function of the natural muscle. The engineered tissue holds potential as a transplantable material that can help regeneration *in vivo*.

In this thesis, we used different methodologies to recapitulate the natural skeletal muscle and enhance muscle development. The first part of the thesis uses physical approach to engineer functional skeletal muscle. A grooved substrate with controlled width was used to promote myogenic differentiation and enhance muscle maturity. After the mature muscle was generated, we cultured neural stem cells and let them innervate into the skeletal muscle to form a neuron-muscle interface to finally engineer a functional skeletal muscle (Chapter 3). The next study focuses on chemically stimulating the skeletal myoblasts to express more gap junction proteins and prolong the expression time. After confirming the genetic changes occurring in the muscle cells, we assembled a pump-bot device with the pre-stimulated skeletal muscle tissue engineered in a 3D ring. We compared how the fluid movement in the pump-bot was changed when the myoblasts had been chemically stimulated (Chapter 4). Lastly, we biologically modified the skeletal myoblasts to express gap junction proteins in myotubes (Chapter 5). We delivered connexin genes to the skeletal myoblasts. We examined how the presence of connexin in the cells contributes to myogenic differentiation and muscle development. Overall, the studies herein will be useful to engineer skeletal muscle for biomedical uses such as developing platforms for *in vitro* drug screening, engineering tissue for transplantation, and assembling a biologically actuated machinery.

ACKNOWLEDGEMENTS

With my deepest respect and gratitude, I want to thank my advisor Professor Hyunjoon Kong and Professor Rashid Bashir for their encouragement, guidance and support throughout my doctoral research. I was able to become a better researcher with help of their wonderful mentorship. I would also like to thank my committee members, Professor Taher Saif and Professor Martha Gillette for their insightful suggestions and support. Working in the EBICS group for the last five years was amazing.

I would like to thank all the lab members in the Kong lab and Bashir lab for their support. I have enjoyed all the collaboration and conversation we have had. Particularly, I would like to thank the EBICS subgroup for their significant contributions to all of my projects. Also, Dr. Caroline Cvetkovic who was a wonderful senior student. All of my works could not have been done without your help. I would also like to thank Professor Marni Boppart, Dr. Ziad Mahamassani, Professor Im, Dr. Seung Jung Yu, Onur Aydin, Dr. Zhengwei Li, and many, many others. Thank you, Professor Rohit Bharghava, and Professor Rex Gaskins for your mentorship while I was part of the NIH-T32 program.

Thanks to all my friends who have always been next to me during graduate school, especially, Minjeong, Yoomin, and Donghyuk. Finally, I cannot thank my family enough for their love and support. Thank you for always having trust in me and supporting me unconditionally.

The work described in this thesis was made possible by the support of National Institute of Biomedical Imaging and Bioengineering of the National Institutes of Health under Award Number T32EB019944, National Science Foundation (STC-EBICS Grant CBET-0939511), National Science Foundation Integrative Graduate Education and Research Traineeship, (CMMB-IGERT).

TABLE OF CONTENTS

LIST OF TABLES AND FIGURES

CHAPTER 1: INTRODUCTION

1.1 Motivation

In the field of tissue engineering, understanding how cells behave and respond to a controlled stimulus is crucial. Generally, different types of cells require distinct stiffness, topography, chemical stimulus to become a functional tissue. Researchers utilize a combination of biochemical as well as biophysical stimuli to provide a controlled environment for the cells. The main hypothesis of this dissertation is that microenvironment can control cellular emergence which may result in physiological and functional change of the engineered tissue. The microenvironments can be modulated by changing the physical, chemical, and biological cues of the surroundings. As we have thorough understanding of the interface of cells and materials, we can build functional tissues which can be used for various biomedical applications such as drug screening, transplantation, or building biological machinery.

1.2. Project Overview

This thesis seeks to enhance the quality of engineered muscle by controlling the maturity and functionality of the skeletal muscle tissue. To do so, different methodologies were employed to modulate the microenvironment of the skeletal muscle. For example, substrates with controlled topography were used to promote skeletal muscle maturity. A graphene-based nanomaterial was incorporated into the skeletal myoblasts to investigate the biological changes which resulted in myotube maturity. Furthermore, the myoblast cells were genetically modified to enhance the maturity and function after differentiation.

In chapter 3, we modulated the physical microenvironment. We used substrates with grooved topography with controlled width to promote skeletal myoblast maturation and neural

innervation. We examined if the groove size similar to the extracellular matrices or the myofibril enhanced maturation of the myotubes. Then, we studied how the maturation and alignment of the myotubes aid differentiation of the neural stem cells to become motor neuron progenitor cells and, subsequently, innervate into the skeletal myotubes. Furthermore, we tested the functionality of the engineered neuron-muscle interface by treating the tissue with a neural stimulator glutamate, and an antagonist, curare.

In chapter 4, we provided chemical cues to the skeletal myoblasts. We treated the skeletal myoblasts with reduced graphene oxide and explored how the material interacts with the skeletal myoblasts to enhance muscle maturation. In particular, we examined if the gap junction protein, connexin 43, expression is extended upon treating reduced graphene oxide and this event can promote myogenic differentiation of the myoblasts. In the end, we used the reduced graphene oxide treated skeletal muscles to engineer 3D muscle ring and tested with a pump-bot device.

In chapter 5, biological approach to genetically modify the cells was used to improve the quality of engineered muscle. After transfecting the myoblasts to express connexins, we focused on exploring the role of the gap junction proteins on myogenesis and how they can contribute to forming mature myotubes. We used myoblasts that continuously express different types of gap junction proteins after differentiation.

Ultimately, the results from these studies will be useful in engineering functional skeletal muscle tissue with better quality. The findings will broadly benefit developing drug screening platforms for skeletal muscle diseases, building biological actuators, and regeneration therapies.

CHAPTER 2: LITERATURE REVIEW ON SKELETAL MUSCLE TISSUE ENGINEERING

2.1 Skeletal Muscle Tissue Engineering

Skeletal muscle related diseases including muscular dystrophy, atrophy, myopathy and traumatic injuries cause loss and weakness in the muscle. Since muscle comprise approximately 40% of the body mass and is responsible for locomotion, skeletal muscle injury may significantly affect the quality of life of the patients[1]. Although skeletal muscle can self-regenerate up to a certain threshold, the tissue cannot fully recover the function beyond this point. Generally, if the volumetric muscle loss exceeds 20%, the patient needs to go through a surgical procedure or a physical therapy.[2]

During the surgical procedure, an autologous muscle is transferred from a donor site to the injured site. Latissimus dorsi muscle and gracilis muscle are the two largest sources used for autonomous transplantation. In addition, physical therapy is often performed after the surgery to prevent additional muscle loss around the injured site. However, the reconstruction surgery often results in failure in grafting, morbidity around the donor site, and insufficient neuron innervation. Furthermore, physical therapy alone cannot regenerate the skeletal muscle and restore volumetric muscle loss completely.[3] Another strategy to inject muscle cells *ex vivo* exists but this method also has limitations due to poor cell survival, migration and immune response.[3]

Skeletal muscle tissue engineering targets to recapitulate the structure and function of the natural tissue. After successfully engineering the skeletal muscle tissue, the construct holds potential as a transplantable material to an *in vivo* model, or an *in vitro* platform that can screen drugs. There are mainly two approaches to perform skeletal muscle tissue engineering. First, to develop mature myotubes and assemble a functional tissue *in vitro*. After the tissue is fully

developed, the construct can be transplanted at the injured site. However, innervation of the neurons into the skeletal muscle after transplantation, restoration of the physically relevant contraction force, vascularization to maintain viability of the tissue, and construction of a highly dense fiber bundle still remain as challenge.[4-5] On the other hand, the other strategy is to transplant cells and supporting those cells to undergo myogenesis *in vivo*. The purpose of this method is to provide cues to the host cells to undergo endogenous regeneration. A supportive material to provide a niche is often used together in this case. This strategy, however, also holds limitation due to immune response of the host and loss in cell number after transplantation.[6] Thus, it is important to balance each factor to maximize the regeneration efficacy after transplanting the engineered skeletal muscle tissue.

2.2 Importance of the cell-material interface

The choice of cell for skeletal muscle tissue engineering requires consideration of several characteristics. First, the cells should be accessible and should maintain their growth and differentiation well *in vitro*. The cells sources should also hold potential to develop into physiologically and functionally relevant muscle tissue.[7] A large range of cells fall into the category including satellite cells, muscle stem cells, myoblasts, mesenchymal stem cells, induced pluripotent stem cells, embryonic stem cells, and pericytes.[7-8] Systematic or local delivery of these cells allows the cells to develop into myofibers and aid regeneration at the injured site.[9-10] This, however, may result in loss of cells during delivery. Furthermore, the cells to differentiate and develop into mature muscle takes a long time. Thus, to potentiate the myogenic potential of the cells and improve the function after transplantation, researchers have focused on investigating the cell-material interface.

Skeletal muscle tissue engineering utilizes a broad range of biomaterials that can overcome current limitations. These biomaterials allow the cells to form functional and self-regenerative skeletal muscles, innervated and vascularized to closely recapitulate the natural skeletal muscle. For example, numerous blood vessels supply nutrient to the skeletal muscle following the connective tissues and each muscle fiber is innervated by motor neurons that stimulate the skeletal muscle to contract.[11-12] In fact, a highly porous poly-L-lactic acid (PLLA) and polylactic-glycolic acid (PLGA) substrate was used for co-culturing myoblasts, embryonic fibroblasts, and endothelial cells.[13] The skeletal muscle tissue engineered with the endothelial cells showed improved blood perfusion and survival rate after being transplanted to an *in vivo* animal model.

To maximize the effects of biomaterials for skeletal muscle tissue engineering, the platform should be developed with appropriate physical, chemical, and biological cues. These cues also must support myoblast proliferation, differentiation, maturation, and health. In the following sections, different approaches to provide each cue to the skeletal myoblasts are discussed in more details.

2.3 Physical Approach

Physical cues of the material are important factors in tissue development and can control cell function and fate. There are different methods to manipulate the physical property of material such as changing the geometry, stiffness, or topography of the substrate.[14] To physically manipulate the microenvironment, we must first understand the physiological characteristic of the skeletal muscle. Skeletal muscles consist of multiple bundles of muscle fibers, comprised of multinucleated myotubes.[15] These fiber bundles are surrounded by connective tissues which

supports the uniaxial shape and longitudinal movement. The actin and myosin in the bundles are pulled along the aligned tissue. Thus, the architecture of the skeletal muscle directly relates to the contraction of the skeletal muscle.[16] Thus, providing an appropriate physical stimulus to the skeletal muscle cells is advantageous to create a skeletal muscle tissue with better function.[15]

Linear topography is known to facilitate skeletal myoblasts to uniaxially align and form myotubes similar to the natural skeletal muscle.[17-19] As mentioned above, the alignment directly influences the functionality of the tissue *in vivo*, thus, this feature is considered significant for *in vitro* muscle tissue engineering. For example, the skeletal muscle tissue engineered with pre-aligned myotubes generated 2-fold increased contraction force compared to the tissue engineered with randomly oriented myotubes.[20] The myoblasts were pre-cultured on a micropatterned polydimethylsiloxane pattern and the muscle layer was transferred on a fibrin gel where the cells self-organized into a 3D muscle construct.

Substrate stiffness also plays a significant role in skeletal muscle development. The modulus varies as the muscle develops, but the Young's modulus of the skeletal muscle tissue is known to be between 10-20 kPa.[21-22] In fact, substrate stiffness around 10-20 kPa has shown to facilitate myogenic differentiation and maturation of myotubes of the skeletal myoblasts as well as mesenchymal stem cells.[14, 23] However, there are also controversial reports that stiffer substrates enhance myotube striation.

In addition, electrical stimulus is another commonly used method to physically manipulate the microenvironment.[24-25] This approach is widely used to both stimulate myoblasts during differentiation and after myotube formation. Interestingly, stimulating the myoblasts during differentiation allows more mature myotube formation during myogenesis showing better multinucleation and more number of myotubes.[26] Furthermore, when myotubes are stimulated

electrically, they can produce higher force.[27] Mechanical stimulation such as exercise is another way to provide physical cues to the engineered skeletal muscle. This strategy is similar to the physical therapy performed with the patients after a muscle transplantation surgery.[28-29]

Some studies use multiple features to physically stimulate the skeletal myoblasts. For example, a micropatterned gelatin hydrogel can enhance more mature myotube formation and long term culture compared to the polydimethylsiloxane substrate, a stiffer substrate, without the grooves.[30] The myotubes formed on the micropatterned gelatin hydrogels formed thicker, longer myotubes with better striation after 3 weeks of differentiation.

In conclusion, various methods are available to provide physical cues for the skeletal myoblasts from changing the property of the material to mechanically or electrically stimulating the cells.

2.4 Chemical Approach

Together with the physical cues, the extracellular matrix (ECM) provides cells with a wide range of chemical cues that modulates the morphology, adhesion, proliferation, differentiation, and apoptosis.[31-32] For instance, ECM holds adhesion proteins that support cell adhesion including fibronectin, collagen, vitronectin, and laminin.[31] Usually, the cellular response to these chemical cues is studied by immobilizing these proteins on a substrate.[33] In skeletal muscle, collagen is the major ECM protein which preserves 10% of the total muscle mass.[34] Collagen type I and III are predominant among the many types. Proteoglycans are also present in the connective tissue and they interact with the collagen to maintain the structure and organization of the matrix. In addition, glycoproteins such as laminins, integrins, and fibronectins link type IV collagen in the basement membrane. Some matrix remodeling enzymes such as matrix metalloprotease (MMP) also exists.

The secreted MMPs degrade collagen, fibronectin, proteoglycans, and laminins to remodel and regulate skeletal muscle function and development. The membrane bound MMPs are responsible for the proteolytic functions near the cell surface.

The adhesion proteins, mentioned above, mediate cellular attachment by integrin, a transmembrane receptor protein. This protein family mediate both cell-matrix and cell-cell interaction in skeletal muscle.[35-36] Particularly, the integrins helps the myoblasts to migrate and fuse together during myogenesis. In addition, disruption in the integrin-mediated adhesion in skeletal muscle cause myopathy.[37] Thus, chemical modification of the substrate or cells using the tripeptide sequence, arginylglycylaspartic acid (RGD), is widely used to investigate the role of the adhesion proteins in skeletal muscle. This sequence is present in fibronectin, vitronectin, fibrinogen, laminin and collagen, dominant ECM proteins in myoblasts.[38] The most commonly used method to introduce this chemical cue to the myoblast is by manipulating the substrate with the RGD sequence. Immobilization of the RGD-containing peptide on a poly-L-lysine and poly-L-glutamic acid substrate promoted myogenic differentiation by showing increased fusion index, striation, and myogenic positive nuclei.[39]

Moreover, the chemical composition of the ECM is significant for skeletal muscle differentiation and myogenesis when using multiple chemical cues to engineer skeletal muscle.[40] Previously, it was reported that the composition of the collagen I, fibrin and Matrigel change the myotube diameter, length and force generation. Matrigel is basement membrane which contains ECM proteins such as collagen IV, laminin, etactin, and growth factors including transforming growth factor beta, epidermal growth factor, insulin-like growth factor 1, and basic fibroblast growth factor.[41] These components promote myogenic differentiation by providing structurally organized environment and various myogenesis stimulating signals. Thus, higher Matrigel

concentration yielded a densely packed skeletal muscle fiber and larger myotube.[40] The intracellular calcium transients was also higher when the muscle fiber was engineered with higher Matrigel concentration.

Other growth factors or small molecules secreted from the surroundings also regulate skeletal muscle formation. Insulin like growth factor (IGF)-1 is a growth hormone that primarily works to promote growth and differentiation of the skeletal muscle via autocrine and paracrine mechanisms.[42] In the *in vivo* system, the IGF-1 also mediates muscle regeneration after damage and is related to the measures of muscular endurance. Thus, IGF-1 is a popularly used growth hormone for skeletal muscle tissue engineering. The pathway of IGF-1 affects skeletal muscle growth by protein synthesis and degradation. Once IGF-1 binds to the transmembrane protein IGF-1 receptor, the PI3K/Akt pathway is activated.[43] This activation results in hypertrophy and inhibition of the key ubiquitin ligase.

To successfully guide innervation of motor neurons, agrin, an acetylcholine receptor cluster inducing factor, is often incorporated into the culture system. Agrin is trophic factor released from the motor neurons and it stimulates phosphorylation of the muscle specific kinase (MuSK).[44-45] This event localizes acetylcholine receptor (AchR) to the synaptic sites and aids neuromuscular junction formation. Due to the importance of neural innervation in functional muscle engineering, agrin has been widely used to promote neuromuscular junction. An agrin treated C2C12 myoblasts were shown to express more acetylcholine receptors and promote a greater number of neuromuscular junction formation as well as enhanced blood vessels.

As such, controlled chemical cues provided to the niche will promote growth, migration, and differentiation of the myoblasts. With necessary ECM protein present on the environment and

soluble growth factors present in the medium, the engineered skeletal muscles will show better maturity and function more actively.

2.5 Biological Approach

Delivering genetical materials into the cells is a widely used method to biologically manipulate the microenvironment. Gene therapy generates a therapeutic effect by correcting the diseased gene in cell or introduce new function.[46-47] This technique holds promising potential because it can possibly be used to correcting inherited genetic disorders as well as acquired diseases. Transfection is a method used for gene therapy to introduce foreign nucleic acid to genetically modify the cells.[48] The engineered cell can express multiple phenotypic characteristics or functions depending on the delivered gene. The purpose of gene delivery is mainly to study the regulatory function of specific gene and investigate the protein product.

To enhance muscle function, researchers have tried to activate the signaling pathways involved in myogenesis and muscle development. For instance, IGF-1 gene was transduced into the C2C12 skeletal myoblasts to enhance the contractile force.[49] A retroviral vector was used to deliver IGF-1 gene to the C2C12 cells, which consequently enhanced growth and differentiation of the myoblasts. The myotubes formed with the genetically engineered myoblasts showed increase in myotube width, myotube area, muscle creatine kinase activity, and contractile force.

After a skeletal muscle tissue is formed *in vitro*, enough nutrient and oxygen must be supplied to the myotubes to maintain the viability and function. This is more important when the tissue is engineered in 3D form since the center part often goes through necrosis or apoptosis due to insufficient nutrient supply.[50] B-cell lymphoma 2 (BCL-2) protein is an apoptosis regulator that inhibits the mitochondrial dependent cell death.[51] Based on this fact, BCL-2 gene was transferred

to C2C12 myoblasts with retroviral vector to investigate the function of the engineered muscle under stressed conditions.[52] The skeletal myotube bundles formed with BCL-2 transfected C2C12 cells allowed the myotubes to form a densely bundled structure with higher viability. However, the engineered muscle bundles without BCL-2 overexpression showed cell death at the central region. Another study delivered both IGF-1 and BCL-2 to the C2C12 myoblasts to improve force production while minimizing cell apoptosis and necrosis.[53] In this study, the myotubes were further stimulated electrically to synergistically improve the force production.

Sometimes, genes that does not directly enhance myogenesis, but aids engraftment or migration are used to modify the myoblasts. Matrix metalloproteinase type 1 (MMP 1) is a well-known collagen-digesting enzyme. This gene was transfected to the myoblasts to eliminate scar tissue formation and enhance regeneration after transplantation.[54-56] The transfected myoblasts showed enhanced myogenic differentiation yielding myotubes with higher fusion index. More importantly, the transplanted MMP1 expressing myoblasts improved migration of the cells to the injured site and engraftment of the transplanted cells to the host tissue.

As mentioned in the previous section, agrin is secreted by the pre-synaptic axon terminals of the neuromuscular junction and this induce AchR aggregation at the post synaptic region. To investigate the effect of agrin at the post-synaptic muscle, myoblasts were transfected with gene that encodes agrin.[45]

To this end, modulating biological cues is useful to study the effect and function of various genes. Particularly, gene transfection could generate a variety of myoblasts with enhanced survival rate, differentiation efficiency, myogenesis, or functionality.

2.6. Summary and Future Perspectives

This review highlights the potential usage of skeletal muscle tissue engineering in clinical and laboratory applications. To successfully reconstruct a skeletal muscle tissue *in vitro*, there must be a thorough understanding of the physiology and function of skeletal muscle. The cells used for skeletal muscle tissue engineering requires microenvironment similar to the natural skeletal muscle tissue, physically, chemically, and biologically similar. Once the cells are provided with a combination of optimal cues, the cells will form a skeletal muscle tissue with better morphology and function.

Current trends in skeletal muscle tissue engineering is more focused on combining different approaches. For instance, combination of a physical and chemical stimulation can potentiate myogenic differentiation. A substrate introduced with grooved pattern and a cell-adhesive peptide, RGD, can promote adhesion, growth, and differentiation better than a substrate with only grooved pattern or RGD peptide.[57] Some studies have shown combinatorial usage of the biological and physical approaches by transplanting transfected cells loaded on a decellularized matrix and physically training the transplanted tissue.[29] Providing mechanical stimulation to the skeletal muscle co-cultured with vascular channel also improved myogenesis and muscle regeneration.[58]

Altogether, physical, chemical and biological cues must be considered when designing a culture system for engineering skeletal muscle. With appropriate signals provided to the myoblasts, the engineered muscle will both physiologically and functionally resemble the natural tissue.

2.7. References

1. Brook, M.; Wilkinson, D.; Phillips, B.; Perez-Schindler, J.; Philp, A.; Smith, K.; Atherton, P., Skeletal Muscle Homeostasis and Plasticity in Youth and Ageing: Impact of Nutrition and Exercise. *Acta physiologica* **2016,** *216* (1), 15-41.

2. Liu, J.; Saul, D.; Böker, K. O.; Ernst, J.; Lehman, W.; Schilling, A. F., Current Methods for Skeletal Muscle Tissue Repair and Regeneration. *BioMed research international* **2018,** *2018*.

3. Palmieri, B.; Tremblay, J. P.; Daniele, L., Past, Present and Future of Myoblast Transplantation in the Treatment of Duchenne Muscular Dystrophy. *Pediatric transplantation* **2010,** *14* (7), 813-819.

4. Qazi, T. H.; Mooney, D. J.; Pumberger, M.; Geissler, S.; Duda, G. N., Biomaterials Based Strategies for Skeletal Muscle Tissue Engineering: Existing Technologies and Future Trends. *Biomaterials* **2015,** *53*, 502-521.

5. Kwee, B. J.; Mooney, D. J., Biomaterials for Skeletal Muscle Tissue Engineering. *Current opinion in biotechnology* **2017,** *47*, 16-22.

6. Liu, Y.; Wang, L.; Kikuiri, T.; Akiyama, K.; Chen, C.; Xu, X.; Yang, R.; Chen, W.; Wang, S.; Shi, S., Mesenchymal Stem Cell–Based Tissue Regeneration Is Governed by Recipient T Lymphocytes Via Ifn-Γ and Tnf-A. *Nature medicine* **2011,** *17* (12), 1594.

7. Fan, Y.; Maley, M.; Beilharz, M.; Grounds, M., Rapid Death of Injected Myoblasts in Myoblast Transfer Therapy. *Muscle & Nerve: Official Journal of the American Association of Electrodiagnostic Medicine* **1996,** *19* (7), 853-860.

8. Shadrach, J. L.; Wagers, A. J., Stem Cells for Skeletal Muscle Repair. *Philosophical Transactions of the Royal Society B: Biological Sciences* **2011,** *366* (1575), 2297-2306.

9. Darabi, R.; Gehlbach, K.; Bachoo, R. M.; Kamath, S.; Osawa, M.; Kamm, K. E.; Kyba, M.; Perlingeiro, R. C., Functional Skeletal Muscle Regeneration from Differentiating Embryonic Stem Cells. *Nature medicine* **2008,** *14* (2), 134.

10. Dellavalle, A.; Sampaolesi, M.; Tonlorenzi, R.; Tagliafico, E.; Sacchetti, B.; Perani, L.; Innocenzi, A.; Galvez, B. G.; Messina, G.; Morosetti, R., Pericytes of Human Skeletal Muscle Are Myogenic Precursors Distinct from Satellite Cells. *Nature cell biology* **2007,** *9* (3), 255.

11. Olfert, I. M.; Baum, O.; Hellsten, Y.; Egginton, S., Advances and Challenges in Skeletal Muscle Angiogenesis. *American journal of physiology-heart and circulatory physiology* **2015,** *310* (3), H326-H336.

12. Mars, T.; King, M.; Miranda, A.; Walker, W.; Mis, K.; Grubic, Z., Functional Innervation of Cultured Human Skeletal Muscle Proceeds by Two Modes with Regard to Agrin Effects. *Neuroscience* **2003,** *118* (1), 87-97.

13. Levenberg, S.; Rouwkema, J.; Macdonald, M.; Garfein, E. S.; Kohane, D. S.; Darland, D. C.; Marini, R.; Van Blitterswijk, C. A.; Mulligan, R. C.; D'Amore, P. A., Engineering Vascularized Skeletal Muscle Tissue. *Nature biotechnology* **2005,** *23* (7), 879.

14. Engler, A. J.; Sen, S.; Sweeney, H. L.; Discher, D. E., Matrix Elasticity Directs Stem Cell Lineage Specification. *Cell* **2006,** *126* (4), 677-689.

15. Ostrovidov, S.; Hosseini, V.; Ahadian, S.; Fujie, T.; Parthiban, S. P.; Ramalingam, M.; Bae, H.; Kaji, H.; Khademhosseini, A., Skeletal Muscle Tissue Engineering: Methods to Form Skeletal Myotubes and Their Applications. *Tissue Engineering Part B: Reviews* **2014,** *20* (5), 403-436.

16. Cittadella Vigodarzere, G.; Mantero, S., Skeletal Muscle Tissue Engineering: Strategies for Volumetric Constructs. *Frontiers in physiology* **2014,** *5*, 362.

17. Arab, W.; Rauf, S.; Al-Harbi, O.; Hauser, C. A., Novel Ultrashort Self-Assembling Peptide Bioinks for 3d Culture of Muscle Myoblast Cells. *Int. J. Bioprint.* **2018,** *4*, 129.

18. Gingras, J.; Rioux, R. M.; Cuvelier, D.; Geisse, N. A.; Lichtman, J. W.; Whitesides, G. M.; Mahadevan, L.; Sanes, J. R., Controlling the Orientation and Synaptic Differentiation of Myotubes with Micropatterned Substrates. *Biophysical journal* **2009,** *97* (10), 2771-2779.

19. Bajaj, P.; Reddy Jr, B.; Millet, L.; Wei, C.; Zorlutuna, P.; Bao, G.; Bashir, R., Patterning the Differentiation of C2c12 Skeletal Myoblasts. *Integrative Biology* **2011,** *3* (9), 897-909.

20. Lam, M. T.; Huang, Y.-C.; Birla, R. K.; Takayama, S., Microfeature Guided Skeletal Muscle Tissue Engineering for Highly Organized 3-Dimensional Free-Standing Constructs. *Biomaterials* **2009,** *30* (6), 1150-1155.

21. Engler, A. J.; Griffin, M. A.; Sen, S.; Bönnemann, C. G.; Sweeney, H. L.; Discher, D. E., Myotubes Differentiate Optimally on Substrates with Tissue-Like Stiffness: Pathological Implications for Soft or Stiff Microenvironments. *J Cell Biol* **2004,** *166* (6), 877-887.

22. Ogneva, I. V.; Lebedev, D. V.; Shenkman, B. S., Transversal Stiffness and Young's Modulus of Single Fibers from Rat Soleus Muscle Probed by Atomic Force Microscopy. *Biophysical Journal* **2010,** *98* (3), 418-424.

23. Boontheekul, T.; Hill, E. E.; Kong, H.-J.; Mooney, D. J., Regulating Myoblast Phenotype through Controlled Gel Stiffness and Degradation. *Tissue engineering* **2007,** *13* (7), 1431-1442.

24. Kaji, H.; Ishibashi, T.; Nagamine, K.; Kanzaki, M.; Nishizawa, M., Electrically Induced Contraction of C2c12 Myotubes Cultured on a Porous Membrane-Based Substrate with Muscle Tissue-Like Stiffness. *Biomaterials* **2010,** *31* (27), 6981-6986.

25. Banan Sadeghian, R.; Ebrahimi, M.; Salehi, S., Electrical Stimulation of Microengineered Skeletal Muscle Tissue: Effect of Stimulus Parameters on Myotube Contractility and Maturation. *Journal of tissue engineering and regenerative medicine* **2018,** *12* (4), 912-922.

26. Quigley, A. F.; Razal, J. M.; Kita, M.; Jalili, R.; Gelmi, A.; Penington, A.; Ovalle-Robles, R.; Baughman, R. H.; Clark, G. M.; Wallace, G. G., Electrical Stimulation of Myoblast Proliferation and Differentiation on Aligned Nanostructured Conductive Polymer Platforms. *Advanced healthcare materials* **2012,** *1* (6), 801-808.

27. Raman, R.; Cvetkovic, C.; Uzel, S. G.; Platt, R. J.; Sengupta, P.; Kamm, R. D.; Bashir, R., Optogenetic Skeletal Muscle-Powered Adaptive Biological Machines. *Proceedings of the National Academy of Sciences* **2016,** *113* (13), 3497-3502.

28. Powell, C. A.; Smiley, B. L.; Mills, J.; Vandenburgh, H. H., Mechanical Stimulation Improves Tissue Engineered Human Skeletal Muscle. *American Journal of Physiology-Cell Physiology* **2002**.

29. Quarta, M.; Cromie, M.; Chacon, R.; Blonigan, J.; Garcia, V.; Akimenko, I.; Hamer, M.; Paine, P.; Stok, M.; Shrager, J. B., Bioengineered Constructs Combined with Exercise Enhance Stem Cell-Mediated Treatment of Volumetric Muscle Loss. *Nature communications* **2017,** *8*, 15613.

30. Bettadapur, A.; Suh, G. C.; Geisse, N. A.; Wang, E. R.; Hua, C.; Huber, H. A.; Viscio, A. A.; Kim, J. Y.; Strickland, J. B.; McCain, M. L., Prolonged Culture of Aligned Skeletal Myotubes on Micromolded Gelatin Hydrogels. *Scientific reports* **2016,** *6*, 28855.

31. Watt, F. M.; Huck, W. T., Role of the Extracellular Matrix in Regulating Stem Cell Fate. *Nature reviews Molecular cell biology* **2013,** *14* (8), 467.

32. Bonnans, C.; Chou, J.; Werb, Z., Remodelling the Extracellular Matrix in Development and Disease. *Nature reviews Molecular cell biology* **2014,** *15* (12), 786.

33. von der Mark, K.; Park, J.; Bauer, S.; Schmuki, P., Nanoscale Engineering of Biomimetic Surfaces: Cues from the Extracellular Matrix. *Cell and tissue research* **2010,** *339* (1), 131.

34. Gillies, A. R.; Lieber, R. L., Structure and Function of the Skeletal Muscle Extracellular Matrix. *Muscle & nerve* **2011,** *44* (3), 318-331.

35. Mayer, U., Integrins: Redundant or Important Players in Skeletal Muscle? *Journal of Biological Chemistry* **2003,** *278* (17), 14587-14590.

36. McDonald, K. A.; Horwitz, A. F.; Knudsen, K. A. In *Adhesion Molecules and Skeletal Myogenesis*, seminars in DEVELOPMENTAL BIOLOGY, Elsevier: 1995; pp 105-116.

37. Perkins, A. D.; Ellis, S. J.; Asghari, P.; Shamsian, A.; Moore, E. D.; Tanentzapf, G., Integrin-Mediated Adhesion Maintains Sarcomeric Integrity. *Developmental biology* **2010,** *338* (1), 15-27.

38. Ruoslahti, E., Rgd and Other Recognition Sequences for Integrins. *Annual review of cell and developmental biology* **1996,** *12* (1), 697-715.

39. Gribova, V.; Gauthier-Rouvière, C.; Albigès-Rizo, C.; Auzely-Velty, R.; Picart, C., Effect of Rgd Functionalization and Stiffness Modulation of Polyelectrolyte Multilayer Films on Muscle Cell Differentiation. *Acta biomaterialia* **2013,** *9* (5), 6468-6480.

40. Hinds, S.; Bian, W.; Dennis, R. G.; Bursac, N., The Role of Extracellular Matrix Composition in Structure and Function of Bioengineered Skeletal Muscle. *Biomaterials* **2011,** *32* (14), 3575-3583.

41. Shahini, A.; Vydiam, K.; Choudhury, D.; Rajabian, N.; Nguyen, T.; Lei, P.; Andreadis, S. T., Efficient and High Yield Isolation of Myoblasts from Skeletal Muscle. *Stem cell research* **2018,** *30*, 122-129.

42. Cohick, W.; Clemmons, D., The Insulin-Like Growth Factors. *Annual review of physiology* **1993,** *55* (1), 131-153.

43. Song, Y.-H.; Song, J. L.; Delafontaine, P.; Godard, M. P., The Therapeutic Potential of Igf-I in Skeletal Muscle Repair. *Trends in Endocrinology & Metabolism* **2013,** *24* (6), 310-319.

44. Glass, D. J.; Bowen, D. C.; Stitt, T. N.; Radziejewski, C.; Bruno, J.; Ryan, T. E.; Gies, D. R.; Shah, S.; Mattsson, K.; Burden, S. J., Agrin Acts Via a Musk Receptor Complex. *Cell* **1996,** *85* (4), 513-523.

45. Cohen, I.; Rimer, M.; Lømo, T.; McMahan, U., Agrin-Induced Postsynaptic-Like Apparatus in Skeletal Muscle Fibersin Vivo. *Molecular and Cellular Neuroscience* **1997,** *9* (4), 237-253.

46. Nayerossadat, N.; Maedeh, T.; Ali, P. A., Viral and Nonviral Delivery Systems for Gene Delivery. *Advanced biomedical research* **2012,** *1*.

47. Verma, I. M.; Naldini, L.; Kafri, T.; Miyoshi, H.; Takahashi, M.; Blömer, U.; Somia, N.; Wang, L.; Gage, F., Gene Therapy: Promises, Problems and Prospects. In *Genes and Resistance to Disease*, Springer: 2000; pp 147-157.

48. Kim, T. K.; Eberwine, J. H., Mammalian Cell Transfection: The Present and the Future. *Analytical and bioanalytical chemistry* **2010,** *397* (8), 3173-3178.

49. Sato, M.; Ito, A.; Kawabe, Y.; Nagamori, E.; Kamihira, M., Enhanced Contractile Force Generation by Artificial Skeletal Muscle Tissues Using Igf-I Gene-Engineered Myoblast Cells. *Journal of bioscience and bioengineering* **2011,** *112* (3), 273-278.

50. Farris, A. L.; Rindone, A. N.; Grayson, W. L., Oxygen Delivering Biomaterials for Tissue Engineering. *Journal of Materials Chemistry B* **2016,** *4* (20), 3422-3432.

51. Hengartner, M. O., The Biochemistry of Apoptosis. *Nature* **2000,** *407* (6805), 770.

52. Sato, M.; Ito, A.; Akiyama, H.; Kawabe, Y.; Kamihira, M., Effects of B-Cell Lymphoma 2 Gene Transfer to Myoblast Cells on Skeletal Muscle Tissue Formation Using Magnetic Force-Based Tissue Engineering. *Tissue Engineering Part A* **2012,** *19* (1-2), 307-315.

53. Ikeda, K.; Ito, A.; Sato, M.; Kawabe, Y.; Kamihira, M., Improved Contractile Force Generation of Tissue-Engineered Skeletal Muscle Constructs by Igf-I and Bcl-2 Gene Transfer with Electrical Pulse Stimulation. *Regenerative Therapy* **2016,** *3*, 38-44.

54. Pan, H.; Vojnits, K.; Liu, T. T.; Meng, F.; Yang, L.; Wang, Y.; Huard, J.; Cox, C. S.; Lally, K. P.; Li, Y., Mmp1 Gene Expression Enhances Myoblast Migration and Engraftment Following Implanting into Mdx/Scid Mice. *Cell adhesion & migration* **2015,** *9* (4), 283-292.

55. Bedair, H.; Liu, T. T.; Kaar, J. L.; Badlani, S.; Russell, A. J.; Li, Y.; Huard, J., Matrix Metalloproteinase-1 Therapy Improves Muscle Healing. *Journal of applied physiology* **2007,** *102* (6), 2338-2345.

56. Kaar, J. L.; Li, Y.; Blair, H. C.; Asche, G.; Koepsel, R. R.; Huard, J.; Russell, A. J., Matrix Metalloproteinase-1 Treatment of Muscle Fibrosis. *Acta biomaterialia* **2008,** *4* (5), 1411-1420.

57. Wang, P. Y.; Thissen, H.; Tsai, W. B., The Roles of Rgd and Grooved Topography in the Adhesion, Morphology, and Differentiation of C2c12 Skeletal Myoblasts. *Biotechnology and bioengineering* **2012,** *109* (8), 2104-2115.

58. Osaki, T.; Sivathanu, V.; Kamm, R. D., Crosstalk between Developing Vasculature and Optogenetically Engineered Skeletal Muscle Improves Muscle Contraction and Angiogenesis. *Biomaterials* **2018,** *156*, 65-76.

CHAPTER 3: MATRIX TOPOGRAPHY REGULATES SYNAPTIC TRANSMISSION AT THE NEUROMUSCULAR JUNCTION

Acknowledgments

This work was supported by the National Science Foundation (CBET-140349 & STC-EBICS Grant CBET-0939511) and the National Institute of Biomedical Imaging and Bioengineering of the National Institutes of Health under Award Number T32EB019944. I would like to thank Dr. Seung Jung Yu for providing the material platform, Dr. Ziad Mahmassani for providing the primary cells, and Gelson J. Pagan-Diaz for his help in analyzing the functionality data. This chapter is adapted from Ko, E.; Yu, S. J.; Pagan-Diaz, G. J.; Mahmassani, Z.; Boppart, M. D.; Im, S. G.; Bashir, R.; Kong, H. Matrix Topography Regulates Synaptic Transmission at the Neuromuscular Junction. Advanced Science 2018, advs.201801521. Copyright Wiley-VCH Verlag GmbH & Co. KGaA. Reproduced with permission. Wiley-VCH hereby licenses back to the Contributor the following rights with respect to the final published version of the Contribution:

3.1 Introduction

Skeletal muscle injuries characterized with strain and contusion often lead to significant reduction in the mass and strength of skeletal muscle. Without proper treatments, these pathological conditions may lead to discomfort, pain, disability, and ultimately death. In many cases, the muscular impairment accompanies regression and limited self-regeneration of neuromuscular junctions. The neuromuscular junction is a specialized synapse at the junction of the motor neuron and myofiber, a critical site that supports neural transmitter release and subsequent regulation of muscle contraction.[1-2] Morbid or dysfunctional neuromuscular junction

causes a series of neuromuscular disorders and diseases.[3-5] Thus, the formation and impairment of the neuromuscular junction have been extensively studied, largely through *in vivo* studies.

Recently, engineering a muscle tissue innervated by neurons has gained attention because the system potentially allows physiological studies of both normal and impaired tissues at varied length scales. Moreover, the engineered neuromuscular junction could be useful for screening newly developed medicine related to muscular disorders and creating stimulatory devices.[6-7] The neuromuscular junctions are commonly reproduced by co-culturing the skeletal myoblasts and neuronal cells.[7-10] For example, a muscle strip co-cultured with stem cell-derived motor neurons exhibits a contraction profile by a natural neurotransmitter (e.g. glutamate) and an antagonist (e.g. curare).[10] In addition, a microfluidic system was used to spatially organize myotubes and motor neurons and induce neural innervation into the myotubes.[7] These studies largely focused on evaluating capability of stem cell-derived neural cells to innervate muscle tissue. Despite these impressive successes, the underlying basis for cross-talk between muscle and neurons at the neuron-muscle interface is still not sufficiently understood.

Previous studies conducted *in vivo* suggest that communication between the muscle and motor neurons guide neural innervation.[11-12] These studies reported that myogenic differentiation in the post-synaptic region can guide synaptogenesis.[11] For instance, the muscle intrinsically activates muscle-specific kinase that mediates the expression of acetylcholine receptors, which act as a physical pattern at the post-synaptic region. The innervating neurons, on the other hand, secrete agrin proteins that phosphorylates the muscle-specific kinase and stabilize the clustered acetylcholine receptors in the muscle.[13-14] The muscle and neurons communicate during these reciprocal events to form neuromuscular junctions. These results imply that a series of intercellular signaling events in the muscle can mediate the neural innervation.

In this study, we hypothesized that the maturity and alignment of myotubes engineered *in vitro* would affect the expression of acetylcholine receptors in myotubes and responsiveness of neuron-innervating muscle to the neurotransmitter and antagonist. First, we cultured primary or C2C12 skeletal myoblasts on the Matrigel-coated poly(urethane acrylate) (PUA) substrates with grooved patterns (Figure 3.1). The groove width was varied from 200 nm to 800 and 1,600 nm, which encompasses the geometry of collagen fibers in an extracellular matrix (ECM) and myofibrils of the muscle fiber.[15-16] A flat PUA substrate was used as a control. Next, on the pre-formed myotubes, we plated neural stem cells (NSCs) and differentiated them into motor neuron progenitor cells. We examined the differentiation lineage and angular alignment of NSCs via immunofluorescence imaging. Lastly, the neural innervation into myotubes were evaluated by immunofluorescently staining the myosin heavy chain (MHC), acetylcholine receptor, and presynaptic ends of the neurons. The physiological function of the neuromuscular junction was also assessed by measuring the contraction frequency upon exposure to an excitatory neurotransmitter (i.e., glutamate) and a neuromuscular antagonist (i.e., curare).[9]

3.2 Results and Discussion

3.2.1 Engineering Myotubes on the Grooved Substrates

First, we prepared PUA substrates with controlled patterns of grooves ranging from 200 to 1,600 nm. These substrates were fabricated by placing PUA resin and poly (ethylene terephthalate) (PET) film on the silicon molds as previously described (Figure 3.2A).[17] The topographical feature of the pattern was confirmed by scanning electron microscopy images (Figure 3.2B). These grooved substrates were inspired by the structure of muscle.[17] The cross-sectional diameter of a

myofibril is around 1 μm.[18] In contrast, collagen fibers, the ECM protein surrounding the skeletal muscle, have cross-sectional diameters ranging between 200 and 400 nm.[19]

We investigated if the grooved substrates modulate the organization of cytoskeletal actin filaments and focal adhesion proteins of the primary and C2C12 myoblasts (Figure 3). According to the immunofluorescence images of F-actin, the F-actin filaments of primary myoblasts aligned anisotropically on the grooved substrates, while the orientation was random on a flat substrate (Figure 3.3A, B). Vinculin was elongated in parallel with the linear pattern of the grooves in the immunofluorescence images. The linear orientation and elongation in the morphology of the focal adhesion complex may contribute to enhanced myogenic differentiation and muscle function after myoblasts differentiate into myotubes.[20-21] In addition, the primary myoblasts displayed slightly increased expression levels of vinculin, on the substrate with the groove width of 1,600 nm (Figure 3.3C).

The angular orientations of the cells were quantified with the optical images of cells (Figure 3.4). According to the optical images, both primary and C2C12 myoblasts cultured on the grooved substrates aligned in parallel with the grooves. The cells cultured on the flat substrate were, however, randomly oriented. The angular orientation was plotted from 0º to 180º on a histogram using the Directionality plugin in Image J software. This process yielded the histograms in Figure 4 B and D. The y axis indicates the magnitude of Fourier component and the x axis shows the degree. A single high peak with a low dispersion value, and high goodness of fit in the grooved groups suggest that the cells recognize the grooved patterns and align to each other. The flat group showed high dispersion value with low goodness of fit indicating the random orientation of cells.

The role of substrate topography on myogenic differentiation level was evaluated by examining the alignment and maturity of the multinucleated myotubes. After 10 days of culture in

the myogenic differentiation medium, the myotubes were stained for F-actin, myosin heavy chain (MHC), and cell nuclei (Figure 3.5). All three substrates prompted myoblasts to form MHC-positive myotubes characterized with multinucleation. (Figure 3.5A, B). As expected, the grooved substrates guided the myotubes to align anisotropically while myotubes formed on the flat substrate developed in random directions. We further confirmed the myogenic maturation by examining the sarcomeric striation (Figure 3.5 C, D and Figure 6). The myotubes formed with both primary and C2C12 myoblasts cultured on the grooved substrates promoted striation of the myotubes. The relative number of striated myotubes was higher when myoblasts were cultured on the grooved substrates compared to the flat substrate.

With the immunofluorescence images, we performed a morphometric analysis by measuring the width, length, area, and fusion index of MHC-positive myotubes. These morphometric parameters represent maturity of myotubes. There were significant differences in the size of myotubes between conditions. The myoblasts cultured on the substrate with the groove width of 1,600 nm developed MHC-positive myotubes with the largest width and length (Figure 3.5E, F). The MHC-positive area of myotubes was also proportional to the width of the grooves. The dependency was more noticeable with primary myoblasts than C2C12 myoblasts (Figure 3.5G). The fusion index was quantified by dividing the number of nuclei present in the multinucleated myotubes by the total number of nuclei present (Figure 3.5H). The fusion index of cells cultured on the grooved substrates was higher than that on the flat substrate, indicating that grooved substrates are advantageous to stimulating mature myotube formation.

We also examined the MHC-positive myotubes formed on the substrate with the groove width of 800 nm. These myotubes showed minimal differences in the myotube width and area, compared with those formed on the substrate with the groove width of 200 nm (Figure 3.3.7).

Therefore, we used substrates with the groove width of 200 and 1,600 nm for the following co-culture study.

3.2.2 Analysis of Neuronal Differentiation of NSCs on Engineered Myotubes

We studied if the maturity and alignment of myotubes formed on the flat and grooved substrates affect the differentiation lineage of NSCs and the orientation of the differentiated NSCs. We used NSCs because of their potential to differentiate into motor neurons. [10, 22-23] As the first step, we prepared a myotube layer, which covered the flat or grooved substrates entirely. Then, we plated the globular clusters of NSCs, denoted as neurospheres, on the myotubes layer. This allows the NSCs to recognize the orientation of the myotubes instead of the topology of the substrates. Within 3 days, single cells migrated from the neurospheres and adhered on the myotubes. [10, 24]

The cells migrated from the neurospheres differentiated into motor neuron progenitor cells spontaneously, as confirmed with motor neuron markers, including islet 1 and neurogenin 2 (Figure 3.8A-D). Islet 1 is a transcription factor essential for differentiating into motor neurons and neurogenin 2 is a transcription factor that specifies motor neuron identity.[25-28] The motor neuron progenitor cells positively stained by antibodies to islet 1 and neurogenin 2 stretched their axons in parallel to the myotubes, particularly those formed on the grooved substrate. The motor neuron progenitor cells oriented randomly on the myotubes formed on the flat substrate. The differentiated NSCs were also stained with a neuronal marker, microtubule-associated protein 2 (MAP2) and a glial marker, glial fibrillary acidic proteins (GFAP). These immunofluorescence images exhibited that the NSCs differentiated into neuronal cells more actively than glial cells when the myotube layer was present (Figure 3.9 A, B). The spontaneous neuronal differentiation

of NSCs was observed without the myotubes, as confirmed with positive staining for MAP2, neurofilament, islet 1 and neurogenin 2 (Figure 3.9C). However, in this condition, differentiated NSCs also expressed GFAP.

The immunofluorescence images of differentiated neurons were analyzed with ImageJ software to determine the angular orientation. Angular orientation was plotted as histograms, and the direction (population mean) and dispersion (standard deviation) were obtained (Figure 3.8 E, F). The neurons cultured on myotubes aligned by the grooved substrates showed two high peaks localized at single peak, with a small dispersion value confirming anisotropic alignment of neurons (Figure 3.8E, F). The goodness of fit values were above 0.8 indicating that the myoblasts anisotropically aligned better compared to the myoblasts cultured on the flat substrate. Neurons on the myotubes formed on the flat substrates showed a large dispersion value with a low goodness of fit. Thus, the cells were more randomly oriented.

The linear topographical features are known to regulate the differentiation level of NSCs and the spatial organization of the differentiated neurons.[28-29] The axons of neurons tend to extend more on the linear topography where neurotrophic factors are immobilized.[30] Apart from these prior studies, this study was conducted by culturing the neurospheres on the myotube layer, which shadowed the substrate pattern. Therefore, this anisotropic alignment of differentiated neurons with myotubes addresses that myotubes can guide the orientation of neurons during this sequential co-culture. Moreover, the anisotropically aligned ECM molecules produced by the myotubes, such as collagen, could have guided the orientation of the differentiated neurons. The axons stretching to relatively random directions on the flat substrate support this interpretation.

3.2.3 Morphological Analysis of the Neuron-Muscle Interface

We examined the mutual interaction between the myotubes and neurons by examining the acetylcholine receptor expression on the myotubes and the neural innervation. Again, myoblasts were cultured on the grooved substrates to form mature myotubes, and neurospheres were plated on the myotubes subsequently. The acetylcholine receptors, MHC, and neurofilaments of differentiated neurons were visualized via immunostaining. On the flat substrate, myotubes and neurons were extended in random directions, as shown with isotropic orientations of the MHCs and neurofilaments (Figures 7A, C). The myotubes on the grooved substrates aligned together with the differentiated neurons, as displayed with the same orientations of MHCs and neurofilaments. Moreover, myotubes formed on the substrates with the groove width of 1,600 nm presented larger number of acetylcholine receptors than those formed on the flat substrate, particularly with myotubes formed with primary myoblasts (Images in the first rows of Figures 7A and 7C). Then, we visualized synaptophysin (pre-synaptic marker) and acetylcholine receptor (post-synaptic marker) to locate the sites where neurons innervate (Figures 7B and 7D). All conditions showed synaptophysin-positive nerve ends on myotubes. To confirm the nerve ends, differentiated NSCs were additionally stained with MAP2 for the primary myoblast condition.

Based on the immunofluorescence images, we quantified the relative acetylcholine receptor positive area per myotube in the immunofluorescence image and the area of co-localization of the acetylcholine receptors, MHC, and neurofilaments per myotube. According to the quantitative analysis with immunofluorescence images, myotubes developed on the grooved substrates expressed a higher level of acetylcholine receptors than those on the flat substrate (Figure 3.10E). Increasing the groove width from 200 to 1,600 nm led to a 1.7-fold increase in the acetylcholine receptors expression level in primary myoblast-derived myotubes. With C2C12 myoblast-derived

myotubes, the substrate with the groove width of 1,600 nm led to the fivefold higher acetylcholine receptor expression than the flat substrate (Figure 3.10G).

Likewise, primary myoblast-derived myotubes on the substrate with the groove width of 1,600 nm showed a nearly two-fold higher percentage of area co-localized by acetylcholine receptors and neurofilaments than those formed on the flat substrate (Figure 3.10F). This result implies that an increased number of myotubes were innervated by motor neuron progenitor cells on the grooved substrate. The myotubes prepared with C2C12 myoblasts showed a similar trend (Figure 3.10H). The fluorescence channels were separated to show a clearer expression of each marker (Figure 3.11).

3.2.4 Functional Analysis of the Neuron-Muscle Interface

Finally, we evaluated functionality of the motor neuron progenitor cell-innervated myotubes by recording their response upon exposure to the excitatory neurotransmitter, glutamate, and the neuromuscular junction-specific antagonist, curare (Figure 3.12A). Before exposure to glutamate or curare, myotubes showed slightly noticeable spontaneous contraction, regardless of the substrate topography (Figures 8B-E). The myotubes engineered with both primary and C2C12 myoblasts on the substrate with groove width of 1,600 nm responded to glutamate and curare more sensitively. The degree of response was specific to cell types. Upon exposure to glutamate, motor neuron progenitor cell-innervated myotubes on the substrate with groove width of 1,600 nm showed higher contraction frequency and number than those formed on the substrate with groove width of 200 nm (Figure 3.12B, Table 1). The myotubes on the flat substrate exhibited an almost imperceptible increase in the contraction frequency.

When the samples were exposed to curare, motor neuron progenitor cell-innervated myotubes on the substrate with groove width of 1,600 nm instantaneously switched off. The motor neuron progenitor cell-innervated myotubes on the other two substrates showed a lag time ranging from 2 to 5 seconds before the contraction stopped completely (Figure 3.12C).

The difference in muscle contraction between conditions became smaller with myotubes formed with C2C12 myoblasts. Upon exposure to glutamate, there was either proportional increases in the contraction frequency or number with the increase in groove width (Figure 3.12D, Table 1). The muscle contraction was shut down within 5 seconds for all samples when the samples were exposed to curare (Figure 3.12E, Table 1).

The myotubes formed without NSCs did not show a notable response to either glutamate or curare (Figure 3.13). In fact, contraction was either slightly noticeable or not recognizable in the culture. Addition of glutamate to the primary and C2C12 myoblasts did not show significant change in the contraction (Figure 3.13 A, C). Similarly, the myotubes continuously contracted after applying curare to the samples (Figure 3.13 B, D). Because glutamate promotes motor neurons to secrete more acetylcholine molecules from the motor neurons to the skeletal myotubes and enhance contraction, the myotubes without the motor neuron progenitor cells did not respond to glutamate treatment. Curare blocks the acetylcholine receptors in the skeletal myotubes. The blockage of these sites did not have any influence the spontaneous contraction in absence of the motor neuron progenitor cells.

These results address that maturity and orientation of myotubes play important roles in reproducing the neuron-innervated muscle with an increased sensitivity to glutamate and curare. We suggest that the grooves on the substrates present increased contact area for the myotubes and align the cells anisotropically. In fact, grooves with 200 nm-spacing are not wide enough for the

cellular membrane to penetrate and form contacts between a substrate and cells, as confirmed with the electron microscopic images (Figure 3.14).[31] On the other hand, myotubes cultured on the substrate with the groove width of 1,600 nm protrude their membrane into the grooves. Accordingly, myotubes align with the grooved pattern better than those on the 200 nm grooved substrate. We propose that this enhanced contact with the substrate promotes the anisotropic alignment of myotubes along the grooved pattern.

From the analysis of neuron-muscle interface, we propose that myotubes regulate the lineage of the NSCs and the spatial arrangement of the differentiated motor neuron progenitor cells. The maturity of myotubes influences the acetylcholine receptor expression level, which directly promotes the neuronal differentiation.[32] The presence of muscle-derived neurotrophic factors could also contribute to the development and differentiation of NSCs to motor neuron progenitor cells, as maintenance and function of motor neurons depend on secreted factors from the skeletal muscle.[33-34] Moreover, the aligned myotubes express more acetylcholine receptors, thus, increase the number of neuron-innervated myotubes as characterized with the immunofluorescence staining of neuron-muscle interface and the response to glutamate and curare. These results confirm that acetylcholine receptors on the myotubes guide and stimulate neural innervation, as previously suggested with the *in vivo* gene knock-out studies.[35-38] Likely, the agrin molecules secreted by innervating neurons stimulate the aggregation of acetylcholine receptors, which would be systematically examined in future studies.[13-14]

This study provides crucial insights into engineering muscles, morphologically and functionally similar to the natural muscle. To the best of our knowledge, we have demonstrated that the maturity of muscle promotes the neural innervation by mediating the reciprocity between myotubes and neurons for the first time. As a consequence, myotubes display rapid response time,

and increased contraction number in response to a neural simulator and inhibitor. We proposed that this finding make important scientific impacts in understanding the homeostasis of the normal muscle and the regeneration of the functional muscle. In the long term, this system may work as a vital component of controlling the stimulus responsive behavior of a "living" biological machinery, emerged as a new generation of an autonomous robotic system.[39-41]

3.3 Conclusion

In conclusion, this study uncovered an important role of the muscular orientation and maturity in neural innervation and the physiological function of neuromuscular junctions. The nanogrooved substrates with proper groove width facilitated the formation of mature and aligned myotubes compared to the flat substrate. The NSCs subsequently plated on the mature and aligned myotubes differentiated into motor neuron progenitor cells and aligned in the same direction of the pre-formed myotubes. The mature and aligned myotubes formed on the substrate with groove width of 1,600 nm raised the acetylcholine receptor expression level and the percentage of area where motor neuron progenitor cells and acetylcholine receptors are co-localized, compared to myotubes formed on the flat substrate. In consequence, the response of neuron-innervated muscle contraction to glutamate and curare was more evident when myotubes were more aligned and mature. Altogether, results of this study illuminate the reciprocal activity of myotubes and neurons toward the assembly of the physiologically functional muscle. Therefore, these findings would be useful to improving the quality of engineered tissue used for drug screening, muscular disorder treatment, and biological machinery assembly.

3.4 Materials and Methods

3.4.1.Preparation of Nano-Grooved Substrates

The nanogrooved substrates were fabricated with PUA (MINS-311RM, Minuta Tech, Gyeonggi, Korea) by using the capillary force lithography techniques reported previously.[17] Two drops of PUA resin were placed at the center of a nanogrooved Si master and subsequently covered with PET film (Skyrol ®, SKC Co., Ltd., Seoul, Korea). The PUA resin was exposed to ultraviolet light at 20 mW/cm^2 for 10 seconds in the UV curing system (Minuta Tech, Gyeonggi, Korea) (~365 nm). Then, the PET film with the patterned PUA resin was detached from the Si mater and stabilized for 24 hours. The substrates were soaked in isopropyl alcohol for 30 minutes and distilled water for an additional 30 minutes. The flat PUA substrate was prepared on the smooth Si surface by following the same curing and cleaning procedure.

3.4.2 Primary Myoblast Isolation and Culture

Mice were sacrificed using CO_2 inhalation followed by cervical dislocation. Sacrificed mice were placed on ethanol and transferred to a sterile culture hood. Hind limb muscles were dissected and minced in a petri dish 1% (v/v) penicillin/streptomycin antibiotic in sterile phosphate buffer saline (PBS). Enzyme solution containing 10% (w/v) Pronase, 3.5% (w/v) Collagenase, and 2.5mm $CaCl_2$ was introduced to the slurry mix and allowed to incubate for 1 hour at 37 °C with trituration every 10 minutes. The mixture was then passed through a 70μM filter where a volume of inhibition medium (20% (v/v) fetal bovine serum (FBS) and 1% (v/v) penicillin/streptomycin in Hanks' balanced salt solution) equal to the volume of enzyme solution used was added. The solution was, again, passed through a 40μM filter. The conical tubes containing the muscle slurry were spun at 350g for 5 minutes, and the pellet was re-suspended in the growth medium. Cells

were pre-plated on plastic petri dishes for 3 hours, after which the unattached cells were plated on Matrigel coated (1% (v/v) Matrigel in sterile PBS) Petri dishes. Cells were not allowed past 75% confluence during the passage.

3.4.3 Culture of Primary and C2C12 Myoblasts for Myogenic Differentiation

The fabricated PUA substrates were sterilized by using 70 % ethanol and washed with sterile PBS three times before use. The surfaces were coated with Matrigel (Corning, New York, NY, USA) to allow cell adhesion. For the coating process, 1% (v/v) Matrigel in PBS was placed on the PUA substrates and incubated for 1 hour. The excess solution was removed by washing the substrates with PBS 2 times. The primary myoblasts or C2C12 myoblasts (American Type Culture Collection, Rockville, MD, USA) were plated on the PUA substrate at a density of 2×10^4 cells/cm^2. The PUA substrates plated with primary myoblasts were incubated in growth medium consisting of Dulbecco's modified Eagle medium (DMEM) /F12 50:50 (Corning), r-fibroblast growth factor (FGF), 1% penicillin-streptomycin (PS, Gibco, Gaithersburg, MD, USA), 20% FBS (Gibco). The cells were incubated in humidified air containing 5% CO_2 at 37 °C. Separately, the PUA substrate on which C2C12 myoblasts cultured were incubated in DMEM (Gibco) supplemented with 10% FBS (Gibco) and 1% PS. Myogenic differentiation of both primary cells and C2C12 cells was activated by replacing the growth medium with a differentiation medium (DMEM supplemented with 2% horse serum and 1% PS) after 3 days of culture in the growth medium. The cells were incubated in the differentiation medium for additional 7 days.

3.4.4 Culture of NSCs for Neuronal Differentiation

NSCs derived from the mouse brain cortex were purchased from R&D Systems (Minneapolis, MN, USA) and expanded in a neurosphere form by following the manufacturer's protocol. In brief, the cells were plated at a density of 5×10^4 cells/ml and cultured in DMEM/F12 medium supplemented with the N-2 supplement (R&D Systems), the epidermal growth factor (EGF) (R&D Systems), and the basic recombinant human fibroblast growth factor (bFGF) (R&D Systems). Fresh EGF and bFGF were added every day during expansion. After culturing the neurospheres in growth medium for 5 days, the medium was replaced with the neural differentiation medium (DMEM/F12 medium supplemented with N-2 supplement (R&D Systems)). The neurospheres were cultured for 3 days to induce neuronal differentiation before initiating the co-culture with the myotubes.

3.4.5 Co-Culture of the Differentiated Myoblasts and NSC Neurospheres

Primary and C2C12 myoblasts were seeded on the PUA substrates coated with Matrigel and differentiated as above. Then, NSC neurospheres cultured in the neural differentiation medium for 3 days were collected and placed on the engineered muscle layer. The two cell populations were incubated in the NSC differentiation medium overnight for stabilization of NSCs. On the next day, the medium was replaced with NSC differentiation medium containing 2% horse serum. The horse serum was included in the co-culture media to maintain the differentiated myotubes.[42] The myoblasts and NSCs were maintained in the co-culture medium for another 7 days.

3.4.6 Immunofluorescence Staining of F-Actin and Vinculin

Myoblasts cultured on the flat and grooved substrates were stained for F-actin, vinculin, and 4'-6-diamidino-2-phenylindole (DAPI) using the Actin Cytoskeleton and Focal Adhesion Staining Kits

(FAK100) (Millipore, Bedford, MA, USA). In brief, after 3 days of culture, cells on the PUA substrates were fixed with 4% (w/v) paraformaldehyde (Sigma, St. Louis, MO, USA) for 15 min and permeablized with 0.1% (v/v) Triton X-100 (Sigma) for 5 min. After incubating the cells in 2% goat serum for blocking unspecific bindings, the cells were incubated with primary vinculin antibody for one hour at room temperature. Then, vinculin was immunofluorescently labeled with secondary antibodies (Alexa Fluor-594 donkey anti-mouse IgG; Invitrogen, Carlsbad, CA, USA). For double immunofluorescence staining, fluorescein (FITC)-conjugated Phalloidin included in the kit was applied simultaneously. After incubation for 1 hour, the nuclei of the cells were labeled with DAPI (Sigma). The fluorescence signals were collected with a laser scanning confocal microscope (LSM 700, Carl Zeiss, Jena, Germany).

3.4.7 Analysis of Cellular Orientation

The morphology images of the myoblasts were taken with an inverted microscope (Leica DMI 4000B, Leica Microsystems, Wetzlar, Germany) after the myoblasts were cultured in growth medium for 3 days and differentiation medium for 7 days. The directionality of the adhered cells was analyzed by Directionality plugin for ImageJ software. First, the morphology images were converted to 8-bit grayscale images, and these images were processed with Directionality plugin available on the Analyze tab. This plugin derives a histogram that counts the amount of myotubes in each degree from 0º to 180º. A Gaussian fit is calculated from the highest peak in the histogram. Direction of the myotubes in degree (mean) and the dispersion of the myotubes in degree (standard deviation) were derived by the plug in.[43] Similarly, the alignment of NSCs cultured on the myotubes was analyzed by following the same procedure. Immunofluorescence

images of the neurons positively stained for MAP2 were used for this analysis. The goodness of fit R^2 value was averaged to confirm orientation of the myotubes.

3.4.8 Immunofluorescence Staining of Myotubes and Morphometric Analysis

After culturing the myoblasts for 7 days in the myogenic differentiation medium, we immunofluorescently stained the cells. Cells were fixed with 4% (w/v) paraformaldehyde (Sigma) for 15 min, permeablized with 0.1% (v/v) Triton X-100 (Sigma) for 5 min and incubated in blocking solution for 45 min. After blocking, the cells were incubated with MF-20 anti-MHC (1:400) (iT FX, Developmental Studies Hybridoma Bank, The University of Iowa Department of Biology) at 4 °C overnight. Another set of samples were incubated with anti-sarcomeric α-actinin antibody (Abcam Cambridge, U.K.). On the next day, MHC was labeled with fluorescence-tagged secondary antibody (Alexa Fluor-594 goat anti-mouse IgG (1:500) (Invitrogen)) and sarcomeric α-actinin was labeled with Alexa Fluor-568 donkey anti-rabbit IgG (1:500; Invitrogen). Additionally, phalloidin-Alexa Fluor 488 (1:200; Invitrogen) and DAPI (Sigma) were used to stain F-actin and nuclei of the cells, respectively. The length and width of the myotubes were quantified by measuring the length and width of the MHC-stained myotubes present in the immunofluorescence image. The MHC-positive area was calculated by quantifying the number of pixels. The fusion index was quantified by calculating the ratio of the number of nuclei in the differentiated myoblasts. The samples were imaged with the laser scanning confocal microscope (LSM 700, Carl Zeiss).

3.4.9 Immunocytochemical Analysis of Differentiated Neurons

The immunofluorescence staining of NSCs cultured on the myotubes was fixed, permeabilized, and blocked. Then, the samples were incubated with the motor neuron marker, rabbit monoclonal anti-islet 1 (1:100; Abcam) and rabbit polyclonal anti-neurogenin 2 (1:100; Abcam). Islet 1 and neurogenin 2 were labeled with Alexa Fluor-488 donkey anti-rabbit IgG (1:500; Invitrogen). Then, another sample set was incubated with mouse monoclonal anti-glial fibrillary acidic protein (GFAP) (1:200; Millipore), and rabbit polyclonal anti-microtubule- associated protein (MAP2) (1:200; Abcam) at 4°C. The GFAP and MAP2 were labeled with Alexa Fluor-488 donkey anti-rabbit IgG (1:500; Invitrogen) and Alexa Fluor-594 donkey anti-mouse IgG (1:500; Invitrogen), respectively. The nuclei of cells were separately stained with DAPI. The samples were imaged by the confocal microscope (LSM 700, Carl Zeiss).

3.4.10 Immunocytochemical Analysis of the Neuromuscular Junctions

The neuromuscular junctions were identified with a site where acetylcholine receptors on the MHC-positive myotubes and the synaptic ends of the neurofilaments were co-localized. The cells were fixed, permeabilized, and blocked. After blocking, one set of samples was incubated with primary antibodies, MF-20 anti-myosin heavy chain (MHC; 1:400) (iT FX) and neurofilament-H (neurofilament 200) (1:50; Sigma) at 4 °C. Another set of samples was treated with chicken polyclonal anti-MAP2 (1:1000; Abcam), and rabbit monoclonal anti-synaptophysin (1:250; Thermo Fisher Scientific, Rockford, IL, USA) to label the myotubes and pre-synaptic ends of the motor neuron progenitor cells. Lastly, cells treated with MF-20 and neurofilament-H were incubated with Alexa Fluor-488 donkey anti-rabbit IgG (1:500; Invitrogen) and Alexa Fluor-594 goat anti-mouse IgG (1:500) (Invitrogen). The samples treated with anti-MAP2 antibody and

synaptophysin were treated with Alexa Fluor-488 goat anti-chicken IgG (1:500; Invitrogen) and Alexa Fluor-568 donkey anti-rabbit IgG (1:500) (Invitrogen). The cells were also incubated with the α-Bungarotoxin-Alexa Fluor-647 conjugate (1:1000; Invitrogen) to label acetylcholine receptors on the myotubes. Next, the nuclei were stained using DAPI (Sigma). The final samples were observed under a multiphoton confocal microscope (LSM 710, Carl Zeiss).

3.4.11 Functionality Analysis of the Engineered Neuromuscular Junctions

The engineered neuromuscular junctions on the substrates were treated with a neurotransmitter, glutamate (400 μM, Sigma), or an antagonist, (+)-Tubocurarine chloride hydrochloride pentahydrate (curare) (50 μM, Abcam), to stimulate or stop the muscle contraction, respectively. Videos were taken using Zeiss Axiocam ERc 5s (Carl Zeiss) attached on an inverted microscope at 30 fps and later processed using FIJI and MatLAB. The region of interest was determined by selecting 6 active regions in the beginning of data acquisition distributed evenly across the entire field of view. The region of interests were loaded unto MATLAB and tracked displacement of myotube periphery. Modulus of displacement was calculated between each phrase using standard distance formula. Contractions were assigned by selecting positive values after calculating the discreet derivatives of the displacement arrays. Contractions were summed for each frame and plotted against time. The analysis for the control group was performed same as above, but the myotubes were treated without the neural stem cells.

3.4.12 Statistical Analysis

All statistical analyses performed in this study were conducted using unpaired Student's t-test with Graph Pad Prism 6.0 (Graph Pad Software Inc., San Diego, CA, USA). Differences were

considered significant at a *p*-value of less than 0.05. *p*-value smaller than 0.05, were considered statistically significant.

3.5 Figures and Table

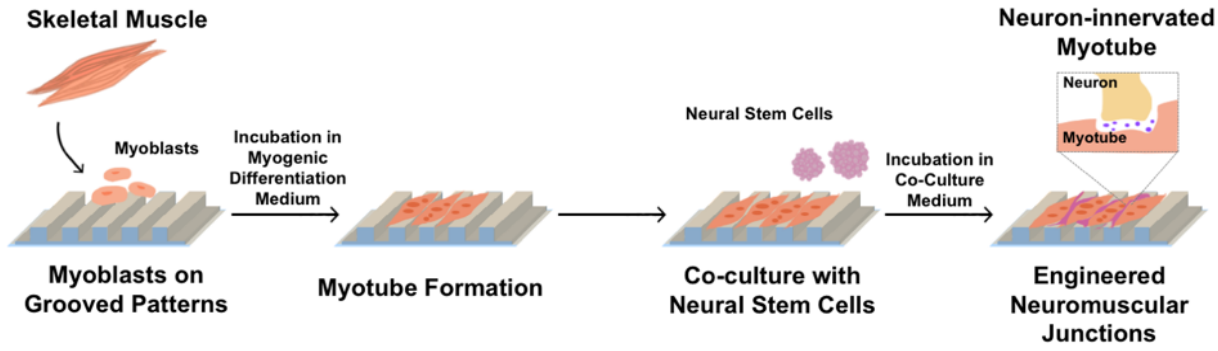

Figure 3.1 Schematic description of engineering the neuromuscular junction through the sequential co-culture of skeletal myoblasts and NSCs on the Matrigel-coated PUA substrates. The substrates were engineered to present grooves with 200, 800, and 1,600 nm width.

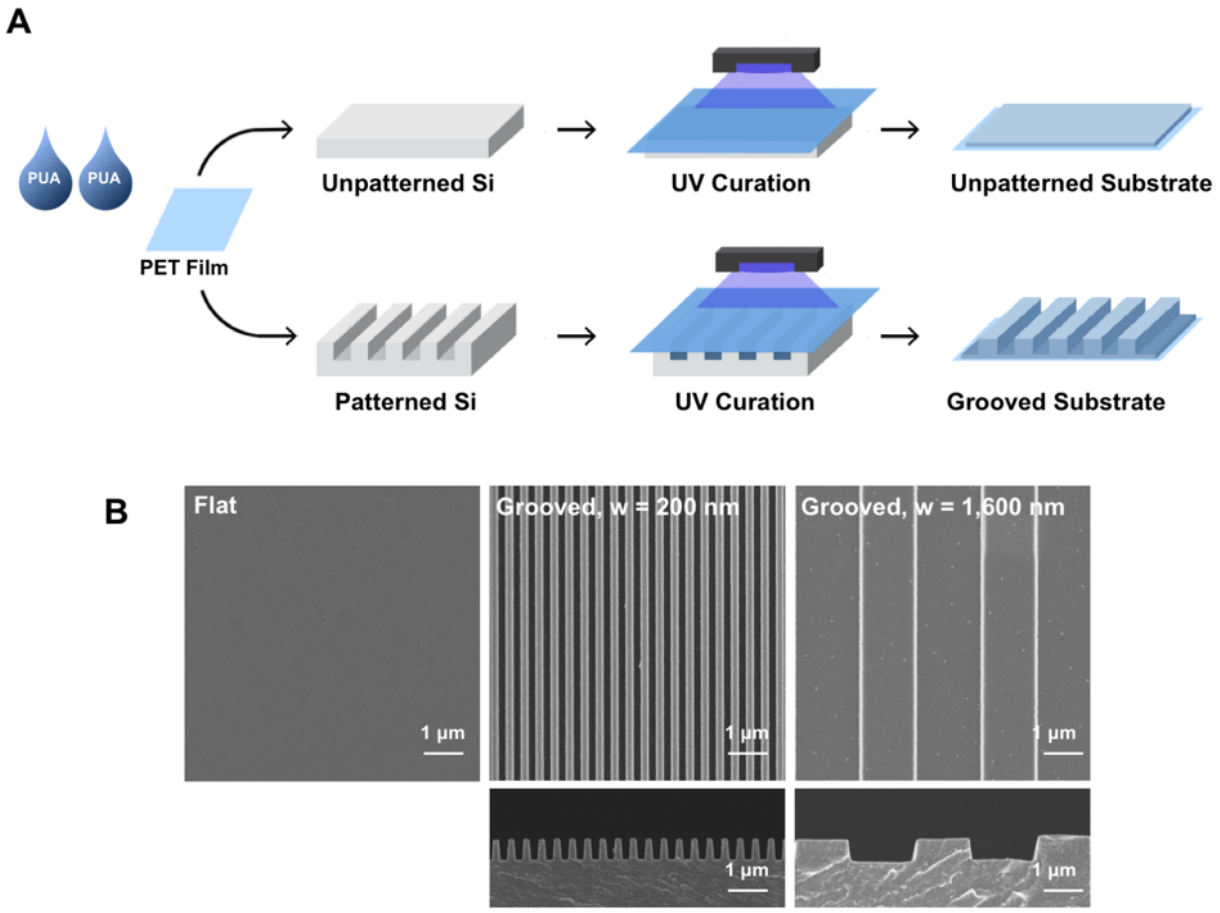

Figure 3.2 Fabrication procedure and analysis of the grooved PUA substrates. (A) Schematic description of the fabrication procedure of the grooved substrates. (B) Scanning electron microscope images of the flat PUA substrate, PUA substrate with 200 nm-groove width (w), and PUA substrate with 1,600 nm-groove width (w). Images in the first and second rows represent the top view and the side view of the substrates, respectively.

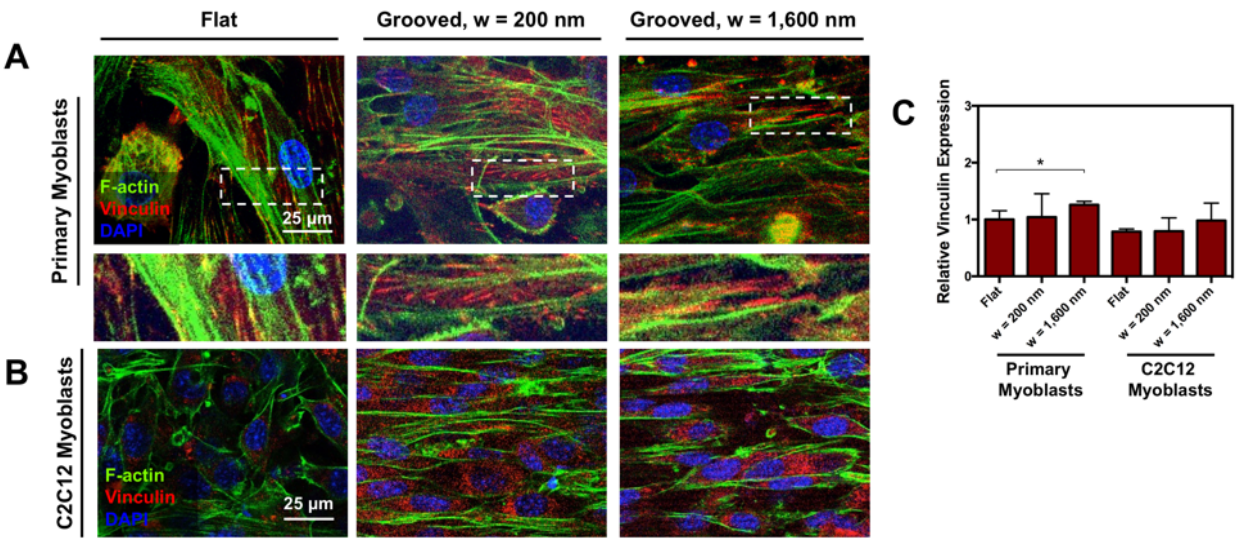

Figure 3.3 Immunofluorescence staining of F-actin (green), vinculin (red), and nucleus (blue) of primary myoblasts (A) and C2C12 myoblasts (B). The images on the second row of A are magnified views of the area boxed in images. Images were captured 3 days after culture. (C) The vinculin expression level quantified with the immunofluorescence images. Each condition was normalized to the vinculin expression value of primary myoblasts adhered to the flat substrate. * represent the statistical significance of the difference of the values between conditions noted in brackets (n=4, *$p < 0.05$)

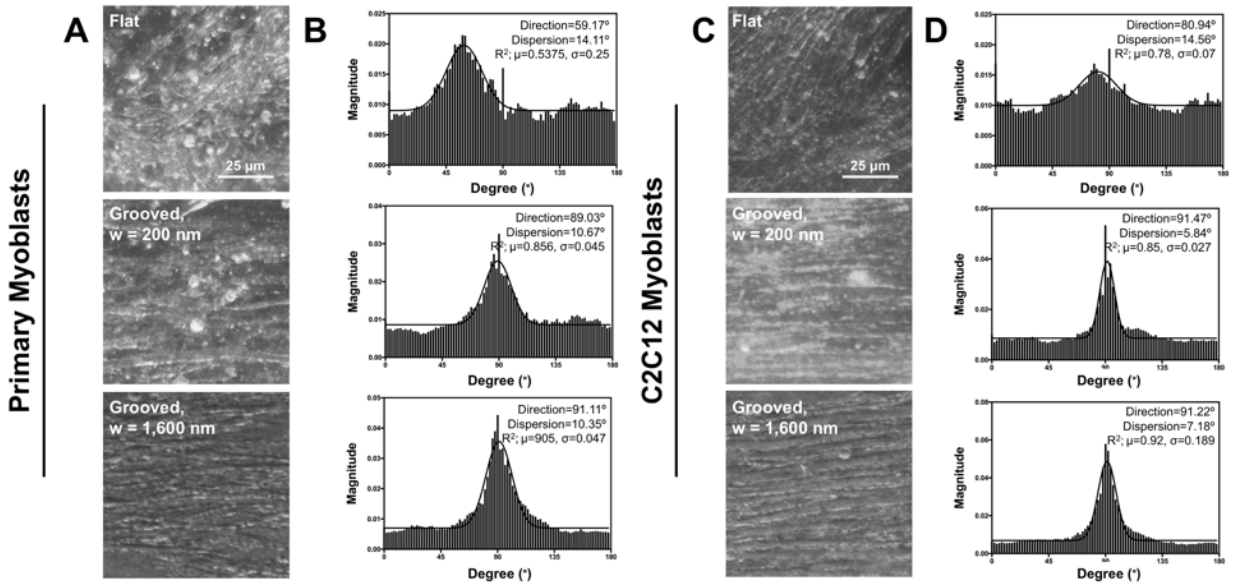

Figure 3.4 Angular orientation analysis of the skeletal myoblasts. The primary myoblasts (A, B) and C2C12 myoblasts (C, D) were cultured for 7 days on the flat substrate, a grooved pattern with 200 nm-width, and grooved pattern with 1,600 nm-width. (A, C) Morphology images of the primary myoblasts and C2C12 myoblasts, respectively. (B, D) Representative histograms of the orientation of primary myoblasts and C2C12 myoblasts. The average value of goodness of fit (R^2) is indicated as μ, and the standard deviation is indicated as σ (n=4).

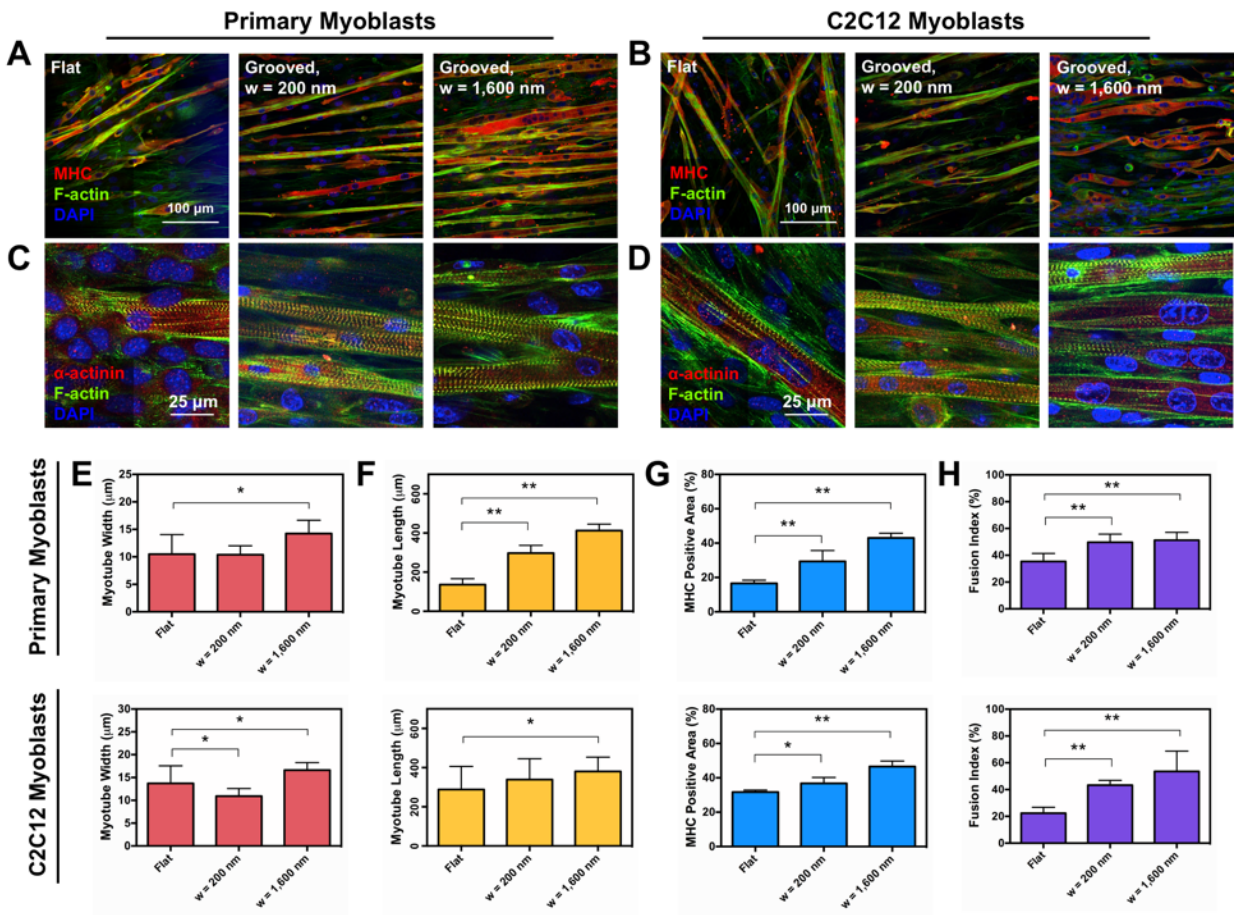

Figure 3.5 Analysis of the myogenic differentiation of skeletal myoblasts. (A, B) Immunofluorescence images of the MHC (red), F-actin (green), and nucleus (blue) in the differentiated primary myoblasts (A) and C2C12 myoblasts (B) taken after 10 days of culture in myogenic differentiation medium. (C, D) Immunofluorescence images of the sarcomeric α-actinin (red), F-actin (green), and nucleus (blue) in the differentiated primary myoblasts (C) and C2C12 myoblasts (D) taken after 10 days of culture in myogenic differentiation medium. (E-H) Morphometric analysis of the differentiated skeletal myoblasts based on the immunofluorescence images. The myotube width (E), myotube lengths (F), MHC-positive area (G), and fusion index (H) were quantitatively examined. In each plot, * and ** represent the statistical significance of the difference of the values between conditions noted in brackets (n=4, *$p < 0.01$, **$p < 0.05$).

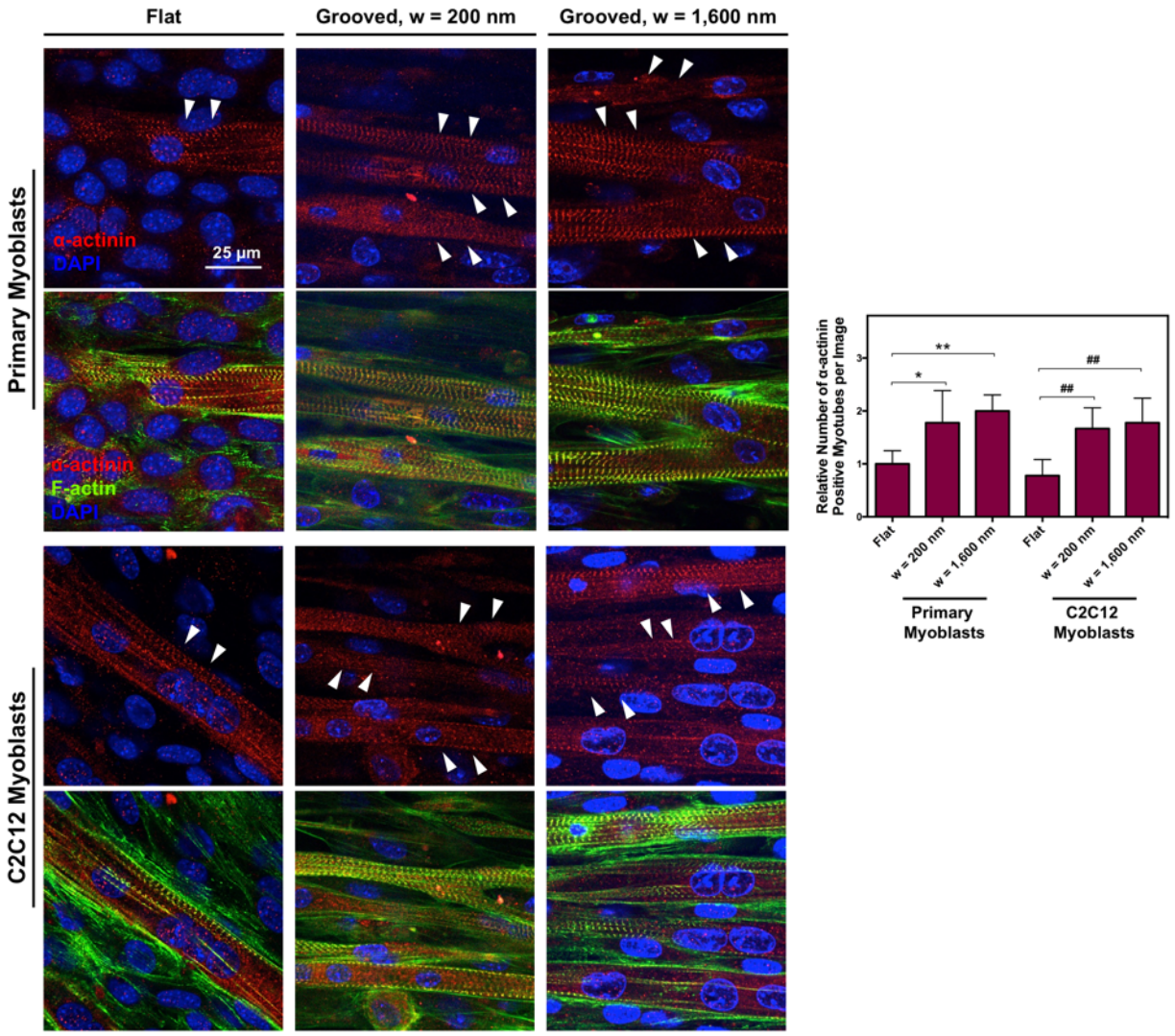

Figure 3.6 Immunofluorescence staining of sarcomeric α-actinin (red), F-actin (green), and nucleus (blue) of primary myoblasts and C2C12 myoblasts. Images were captured 10 days after culture. The graph represents the relative number of α-actinin positive myotubes per image. * and ** represent the statistical significance of the difference of the values between conditions noted in brackets (n=4, *$p < 0.05$).

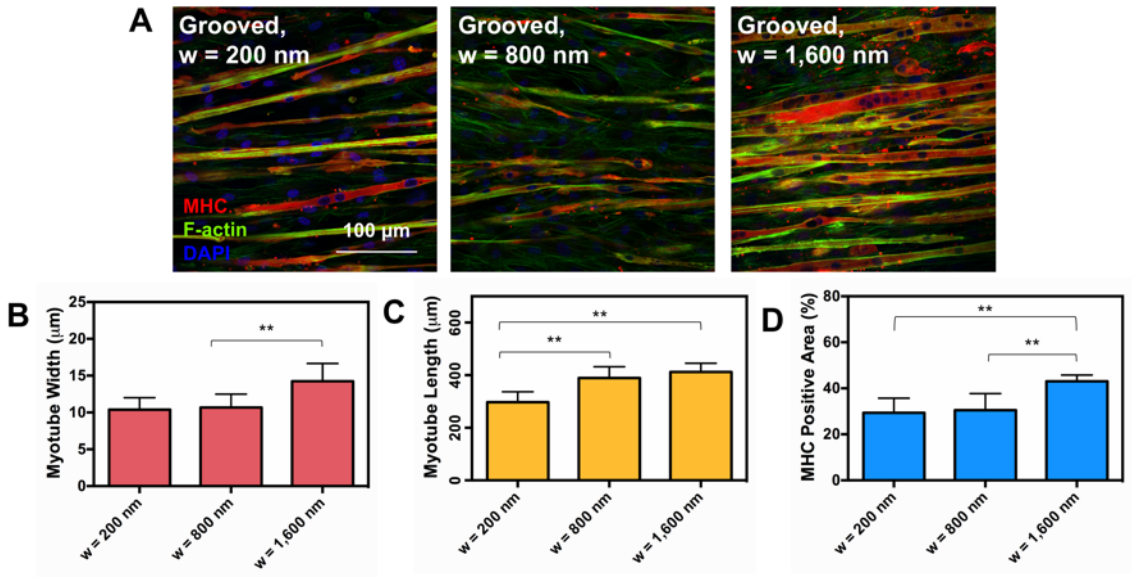

Figure 3.7 Analysis of the myogenic differentiation of primary skeletal myoblasts cultured on substrates with different groove widths. (A) Immunofluorescence images of the MHC (red), F-actin (green), and nucleus (blue) of myoblasts. Images were taken after 10 days of culture in differentiation medium. (B-E) Morphometric analysis of the differentiated skeletal myoblasts based on the immunofluorescence images. The myotube width (B), myotube lengths (C), MHC-positive area (D) were examined quantitatively. In each plot, * and ** represent the statistical significance of the difference of the values between conditions noted in brackets (n=4, *$p < 0.01$, **$p < 0.05$).

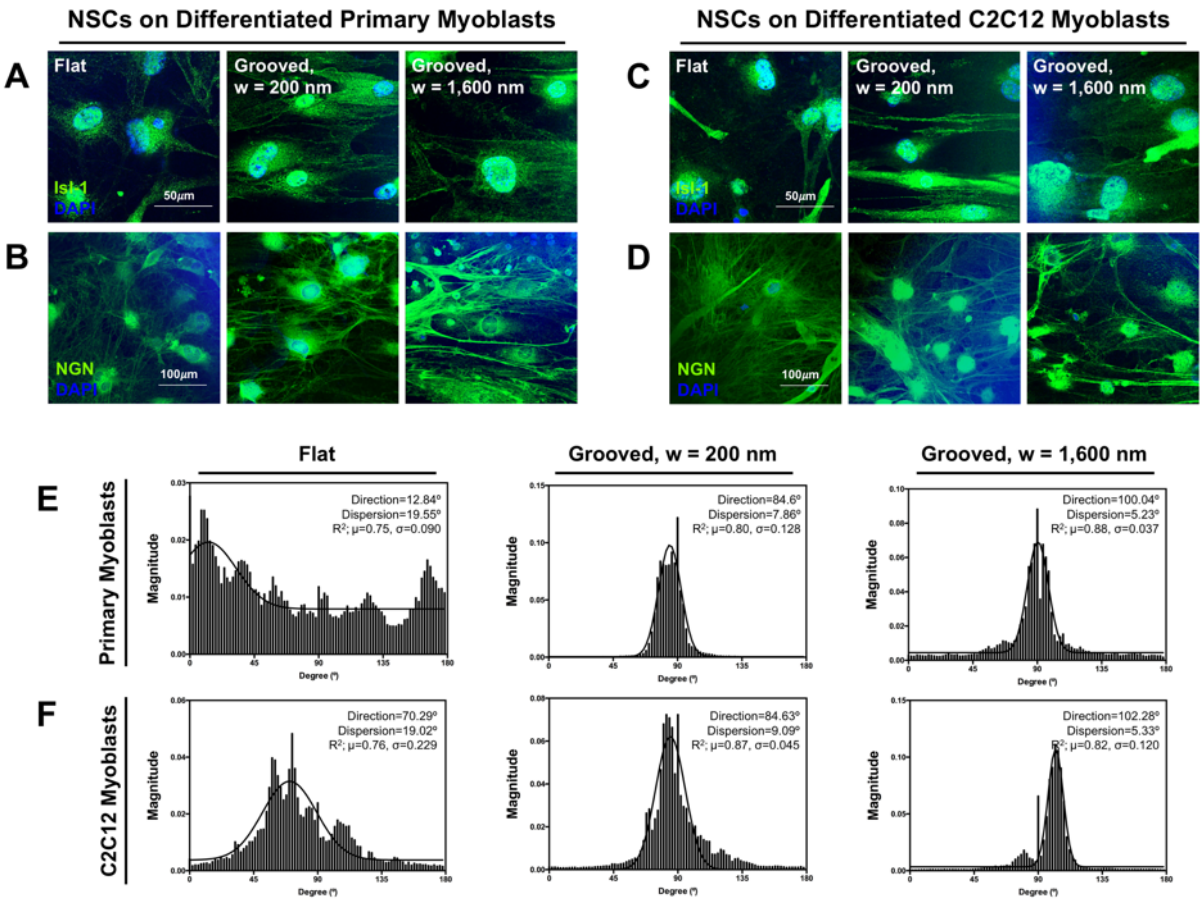

Figure 3.8 Analysis of the differentiation and alignment of NSCs cultured on the myotubes. Immunofluorescence images of the differentiated NSCs on the myotubes formed with primary myoblasts (A, B) and C2C12 myoblasts (C, D). NSCs were stained positively for islet-1 (Isl-1, green in A, C), neurogenin-2 (NGN, green in B, D), and nucleus (blue) after 5 days of culture in the neural differentiation medium. Representative histogram showing the angular orientation of the differentiated NSCs on myotubes formed with primary myoblasts (E) and C2C12 myoblasts (F). The average value of goodness of fit (R^2) is indicated as μ, and the standard deviation is indicated as σ (n=4).

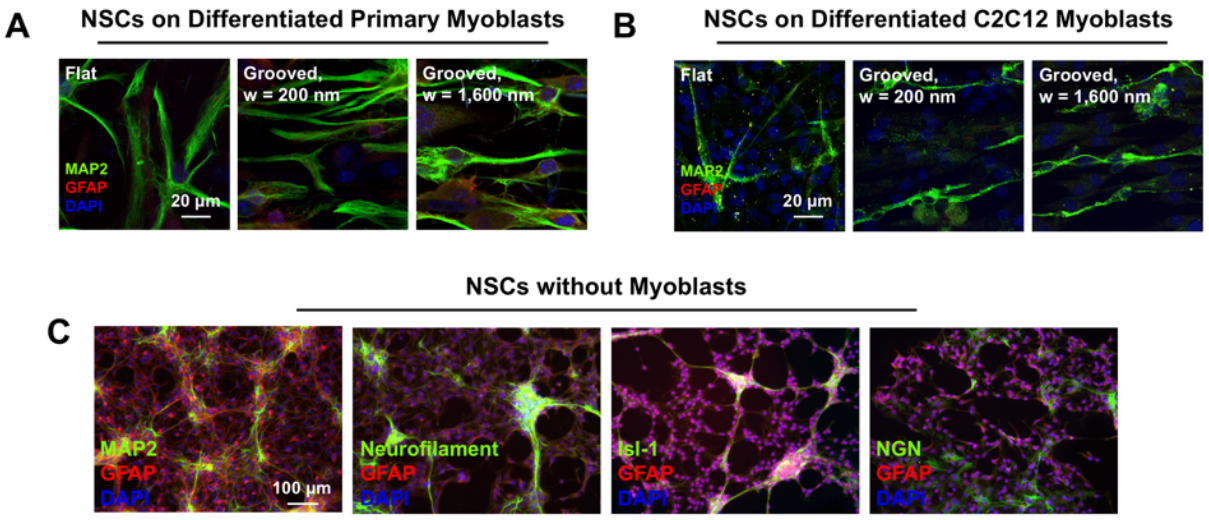

Figure 3.9 Differentiated NSCs on the myotubes formed with primary myoblasts (A), C2C12 myoblasts (B), and without myoblasts (C). In (A) and (B), the cells were labeled with MAP2 (green), GFAP (red), and nucleus (blue). In (C), the cells were labeled with MAP2 (green), neurofilament (green), islet-1 (Isl-1, green), GFAP (red), and nucleus (blue) after 5 days of culture in the neural differentiation medium.

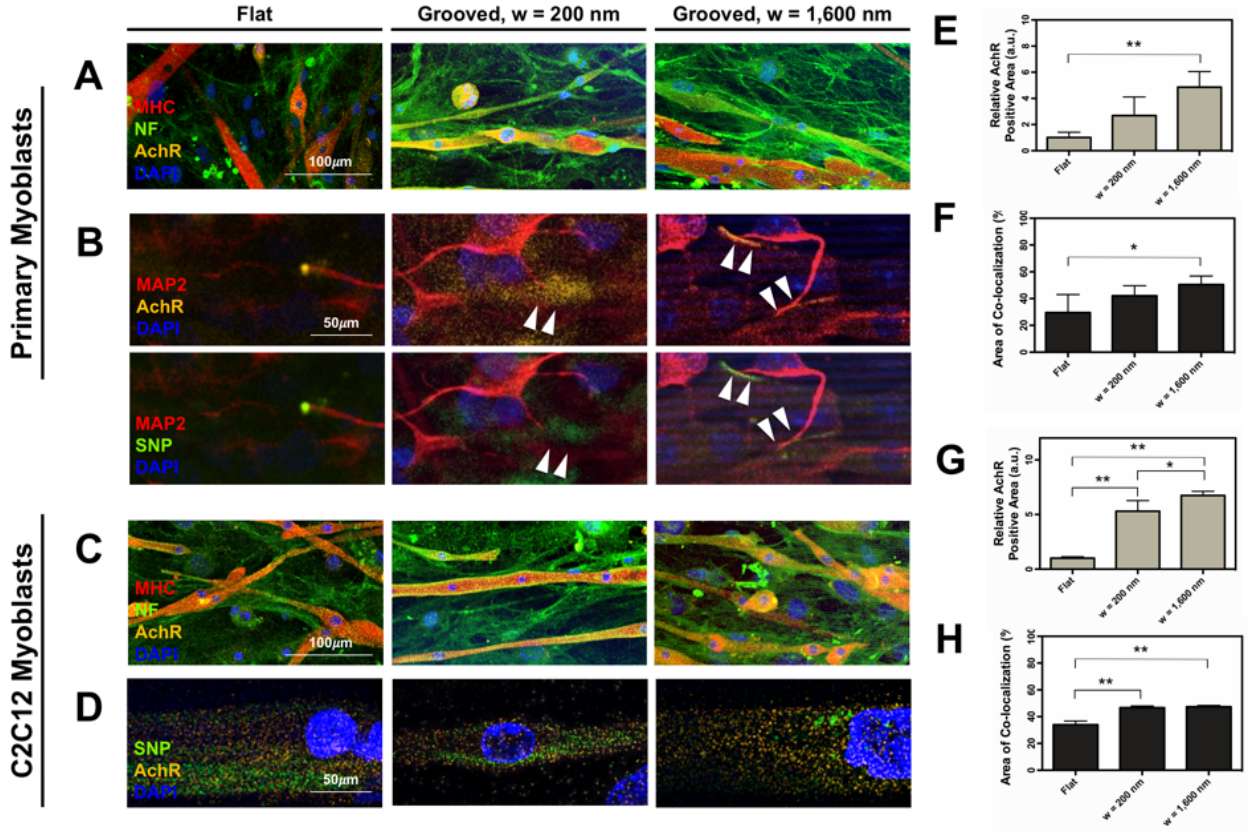

Figure 3.10 Immunocytochemistry of the neuron-innervated myotubes. Images were captured after the co-culture of primary myoblasts and C2C12 myoblasts with NSCs for 7 days. (A, C) Myotubes and neurons stained for MHC (red), neurofilament (NF, green), acetylcholine receptors (AchR, orange), and nucleus (blue). (B, D) Myotubes and neurons stained for synaptophysin (SNP, green), acetylcholine receptors (AchR, orange), and nucleus (blue). The motor neuron progenitor cells were additionally labeled with MAP2 (red) (B). (E, G) Quantified acetylcholine receptor expression levels (n=4, *$p < 0.01$, **$p < 0.05$). The relative acetylcholine receptor expression level was calculated by counting the number of pixels stained positively for acetylcholine receptors in each image and normalizing it to the number obtained with the flat substrate condition. (F, H) Average percentage of area where neurofilaments and acetylcholine receptors are co-localized in the myotubes (n=4, *$p < 0.01$, **$p < 0.05$). Images of (A), (B) and graphs of (C), (D) are the results for primary myoblasts-derived myotubes. Images of (C), (D) and graphs of (G), (H) are the results for C2C12 myoblasts-derived myotubes.

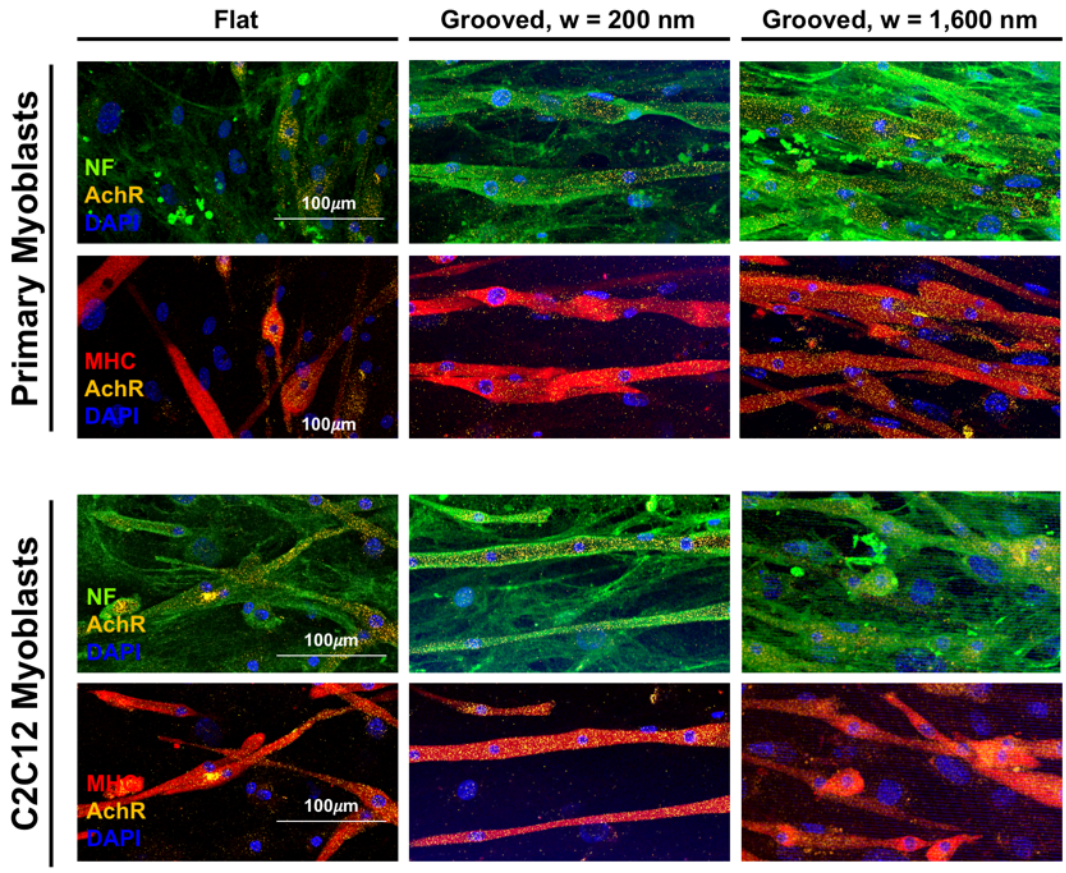

Figure 3.11 Immunocytochemistry of the neuron-innervated myotubes. Images were captured after the co-culture of primary myoblasts and C2C12 myoblasts with NSCs for 7 days. These images are the same images from Figure 10A-C showing separated channel images.

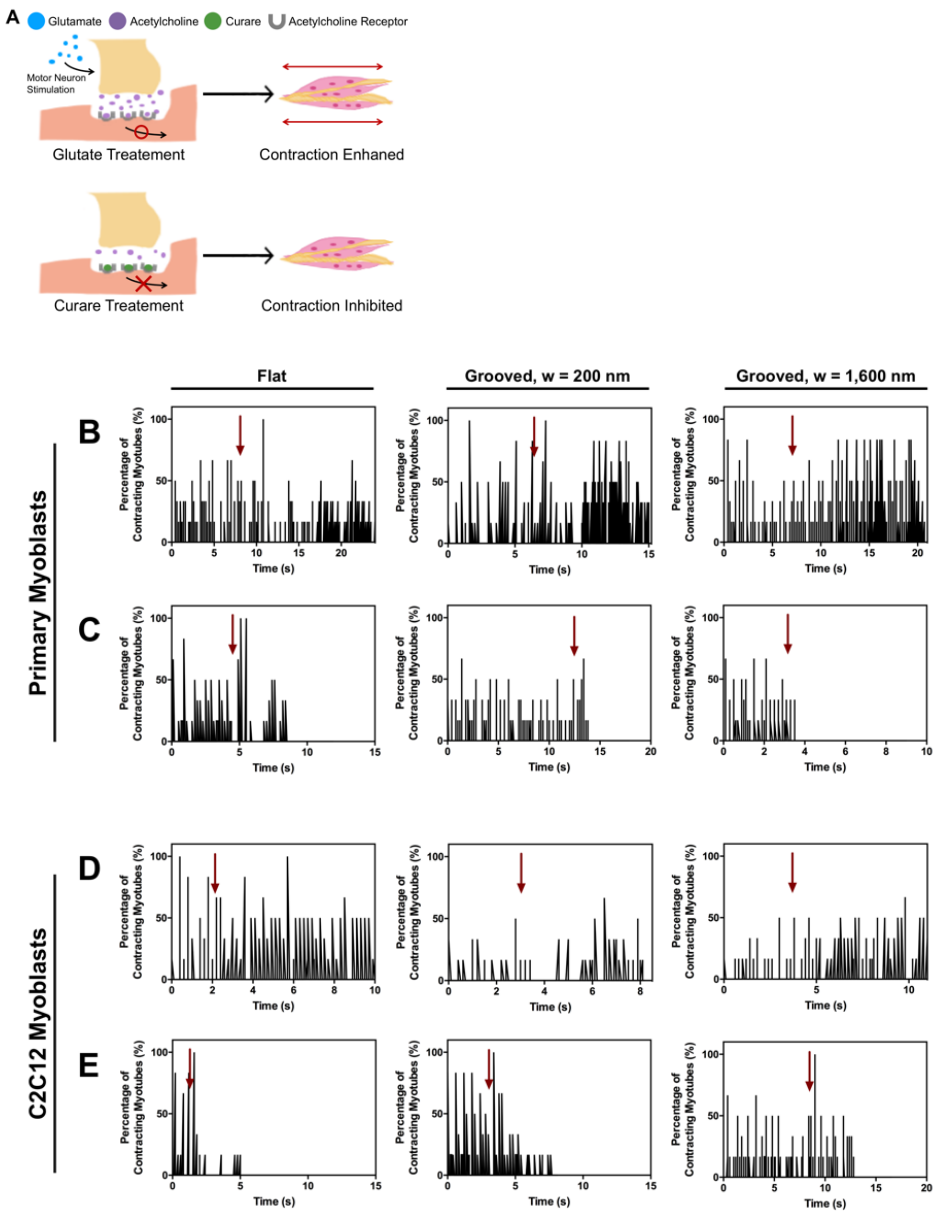

Figure 3.12 Functionality analysis of the neuron-innervated myotubes. (A) Schematic description of the increased contraction of neuron-innervated muscle by glutamate and the inhibited contraction by curare. (B) Triggered contraction of the primary myoblast-derived myotubes with the addition of glutamate. (C) Inhibited contraction of the primary myoblast-derived myotubes upon exposure to curare. (D) Triggered contraction of the C2C12 myoblast-derived myotubes with the addition of glutamate. (E) Inhibited contraction of the C2C12 myoblast-derived myotubes upon exposure to curare. In (B) and (D), arrows indicate the time point when glutamate was added. In (C) and (E), arrows indicate the time point when curare was added.

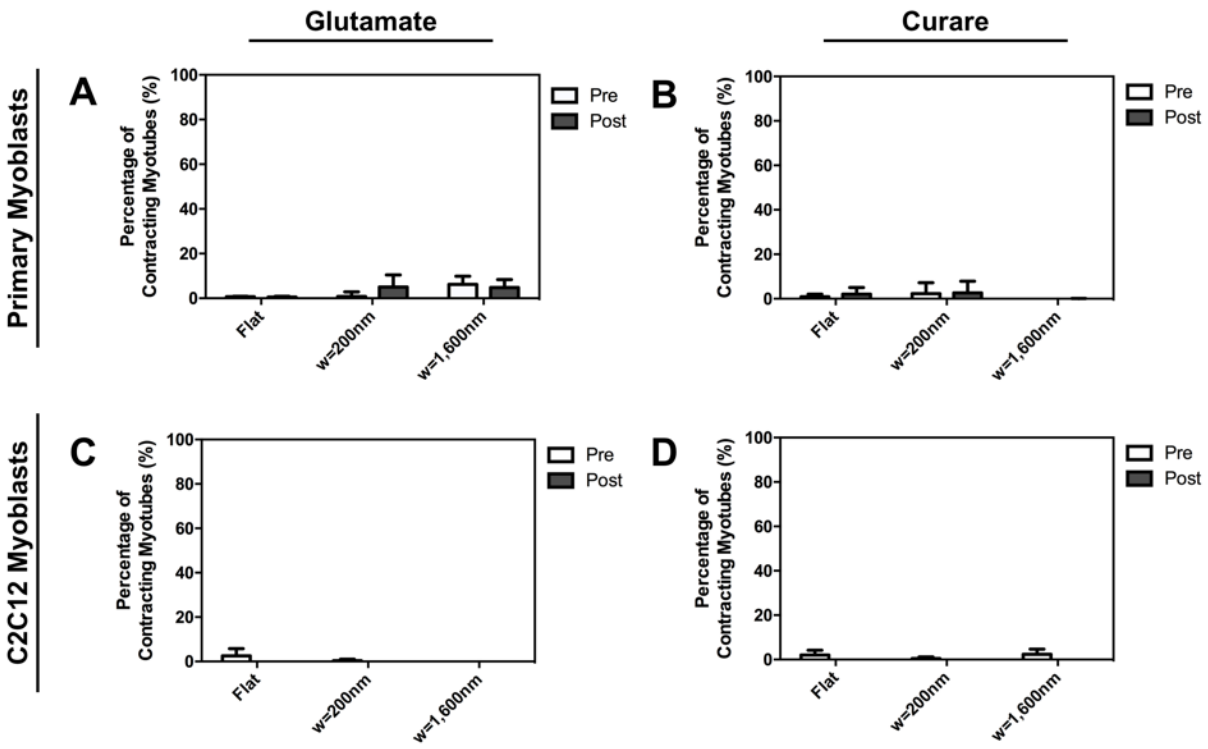

Figure 3.13 Functionality analysis of myotubes without motor neuron progenitor cell innervation. (A) Contraction change of the primary myoblast-derived myotubes with the addition of glutamate. (B) Contraction change of the primary myoblast-derived myotubes upon exposure to curare. (D) Contraction change of the C2C12 myoblast-derived myotubes with the addition of glutamate. (E) Contraction change of the C2C12 myoblast-derived myotubes upon exposure to curare (n=6).

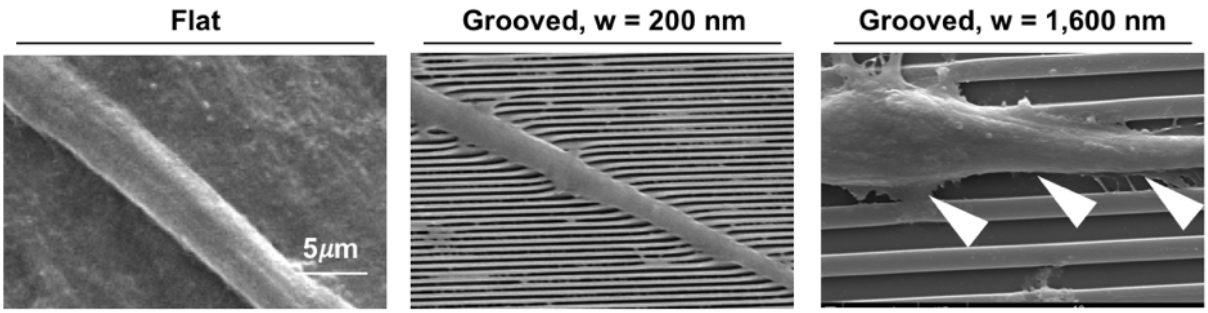

Figure 3.14 Scanning electron microscope images of the primary myoblasts-derived myotubes on flat and grooved substrates. Arrows indicate the sites where the cell membrane was protruded.

Figure Number	Cell Type	Groove Width	Added Chemical	Response Time	Result
Figure 3.12B-Flat-Primary Myoblasts	Primary Myoblasts	Flat	Glutamate	7 seconds	Triggered Contraction
Figure 3.12B-200-Primary Myoblasts	Primary Myoblasts	200 nm	Glutamate	7 seconds	Triggered Contraction
Figure 3.12B-1,600-Primary Myoblasts	Primary Myoblasts	1,600 nm	Glutamate	7 seconds	Triggered Contraction
Figure 3.12C-Flat-Primary Myoblasts	Primary Myoblasts	Flat	Curare	4 seconds	Inhibited Contraction
Figure 3.12C-200-Primary Myoblasts	Primary Myoblasts	200 nm	Curare	12 seconds	Inhibited Contraction
Figure 3.12C-1,600-Primary Myoblasts	Primary Myoblasts	1,600 nm	Curare	3 seconds	Inhibited Contraction
Figure 3.12D-Flat-C2C12 Myoblasts	C2C12 Myoblasts	Flat	Glutamate	2 seconds	Triggered Contraction
Figure 3.12D-200-C2C12 Myoblasts	C2C12 Myoblasts	200 nm	Glutamate	3 seconds	Triggered Contraction
Figure 3.12D-1,600-C2C12 Myoblasts	C2C12 Myoblasts	1,600 nm	Glutamate	4 seconds	Triggered Contraction
Figure 3.12E-Flat-C2C12 Myoblasts	C2C12 Myoblasts	Flat	Curare	2 seconds	Inhibited Contraction
Figure 3.12E-200-C2C12 Myoblasts	C2C12 Myoblasts	200 nm	Curare	4 seconds	Inhibited Contraction
Figure 3.12E-1,600-C2C12 Myoblasts	C2C12 Myoblasts	1,600 nm	Curare	8 seconds	Inhibited Contraction

Table 3.1. Description of the movies which correspond to Figure 3.12 B-E.

3.6 References

1. Wu, H.; Xiong, W. C.; Mei, L., To Build a Synapse: Signaling Pathways in Neuromuscular Junction Assembly. *Development* **2010,** *137* (7), 1017-1033.

2. Witzemann, V., Development of the Neuromuscular Junction. *Cell Tissue Res.* **2006,** *326* (2), 263-271.

3. Gilhus, N. E., Myasthenia and the Neuromuscular Junction. *Current opinion in neurology* **2012,** *25* (5), 523-529.

4. Murray, L.; Talbot, K.; Gillingwater, T., Review: Neuromuscular Synaptic Vulnerability in Motor Neurone Disease: Amyotrophic Lateral Sclerosis and Spinal Muscular Atrophy. *Neuropathol. Appl. Neurobiol.* **2010,** *36* (2), 133-156.

5. McConville, J.; Vincent, A., Diseases of the Neuromuscular Junction. *Current opinion in pharmacology* **2002,** *2* (3), 296-301.

6. Zahavi, E. E.; Ionescu, A.; Gluska, S.; Gradus, T.; Ben-Yaakov, K.; Perlson, E., A Compartmentalized Microfluidic Neuromuscular Co-Culture System Reveals Spatial Aspects of Gdnf Functions. *J Cell Sci* **2015,** *128* (6), 1241-1252.

7. Uzel, S. G.; Platt, R. J.; Subramanian, V.; Pearl, T. M.; Rowlands, C. J.; Chan, V.; Boyer, L. A.; So, P. T.; Kamm, R. D., Microfluidic Device for the Formation of Optically Excitable, Three-Dimensional, Compartmentalized Motor Units. *Science Advances* **2016,** *2* (8), e1501429.

8. Daniels, M. P.; Lowe, B. T.; Shah, S.; Ma, J.; Samuelsson, S. J.; Lugo, B.; Parakh, T.; Uhm, C. S., Rodent Nerve-Muscle Cell Culture System for Studies of Neuromuscular Junction Development: Refinements and Applications. *Microsc. Res. Tech.* **2000,** *49* (1), 26-37.

9. Das, M.; Rumsey, J.; Gregory, C.; Bhargava, N.; Kang, J.-F.; Molnar, P.; Riedel, L.; Guo, X.; Hickman, J., Embryonic Motoneuron-Skeletal Muscle Co-Culture in a Defined System. *Neuroscience* **2007,** *146* (2), 481-488.

10. Morimoto, Y.; Kato-Negishi, M.; Onoe, H.; Takeuchi, S., Three-Dimensional Neuron–Muscle Constructs with Neuromuscular Junctions. *Biomaterials* **2013,** *34* (37), 9413-9419.

11. Lin, W.; Burgess, R. W.; Dominguez, B.; Pfaff, S. L.; Sanes, J. R.; Lee, K.-F., Distinct Roles of Nerve and Muscle in Postsynaptic Differentiation of the Neuromuscular Synapse. *Nature* **2001,** *410* (6832), 1057-1064.

12. Yang, X.; Arber, S.; William, C.; Li, L.; Tanabe, Y.; Jessell, T. M.; Birchmeier, C.; Burden, S. J., Patterning of Muscle Acetylcholine Receptor Gene Expression in the Absence of Motor Innervation. *Neuron* **2001,** *30* (2), 399-410.

13. Reist, N. E.; Werle, M. J.; McMahan, U., Agrin Released by Motor Neurons Induces the Aggregation of Acetylcholine Receptors at Neuromuscular Junctions. *Neuron* **1992,** *8* (5), 865-868.

14. Wallace, B. G.; Zhican, Q.; Richard, H. L., Agrin Induces Phosphorylation of the Nicotinic Acetylcholine Receptor. *Neuron* **1991,** *6* (6), 869-878.

15. Leung, A.; Hwang, J.; Cheung, Y., Determination of Myofibrillar Diameter by Light Diffractometry. *Pflügers Archiv European Journal of Physiology* **1983,** *396* (3), 238-242.

16. Ma, P. X.; Zhang, R., Synthetic Nano-Scale Fibrous Extracellular Matrix. *J Biomed Mater Res* **1999,** *46* (1), 60-72.

17. Yang, H. S.; Lee, B.; Tsui, J. H.; Macadangdang, J.; Jang, S. Y.; Im, S. G.; Kim, D. H., Electroconductive Nanopatterned Substrates for Enhanced Myogenic Differentiation and Maturation. *ADV. Healthc. Mater.* **2016,** *5* (1), 137-145.

18. Gillies, A. R.; Lieber, R. L., Structure and Function of the Skeletal Muscle Extracellular Matrix. *Muscle Nerve* **2011,** *44* (3), 318-331.

19. Hinds, S.; Bian, W.; Dennis, R. G.; Bursac, N., The Role of Extracellular Matrix Composition in Structure and Function of Bioengineered Skeletal Muscle. *Biomaterials* **2011,** *32* (14), 3575-3583.

20. Teo, B. K. K.; Wong, S. T.; Lim, C. K.; Kung, T. Y.; Yap, C. H.; Ramagopal, Y.; Romer, L. H.; Yim, E. K., Nanotopography Modulates Mechanotransduction of Stem Cells and Induces Differentiation through Focal Adhesion Kinase. *ACS Nano* **2013,** *7* (6), 4785-4798.

21. Ahadian, S.; Ramón-Azcón, J.; Ostrovidov, S.; Camci-Unal, G.; Hosseini, V.; Kaji, H.; Ino, K.; Shiku, H.; Khademhosseini, A.; Matsue, T., Interdigitated Array of Pt Electrodes for Electrical Stimulation and Engineering of Aligned Muscle Tissue. *Lab on a Chip* **2012,** *12* (18), 3491-3503.

22. O'Brien, L. C.; Keeney, P. M.; Bennett Jr, J. P., Differentiation of Human Neural Stem Cells into Motor Neurons Stimulates Mitochondrial Biogenesis and Decreases Glycolytic Flux. *Stem cells and development* **2015,** *24* (17), 1984-1994.

23. Lee, H. J.; Kim, K. S.; Ahn, J.; Bae, H. M.; Lim, I.; Kim, S. U., Human Motor Neurons Generated from Neural Stem Cells Delay Clinical Onset and Prolong Life in Als Mouse Model. *PloS one* **2014,** *9* (5), e97518.

24. Itoh, Y.; Moriyama, Y.; Hasegawa, T.; Endo, T. A.; Toyoda, T.; Gotoh, Y., Scratch Regulates Neuronal Migration Onset Via an Epithelial-Mesenchymal Transition-Like Mechanism. *Nat. Neurosci.* **2013,** *16* (4), 416-425.

25. Ma, Y.-C.; Song, M.-R.; Park, J. P.; Ho, H.-Y. H.; Hu, L.; Kurtev, M. V.; Zieg, J.; Ma, Q.; Pfaff, S. L.; Greenberg, M. E., Regulation of Motor Neuron Specification by Phosphorylation of Neurogenin 2. *Neuron* **2008,** *58* (1), 65-77.

26. Mizuguchi, R.; Sugimori, M.; Takebayashi, H.; Kosako, H.; Nagao, M.; Yoshida, S.; Nabeshima, Y.-i.; Shimamura, K.; Nakafuku, M., Combinatorial Roles of Olig2 and Neurogenin2 in the Coordinated Induction of Pan-Neuronal and Subtype-Specific Properties of Motoneurons. *Neuron* **2001,** *31* (5), 757-771.

27. Novitch, B. G.; Chen, A. I.; Jessell, T. M., Coordinate Regulation of Motor Neuron Subtype Identity and Pan-Neuronal Properties by the Bhlh Repressor Olig2. *Neuron* **2001,** *31* (5), 773-789.

28. Qu, Q.; Li, D.; Louis, K. R.; Li, X.; Yang, H.; Sun, Q.; Crandall, S. R.; Tsang, S.; Zhou, J.; Cox, C. L., High-Efficiency Motor Neuron Differentiation from Human Pluripotent Stem Cells and the Function of Islet-1. *Nat. Comm.* **2014,** *5*, 3449.

29. Yang, K.; Jung, K.; Ko, E.; Kim, J.; Park, K. I.; Kim, J.; Cho, S.-W., Nanotopographical Manipulation of Focal Adhesion Formation for Enhanced Differentiation of Human Neural Stem Cells. *ACS Appl. Mater. Interfaces* **2013,** *5* (21), 10529-10540.

30. Yang, K.; Park, E.; Lee, J. S.; Kim, I. S.; Hong, K.; Park, K. I.; Cho, S. W.; Yang, H. S., Biodegradable Nanotopography Combined with Neurotrophic Signals Enhances Contact Guidance and Neuronal Differentiation of Human Neural Stem Cells. *Macromol. Biosci.* **2015,** *15* (10), 1348-1356.

31. Martínez, E.; Engel, E.; López-Iglesias, C.; Mills, C. A.; Planell, J.; Samitier, J., Focused Ion Beam/Scanning Electron Microscopy Characterization of Cell Behavior on Polymer Micro-/Nanopatterned Substrates: A Study of Cell–Substrate Interactions. *Micron* **2008,** *39* (2), 111-116.

32. Takarada, T.; Nakamichi, N.; Kitajima, S.; Fukumori, R.; Nakazato, R.; Le, N. Q.; Kim, Y.-H.; Fujikawa, K.; Kou, M.; Yoneda, Y., Promoted Neuronal Differentiation after Activation of Alpha4/Beta2 Nicotinic Acetylcholine Receptors in Undifferentiated Neural Progenitors. *PLoS One* **2012,** *7* (10), e46177.

33. Tovar-y-Romo, L. B.; Ramírez-Jarquín, U. N.; Lazo-Gómez, R.; Tapia, R., Trophic Factors as Modulators of Motor Neuron Physiology and Survival: Implications for Als Therapy. *Front. Cell. Neurosci.* **2014,** *8*, 61.

34. Kablar, B.; Belliveau, A. C., Presence of Neurotrophic Factors in Skeletal Muscle Correlates with Survival of Spinal Cord Motor Neurons. *Developmental dynamics* **2005,** *234* (3), 659-669.

35. Witzemann, V.; Chevessier, F.; Pacifici, P. G.; Yampolsky, P., The Neuromuscular Junction: Selective Remodeling of Synaptic Regulators at the Nerve/Muscle Interface. *Mechanisms of development* **2013,** *130* (6), 402-411.

36. Gautam, M.; Noakes, P. G.; Moscoso, L.; Rupp, F.; Scheller, R. H.; Merlie, J. P.; Sanes, J. R., Defective Neuromuscular Synaptogenesis in Agrin-Deficient Mutant Mice. *Cell* **1996,** *85* (4), 525-535.

37. Hesser, B. A.; Henschel, O.; Witzemann, V., Synapse Disassembly and Formation of New Synapses in Postnatal Muscle Upon Conditional Inactivation of Musk. *Molecular and Cellular Neuroscience* **2006,** *31* (3), 470-480.

38. Brandon, E. P.; Lin, W.; D'Amour, K. A.; Pizzo, D. P.; Dominguez, B.; Sugiura, Y.; Thode, S.; Ko, C.-P.; Thal, L. J.; Gage, F. H., Aberrant Patterning of Neuromuscular Synapses in Choline Acetyltransferase-Deficient Mice. *J. Neurosci.* **2003,** *23* (2), 539-549.

39. Raman, R.; Cvetkovic, C.; Uzel, S. G.; Platt, R. J.; Sengupta, P.; Kamm, R. D.; Bashir, R., Optogenetic Skeletal Muscle-Powered Adaptive Biological Machines. *Proceedings of the National Academy of Sciences* **2016,** *113* (13), 3497-3502.

40. Cvetkovic, C.; Raman, R.; Chan, V.; Williams, B. J.; Tolish, M.; Bajaj, P.; Sakar, M. S.; Asada, H. H.; Saif, M. T. A.; Bashir, R., Three-Dimensionally Printed Biological Machines Powered by Skeletal Muscle. *Proceedings of the National Academy of Sciences* **2014,** *111* (28), 10125-10130.

41. Cvetkovic, C.; Rich, M.; Raman, R.; Kong, H.; Bashir, R., A 3d Printed Platform for Modular Neuromuscular Motor

Units. *Microsyst. Nanoeng.* **2017,** *3* (17015).

42. Lawson, M. A.; Purslow, P. P., Differentiation of Myoblasts in Serum-Free Media: Effects of Modified Media Are Cell Line-Specific. *Cells Tissues Organs* **2000,** *167* (2-3), 130-137.

43. Pagan-Diaz, G. J.; Zhang, X.; Grant, L.; Kim, Y.; Aydin, O.; Cvetkovic, C.; Ko, E.; Solomon, E.; Hollis, J.; Kong, H., Simulation and Fabrication of Stronger, Larger, and Faster Walking Biohybrid Machines. *Adv. Funct. Mater.* **2018,** *28* (23), 1801145.

CHAPTER 4: STRATEGY TO REGULATE GAP JUNCTION PROTEIN EXPRESSION FOR MATURE MUSCLE DEVELOPMENT AND IMPROVED PUMP-BOT FUNCTION

Acknowledgments

Research in this chapter was conducted through collaborative efforts. The qRT-PCR was conducted by Lauren Grant and the RNA sequencing data was collected with help of Dr. Alvaro G. Hernandez, Dr. Chris L. Wright, Dr. Christopher J. Fields, and Jenny Drnevich. I would like to thank Onur Aydin for his help in measuring and analyzing the pump-bot experiment and Dr. Zhengwei Li for providing the platform.

4.1 Introduction

Skeletal muscle tissue comprises 40% of the body mass and is responsible for locomotion and actuation.[1] Damaged tissue or loss in muscle function cause the patients to experience pain, disability, and sometimes, death.[2, 3] Due to its significant role in the *in vivo* system, extensive *in vitro* studies to regenerate the skeletal muscle have been performed. These studies include creating drug screening devices,[3, 4] developing methodologies to recapitulate the natural muscle tissue[5, 6] and engineering 3D skeletal muscle tissue.[7-9] Engineering muscle tissue in 3D has emerged a useful technique due to its potential applications. For example, a 3D engineered muscle can actuate bio-inspired devices or transplanted to an *in vivo* model.[9-11] To reconstruct the tissue *in vitro*, the engineered muscle must recapitulate the morphological property of the natural tissue and produce enough force. Particularly, force production is a significant factor since it directly relates to the functionality of skeletal muscle. Up to this point, most studies have relied on adding growth factors that promote myotube maturity or performing exercise with the engineered tissue to increase force

production. In addition to these elements, biological changes happening in the myoblasts during differentiation also relates to muscle maturity.

Gap junction proteins connect neighboring cells together allowing exchange of ions and small molecule.[12, 13] During the communication between the adjacent cells, electrical signals as well as interchanging metabolic molecules occur.[14-16] Due to its significant roles in ion exchange and electrical signal transmission, the gap junction proteins, such as connexin 43, are abundant in cardiomyocytes, and skeletal myoblasts.[17, 18] Connexin 43, which propagates action potential signals, are highly expressed in cardiac cells. As the electrical signals are transmitted continuously through these channels, the cardiomyocytes show synchronized contraction. In skeletal myoblasts, however, the connexin 43 proteins are prevalent only during early developmental stage and disappear once the myoblasts fuse together to form myotubes. This is because the muscle fibers are independently innervated by motor neurons to contract.[17, 19]

The role of connexin 43 in skeletal muscle is not clearly revealed. The major function of connexin 43, so far, is known as facilitating the myotube formation during myogenic differentiation.[20-22] Although the exact underlying mechanism is still not well known, reports have shown that myoblasts modified to overexpress connexin 43 forms myotube faster and promote myogenic markers to be expressed in higher extent after differentiation. It also has been reported that overexpression of connexin 43 in rhabdomyosarcoma cells promote gap junctional intercellular communication.[23] The communication between the neighboring cells promoted fusion and myogenesis. Furthermore, the connexin 43 may also contribute to muscle generation since suppression of connexin 43 in osteoblasts in mice damaged skeletal muscle development and resulted in reduce in muscle weight.[24]

Taken together, we hypothesize that extending the expression time of connexin 43 could increase maturity and physiological functionality of engineered skeletal muscle. In particular, delayed downregulation of connexin 43 in myoblasts would contribute to active communication of the differentiating myoblasts during fusion. We cultured C2C12 skeletal myoblasts with ultra-thin, reduced graphene oxide (rGO) flakes which act as glue to increase adhesion of the neighboring cells. (Figure 1). The connexin 43 expression and the maturity of differentiated myotubes were evaluated via immunofluorescence staining and quantitative real time polymerase chain reaction (qRT-PCR) at different time points. Gene sequencing was performed to explore the genetic change occurring at different stages of differentiation. Lastly, we evaluated the contractility of the engineered muscle by operating a biological machine we recently created to control fluid transport in a similar mechanism to an insect's open heart.[25]

4.2 Results and Discussion

4.2.1 Characterization of rGO and Attachment to the C2C12 Myoblasts

Transmission electron microscopy image of the rGO showed micron sized flakes (Figure 4.3 A). The size of the rGO was, in average, 5.37 μm in length and 4.01μm in width. The Raman spectrum of the rGO showed two distinct peaks, known as G band and D band (Figure 4.3 B). As explained above, C2C12 myoblasts used for the experiments were collected on the second day after removing the unattached rGO by centrifugation (Figure 1).

We performed a cytotoxicity test to measure the cytotoxicity of rGO at different concentrations by performing a Tryphan blue assay (Figure 4.5). The relative viability of rGO was measured by comparing the cell number at day 1, 3, 7 and 10. Here, we used 0 μg/ml, 3 μg/ml, 5 μg/ml, and 10 μg/ml rGO dispersed in growth medium. The viability of the C2C12 myoblasts

treated with 3 μg/ml and 5 μg/ml rGO dropped compared to the control group but remained above 70%. The myoblasts treated with 10 μg/ml rGO showed dramatic decrease in viability which dropped to 70% on day 1 and remained between 50 to 55 % on the following days.

Based on the cytotoxicity result, we selected 5 μg/ml concentration to conduct further experiments. We quantified the rGO attached on the myoblasts after removing the unbound rGO and plating the cells on a cell culture dish. As the size of the rGO was in micron scale, the material was visible under an optical microscope (Figure 4.4 A). The total area that rGO occupying in the image was measured to calculate the attachment efficiency (Figure 4.4 B). The total area of rGO in the image was 2012.62 μm^2 in average, which corresponds to 0.83% of the confluent myoblasts.

Treating cells with nanomaterials, such as carbon nanotubes, silver nanowires, as well as graphene, are still controversial because materials under 1 μm size may possibly be internalized by cells.[26, 27] Furthermore, the effects of those materials in the cells are still not well reported. We could avoid the internalization of rGO by using micro scale rGO particle. As shown in our figure (Figure 2D), the particles adhered on the cellular membrane and were visible under a light microscope. Moreover, reduction of cell viability by more than 30% is considered cytotoxic according to the International Organization for Standardization (10993-5). To maximize the effect of rGO while avoiding the cytotoxic effect of rGO, we fixed the concentration of rGO to 5μg/ml for our experiments.

4.2.2 Analysis of Connexin 43 Expression in C2C12 Myoblasts

Connexin 43 expression in C2C12 myoblasts was analyzed by performing immunofluorescence imaging on day 3 (before differentiation), day 7 (early differentiation), and day 14 (terminal differentiation) (Figure 4.6 A). We compared connexin 43 expression in the rGO-

treated C2C12 myoblasts with control C2C12 myoblasts. Connexin 43 (green color) was visible in both groups before differentiation. However, the expression of connexin 43 became lower once we induced differentiation by culturing the cells in differentiation medium. In contrast, rGO-treated C2C12 cells expressed connexin 43 during early differentiation stage. The expression was down-regulated at terminal differentiation stage. This result was confirmed by quantifying the relative mRNA expression level with qRT-PCR (Figure 4.6 B). Relative connexin 43 expression level was measured on day 3, day 7 and day 14. The connexin 43 was 1.2-fold higher on day 3, 1.4-fold higher on day 7, and 1.2-fold higher on day 14. We observed both upregulated connexin 43 mRNA expression and delayed downregulation of connexin 43 mRNA expression with rGO-treated C2C12 myoblasts.

Connexin 43 expression is upregulated in mesenchymal stem cells (MSC) and cardiomyocytes upon treating the cells with rGO.[26, 28] The authors stated that this phenomenon is due to the conductivity of rGO. In addition, rGO has adhesive characteristics to the surrounding proteins and molecules.[29, 30] Therefore, we suggest the conductivity could have contributed to overexpression of connexin 43 on the cellular membrane. Moreover, the adhesive property of rGO would hold the connexin 43 proteins to remain on the cellular membrane longer.

4.2.3 Analysis of Myogenic Differentiation of rGO-Treated C2C12 Myoblasts

The effect of rGO on myogenic differentiation was analyzed by performing immunofluorescence imaging (Figure 4.7) and qRT-PCR (Figure 4.8). The samples were evaluated at 3 different time points; before differentiation, early differentiation, and terminal differentiation. The immunofluorescence images of the myotubes stained for myosin heavy chain (MF20) showed that myotubes formed without rGO showed MF20 expression from early

differentiation stage (Figure 4.7 A, first row). On the other hand, MF20 expression was visible on rGO-treated C2C12 group before differentiation (Figure 4.7 A, second row). The C2C12 myoblasts were stained with F-actin and α-Actinin to observe the attachment on the substrate and confirm that the differentiated myotubes are mature (Figure 4.7 B).

Before differentiation, the C2C12 myoblasts treated with and without rGO showed only F-actin expression. During early differentiation stage, the myotubes showed striation and the F-actin morphology became elongated. The maturity and differentiation level were confirmed again with qRT-PCR (Figure 4.8). We compared different myogenic markers at different time points using desmin (DES), myostatin (MSTN), myogenic factor 5 (MYF5), myogenic factor 5 (MYF5), myoblast determination protein (MYOD), myogenin (MYOG), troponin I (TNNI), and myosin heavy chain 1 (MHC1). These markers include early stage myogenic markers (DES, MYF5, and MYOD), mid stage differentiation marker (MYOG), and late stage differentiation marker (MYH1). As a result, MYF5 (1.38-fold change), MYOD (1.36-fold change), and MYH1 (1.31-fold change) showed significant increase on day 3 upon rGO treatment. Other markers showed slight increase in expression level. On day 7, MYOD (1.30-fold change) and MYOG (1.37-fold change) showed significant increase in mRNA expression level. Although the MYH1 expression was slightly decreased, there was no statistical significance. Lastly, on day 14, MYF5 and MYOD showed 1.24-fold change and 1.47-fold change, respectively.

According to the immunofluorescence images, the rGO-treated C2C12 myoblasts showed myosin heavy chain expression on day 3. However, we could not observe the striated myotubes. This result addresses that the presence of rGO facilitates myogenic differentiation in early stage but the myotubes need more time to become mature myotubes. In addition, since rGO enhanced connexin 43 expression at early differentiation stage, higher expression of the connexin 43 protein

could have caused the cells to differentiate more actively.

In fact, upregulated connexin 43 expression during myogenic differentiation causes myoblasts to communicate with adjacent cells faster.[22] Therefore, it can be interpreted that enhanced connexin 43 expression due to rGO treatment promotes active intercommunication between the myoblasts. This event could have resulted in detection of the MHC marker at early differentiation stage. Furthermore, myotubes formed with rGO-treated C2C12 myoblasts showed higher DES, MYF5, MYOD, MYOG, TNN1, and MYH1 expression. These markers play a significant role during myogenesis and myogenic differentiation.[31]

4.2.4 Genetic Changes in C2C12 Myoblasts after rGO Treatment

We further explored the genetic changes that occurred in C2C12 myoblasts when rGO was present. The cells treated with and without rGO were collected at before differentiation and terminal differentiation stage. We made 5 contrasts for testing the effects of rGO treatment, the effect of time, and lastly the interaction (i.e. the time effect in rGO group vs the time effect in control group) (Table 4.1). First of all, comparison between the time periods generated more differentially expressed genes than the treatment itself. More number of differentially expressed genes were present when we compared before and terminal differentiation stages, both in C2C12 and rGO-treated C2C12 groups. Total number of 10,833 differentially expressed genes were detected with C2C12 cells, and 11,774 with rGO-treated C2C12 cells. The myoblasts cultured with rGO, however, showed a greater number of differentially expressed gene at terminal differentiation stage. Comparison between the C2C12 and rGO-treated C2C12 cells only showed 160 differentially expressed genes before differentiation, but the number increased to 9,452 at terminal differentiation.

Based on the interaction result, we compared the total of 7,474 differentially expressed genes with $p < 0.05$ value and plotted those genes on a heatmap (Figure 4.9). The color key shows if the gene was relatively upregulated (red) or downregulated (blue). We specifically tracked gap junction related genes among the differentially expressed genes (Figure 4.10). Three genes were found including Gja1 (connexin 43), Gjd4 (connexin 39), and Gjb3 (connexin 31). As a result, connexin 43 expression significantly decreased after myogenesis in both groups. The extent of downregulation, however, was much greater without rGO treatment. Connexin 39 is also known to be expressed during muscle embryonic development and fusion.[32, 33] The expression of connexin 39 was enhanced further when rGO was present in culture. Connexin 31, not known to be expressed in skeletal muscle, was downregulated upon rGO treatment.[34]

Genes that directly regulates myogenic differentiation, myogenesis, and muscle regeneration were plotted in two different ways; to show the time effect in presence of rGO and to show the rGO effect at different time points (Figure 4.11). Among the genes that directly regulates myogenic differentiation, myogenesis and muscle regeneration, 17 genes were upregulated with respect to time in C2C12 myoblasts (red bar graph in Figure 4.11 A) and the presence of rGO further upregulated expression of 11 genes among the 17 genes (blue bar graph in Figure 4.11 A). Furthermore, 9 genes were downregulated further in rGO-treated C2C12 group among the 17 downregulated genes in C2C12 myoblasts. We additionally compared how treatment of rGO change these gene expression at different time points (Figure 4.11 B). As a result, we observed early myogenic markers upregulated at before differentiation time point (grey bar graph in Figure 4.11 B) while these markers were downregulated at terminal differentiation time point (black bar graph in Figure 4.11 B). The results were opposite for terminal differentiation markers. The

terminal differentiation markers were upregulated at terminal differentiation stage and downregulated at before differentiation stage.

Next, we plotted the negative regulators of myogenic differentiation, myogenesis and muscle regeneration. We first tracked the gene expression change with respect to time (Figure 4.12). As a result, 4 out of 7 negatively regulators were downregulated when rGO was present during myogenic differentiation (Figure 4.12 A). As we compared how rGO influenced the gene expression change at different time points, 5 genes were downregulated both at before and terminal differentiation stages in presence of rGO (Figure 4.12 B).

Lastly, we plotted other genes that also relates to muscle development and function (Figure 4.13). The presence of rGO during differentiation further upregulated 5 genes (Figure 4.13 A). Specifically, the troponin subunits, troponin C, troponin T3, troponin I were upregulated further compared to C2C12 myoblasts. Interestingly, troponin T2 which plays role in cardiac muscle contraction was downregulated. Other skeletal muscle related gene expressions including actin, and GTP binding protein expressions were upregulated. We also compared these gene expression levels at different time points to examine the effect of rGO (Figure 4.13 B). The troponin expression were especially upregulated at terminal differentiation stage.

The number of differentially expressed genes show how the presence of rGO contributes to myogenic differentiation and myogenesis over time. During myogenic differentiation, multiple signaling pathways change in response to fusion and development.[35-37] The presence of rGO at early stage of differentiation does not show significant gene expression changes but the promotes genetic changes at terminal differentiation stage. Thus, it can be concluded that rGO in skeletal myoblasts can facilitate myogenesis during fusion and dramatically change the gene expression levels after forming myotubes. The mechanism of how rGO triggered certain myogenic genes,

however, should be investigated further.

4.2.5 Decoupling the Conductivity of rGO and Enhancement in Connexin 43 Expression Level

We validated if conductivity of the rGO is enhancing the contraction of muscles under electrical stimuli. We used Channel rhodopsin transfected C2C12 cells which express light-sensitive ion channel. The differentiated myotubes respond to the 470 nm blue LED light and contract.[10, 38] The myotubes with and without rGO were stimulated both optically and electrically to compare the displacement of the myotubes (Figure 4.14). When we electrically stimulated the myotubes, the displacement was 1.41-fold higher upon rGO treatment. However, the fold change was similar when the two groups were stimulated optically. Myotubes formed with C2C12 treated with rGO showed 1.51-fold higher displacement. The fold change in displacement upon different stimuli was also plotted. Both groups showed increased displacement when the cells were electrically stimulated. Interestingly, the fold change was almost the same showing 1.39-fold change in C2C12 group, and 1.31-fold change in rGO treated C2C12 group.

We decoupled the conductivity of rGO and its ability to enhance connexin 43 in myoblasts. The conductivity of the material did not influence the rGO-treated C2C12 group generate greater displacement. Thus, myotube differentiation is mainly a result of connexin 43 enhancement in myoblasts in presence of rGO.

4.2.6 Enhanced Fluid Transport with Skeletal Muscle Treated with rGO

Because our results above revealed that myogenic factor expressions are upregulated when C2C12 myoblasts are treated with rGO, we sought to evaluate the functionality of the differentiated myotubes. Previously, we have developed a platform called “pump-bot,” capable of measuring

fluid flow.[25] We first engineered myotubes in 3D muscle ring and placed the ring on a flexible polyacrylamide hydrogel tube. The tube was assembled to a closed microfluidics system fabricated with polydimethylsiloxane (PDMS). The chamber, where the hydrogel tube and muscle ring were placed, was stimulated electrically to stimulate the muscle to contract and induce fluid flow (Figure 4.15).

First, the rGO treated muscle rings showed black color due to the color of the rGO itself (Figure 4.16 A, muscle ring in black dashed box). The muscle ring fabricated with C2C12 myoblasts was white in color (Figure 4.16 A, muscle ring in red box). In order to compare the tube deformation caused by the muscle rings, we tracked the movement of the hydrogel tube using an image analysis software, Tracker. As we tracked the displacement, the movement caused by the rGO-treated muscle ring was as high as 73 μm (Figure 4.16 B). The displacement caused by the muscle ring without rGO, however, was up to 27 μm.

Then, we analyzed the average flow velocity and the flow rate by tracking the trajectories of the fluorescence beads (Figure 4.17). We divided the inner part of the hydrogel tube to 16 sections and tracked the movement of the fluorescent beads. The average velocity of the beads in each section was plotted on a graph (Figure 4.17 A). The flow profile over the cross section of the gel was parabolic. In addition, the flow rate was higher in rGO treated muscle rings. Based on this movement, the net flow rate of the control group was 8.5 μl/min while rGO treated muscle rings showed 22.5 μl/min (Figure 4.17 B). The net flow rate was 2.65-fold higher with the pump-bot assembled with rGO treated muscle rings.

As a result of enhanced myogenic differentiation due to increased connexin 43 expression in myoblasts, rGO-treated myotubes exhibited more active displacement of the hydrogel tubes compared to the control myotubes. From this result, we could confirm that muscle maturation and

contraction force can be enhanced by rGO treatment.

Troponin acts as a control switch that senses the cytosolic calcium increase and makes the striated muscle to contract and produce force.[39, 40] The protein consists of 3 subunits, troponin C, troponin I and troponin T. We particularly have observed upregulation in troponin I, troponin T3, and troponin C upon treating rGO to the C2C12 myoblasts (Figure 4.13). Thus, upregulated troponin expression may have resulted in active contraction of the skeletal muscle rings and enhanced the force production.

As we have seen our qRT-PCR results that C2C12 treated with rGO exhibited upregulated myogenic marker expression level (DES, MYF5, MYOD, MYOG, TNN1, and MYH1). It has been reported that upregulated expression of these markers contributes to increase in force production.[38] Thus, we expected skeletal muscles engineered in presence of rGO showed more displacement, generated more volumetric fluid flow and accelerated the fluid transfer in a pump-bot device.

4.3 Conclusion

The presence of rGO in C2C12 myoblasts promoted expression of connexin 43 in skeletal myoblasts and prolonged the expression time. In addition, the C2C12 myoblasts formed myotubes in early stage of differentiation, suggesting that presence of rGO shorten the time for the cells to fuse. As a result of enhanced and prolonged connexin 43 in C2C12 myoblasts, treatment of rGO supported enhancement of myogenic differentiation markers in the differentiated myotubes. This result was confirmed further with an RNA sequencing method. The rGO treated myotubes showed increased force production and induced faster fluid flow in a pump-bot system. We suggest further investigation should be performed to study how rGO is enhancing the myoblasts in a molecular level. This system may be useful to study the role of gap junction proteins in myotubes. Potentially,

the 3D muscle with rGO may be useful to build an *in vitro* skeletal muscle studying platform where we can characterize skeletal muscle related diseases or screen drugs to treat those diseases.

4.4 Materials and Methods

4.4.1 Characterization and analysis of rGO

The rGO flakes used for the experiment was purchased from ACS Materials (ACS Material LLC). The rGO was characterized by Raman spectroscopy and Transmission electron microscopy (TEM). TEM analysis was performed using TEM (JEOL 2100 TEM). Based on the obtained TEM images, we measured the length and width of a single rGO sheet using image J software.

4.4.2 Preparation of rGO for cellular assay

A stock of 5 mg/ml rGO in 70% ethanol was prepared. The stock solution was pipetted well and sterilized under UV for 30 min. Then, the stock solution was vortexed at maximum speed for 10 minutes and sonicated in a bath sonicator for an additional 30 minutes. The stock solution was diluted in growth medium at a concentration of 5 µg/ml. The C2C12 myoblasts, which reached 80% confluency, was incubated with the rGO containing medium overnight at 37 °C. On the next day, the unattached rGO was removed and the cells that have rGO on the membrane were collected for further use.

4.4.3 Cytotoxicity test of C2C12 myoblasts

Tryphan blue exclusion assay was used to determine the number of viable cells in culture. The C2C12 myoblasts were treated with 0 µg/ml, 3 µg/ml, 5 µg/ml, and 10 µg/ml of rGO in growth medium. The cells were collected on day 1, 3, 7, and 10 and counted after treating with tryphan

blue solution. Nine sections on the hemocytometer was counted, and total 4 culture samples were collected for single group on each day to verify the result.

4.4.4 Immunocytochemical Analysis

For both Connexin 43 staining and myotube staining, the samples were fixed in 4% (w/v) paraformaldehyde (Sigma) for 30 min, permeablized with 0.1% (v/v) Triton X-100 (Sigma) for 5 min and incubated in blocking solution for 45 min at room temperature. After completing each step, the samples were washed with PBS 2 times. Post blocking, the samples were incubated in primary antibodies at 4 °C overnight. To stain for connexin 43, the samples were incubated in anti-connexin43 (GJA1 antibody, Abcam). To stain for myogenic markers, another set of samples were rather incubated in MF-20 anti-MHC (1:400; iT FX, Developmental Studies Hybridoma Bank, The University of Iowa Department of Biology) or anti-sarcomeric α-actinin antibody (Abcam). On the next day, the samples were washed with PBS 2 times and connexin 43 was labeled with Alexa Fluor-488 donkey anti-rabbit IgG (1:500; Invitrogen). Samples incubated with MF-20 were labeled with Alexa Fluor-488 goat anti-mouse IgG (1:500; Invitrogen), and samples incubated with anti-sarcomeric α-actinin antibody were treated with Alexa Fluor-568 donkey anti-rabbit IgG (1:500; Invitrogen) as well as fluorescein (FITC)-conjugated Phalloidin. All samples were incubated in secondary antibodies for 1 hour. Finally, the nuclei were labeled with 4',6-Diamidino-2-Phenylindole (DAPI, Sigma). The fluorescence images were obtained with a multiphoton confocal microscope (LSM 710, Carl Zeiss).

4.4.5 Quantitative real-time polymerase chain reaction analysis

Quantitative real-time polymerase chain reaction (qRT-PCR) analysis conducted at 3 different

time points; before differentiation (day 3 after seeding), early differentiation (day 7 after seeding) and terminal differentiation (day 10 after seeding). Total RNA from the samples were extracted from C2C12 myoblasts by using RNeasy Mini Kit (Qiagen) following the manufacturer's protocol. After extracting the mRNA, cDNA synthesis was performed with qScript cDNA Super Mix (Quanta Biosciences) from 100 ng of RNA and the reaction was performed according to the manufacturer's protocol. Then, SsoFast EvaGreen Supermix (Bio-Rad) was added to the cDNA and primers and the mixtures were analyzed using CFX Connect Real-Time System (Bio-Rad). For the analysis, the cycle threshold (Ct) values were compared relative to the GAPDH and control samples.

4.4.6 RNA sequencing analysis

The RNA samples were prepared with TruSeq Stranded mRNA-seq Sample Prep kit (Illumina). Differential gene expression analysis was performed using the limma-trend method on the logCPM values. Total 5 contrasts were made for testing the following effects; Before differentiation vs Terminal differentiation in control group, before differentiation vs terminal differentiation in rGO group, rGO vs control group at before differentiation stage, rGO vs control group at terminal differentiation stage and the interaction to compare the time effect in rGO group vs time effect in control group. Multiple testing correction was done separately for each comparison using the False Discovery Rate (FDR) method. The differential expression was considered significant at FDR p-value < 0.05.

4.4.7 3D muscle ring formation for Pump-bot analysis

C2C12 myoblasts were treated with 5µg/ml rGO as mentioned above. On the next day, the cells

were collected to form muscle rings. The cells were first trypsinized and suspended at a concentration of $1.0X10^7$ cells/ml in a mixture composed of growth medium supplemented with 30% v/v Matrigel (BD Biosciences), 4mg/ml fibrinogen (Sigma), 0.5 U/mg thrombin (Sigma). Each well in the PDMS ring mold was supplemented with 150 µl cell mixture and incubated in 37 °C for 1 hour. After the cell mixture compacted, the muscle rings were immersed in growth medium. C2C12 myoblasts without rGO treatment were used to form control group muscle rings.

4.4.8 Hydrogel tube preparation

To fabricate the flexible hydrogel tube, 1mL of 40% w/v aqueous solution of acrylamide, 4 µl of 2% w/v methylene bis-acrylamide, 10 µl of 10% w/v ammonium persulfate, and 2 µl of tetramethylene diamine was mixed together. The mixture was applied on a hallow glass mold and left in room temperature for 30 minutes until the gel was completely cured. Then, the glass mold was removed, and the gel was incubated in water overnight. The fabricated hydrogel tube was 4 mm in outer diameter and 3mm in inner diameter.

4.4.9 Pump-bot assembly and fluid flow measurement

The muscle ring was placed on the fabricated hydrogel tube after being incubated in growth medium for 2 days (Figure 4.16). After the muscle ring was placed on the tube, the ring was incubated for another day in growth medium. On day 3 after the muscle ring was formed, the growth medium was exchanged with differentiation medium. The muscle-tube complex was incubated in differentiation medium for another 7 days. Finally, the muscle-tube complex was placed on the Pump-bot device. While we assembled the muscle-tube complex with the device, FITC tagged fluorescence beads (diameter = 1µm, BD Bioscience) were injected into the hydrogel

tube as well as the channel in the Pump-bot device. The assembled Pump-bot was imaged with Olympus IX81 inverted microscope (Olympus). While imaging, the samples were maintained with 37ºC and 5% CO2 in an environmental chamber. To induce muscle contraction, we stimulated the muscle rings with bipolar electrical pulses (9V amplitude, 50 ms pulse width).

4.4.10 Investigating conductivity of rGO

We used Chennelrhodopsin transfected C2C12 skeletal myoblasts, which respond to the 470 nm blue LED light. The cells were treated with rGO overnight and plated on a tissue culture plate. After the cells were cultured in growth medium for 3 days and differentiation medium for 10 days, the cells were stimulated both optically and electrically. The muscle layer was optically stimulated with a 470 nm LED (Mightex Systems Inc) with 50 ms pulses of 1Hz frequcncy. Additionally, the muscle layer was stimulated electrically with a custom-built electrical stimulation unit. The biphasic electrical pulses of 20 V amplitude and 50 ms pulse width were applied to the muscle layer. All videos for the conductivity analysis was recorded with Olympus ix81 inverted microscope (Olympus).

4.4.11 Statistical analysis

The statistical analyses were performed using unpaired Student's t-test with Graph Pad Prism 6.0 (Graph Pad Software Inc). Statistical differences were considered significant at p-value smaller than 0.05.

4.5 Figures and Table

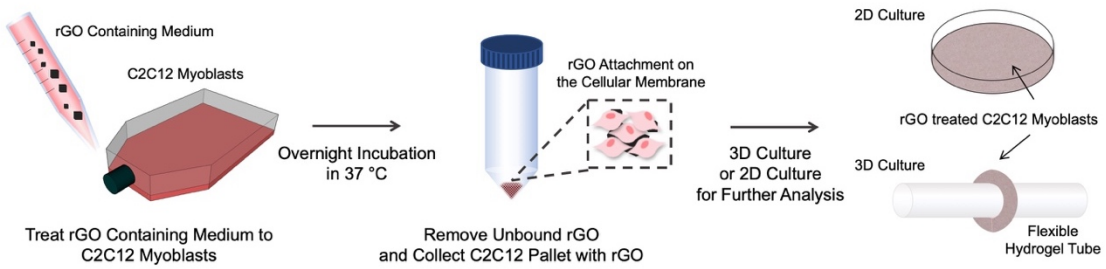

Figure 4.1 Schematic Illustration of the Experimental Procedure. Procedure of Treating C2C12 myoblasts with rGO. The cells are first incubated with rGO containing medium overnight in 37 °C. On the next day, the C2C12 myoblasts with rGO are collected and used for 2D or 3D culture.

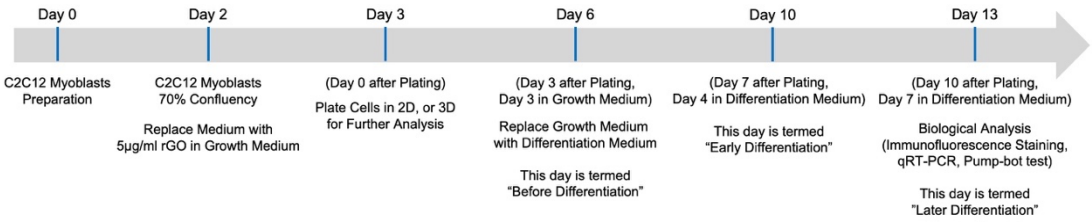

Figure 4.2 Timeline of the experimental procedure. After the C2C12 myoblasts are cultured on the flask, they are treated with 5µg/ml rGO in growth medium and incubated overnight. The cells are collected on the next day and prepared either for 2D or 3D culture. The growth medium is replaced with differentiation medium after the cells are cultured in growth medium for 3 days. After 7 days of culture in differentiation medium, the C2C12 myoblasts were analyzed.

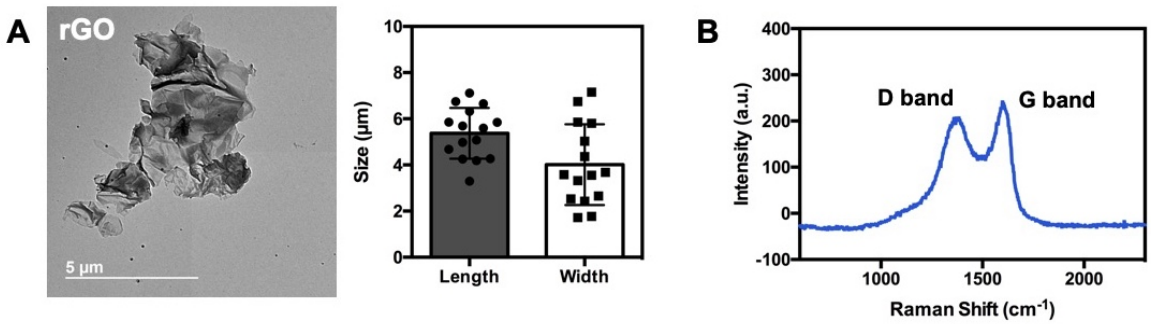

Figure 4.3. Characterization of reduced graphene oxide. (A) Transmission electron microscopy images of the rGO flakes, and size of the flakes based on the images (n=15). (B) Raman spectra of the rGO.

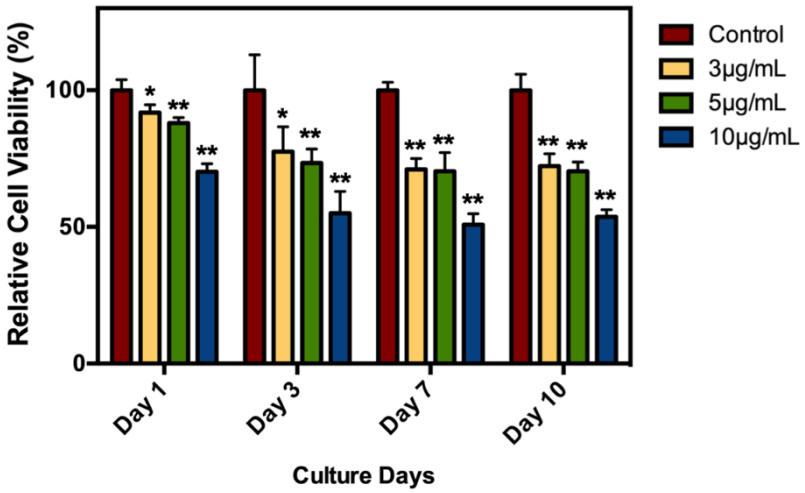

Figure 4.4 Cellular viability of the C2C12 and rGO treated C2C12 myoblasts. The experiment was performed on day 1, 3, 5, 7, and 10 (n=4) with Tryphan Blue Assay. Different concentrations (3µg/mL, 5µg/mL, and 10µg/mL) of rGO was tested and plotted on the graph relative to the control group (* and ** represent the statistical significance between the values. *$p < 0.01$, **$p < 0.05$).

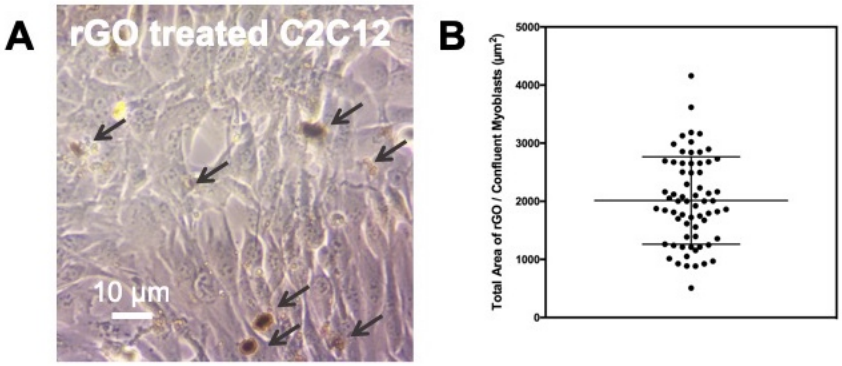

Figure 4.5 Treatment of rGO to C2C12 Myoblasts. (A) Optical image of the C2C12 myoblast after rGO treatment. (B) The concentration of rGO per myotube area. The concentration of rGO was analyzed by measuring the area of rGO in one image with confluent myoblasts (n=60).

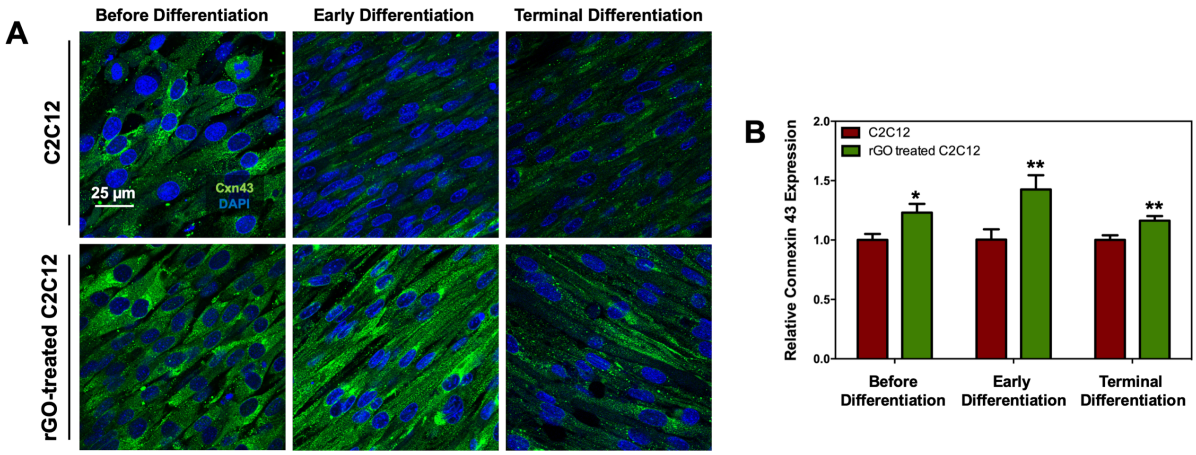

Figure 4.6 Time dependent change of connexin 43 expression in skeletal myoblasts. (A) Immunofluorescence staining of the control C2C12 and rGO treated C2C12 with connexin 43 (Cxn 43, green) and nucleus (DAPI, blue). (B) Quantification of relative connexin 43 mRNA expression level in rGO treated C2C12 myoblasts before differentiation (day 3), early differentiation (day 7), and late differentiation (day 14) (n=3, * and ** represent the statistical significance between the values. *$p < 0.01$, **$p < 0.05$).

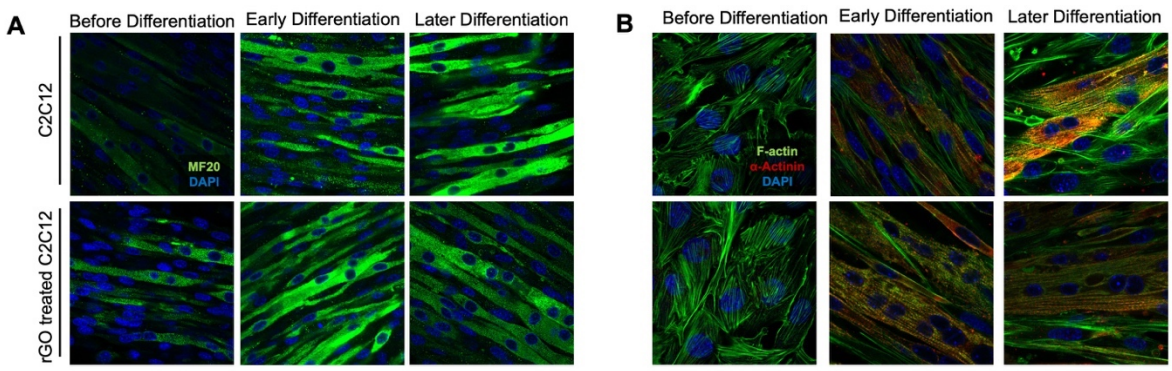

Figure 4.7 Myogenic differentiation of the C2C12 upon rGO addition. (A) Immunofluorescently stained myotubes formed with control C2C12 myoblasts and rGO treated C2C12 myoblasts stained for myosin heavy chain (MF20, green), and nuclei (DAPI, blue). The images were taken before differentiation (day 3), at early differentiation (day 7), and late differentiation (day 14). (B) Striated myotubes of the control C2C12 and rGO treated C2C12 with alpha actinin (α-actinin, green) and nucleus (DAPI, blue).

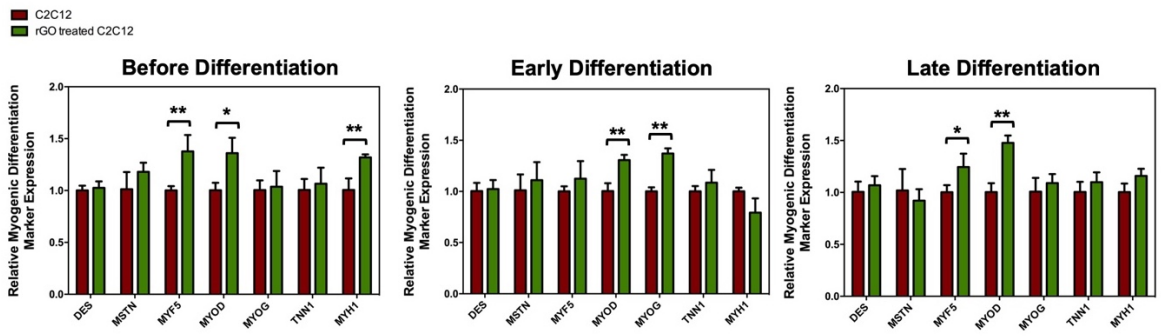

Figure 4.8 Relative myogenic marker expression at different time points. qRT-PCR analysis performed to show relative myogenic marker expression levels in rGO treated C2C12 myoblasts before differentiation (day 3), early differentiation (day 7), and late differentiation (day 14) (n=3, * and ** represent the statistical significance between the values. *$p < 0.01$, **$p < 0.05$).

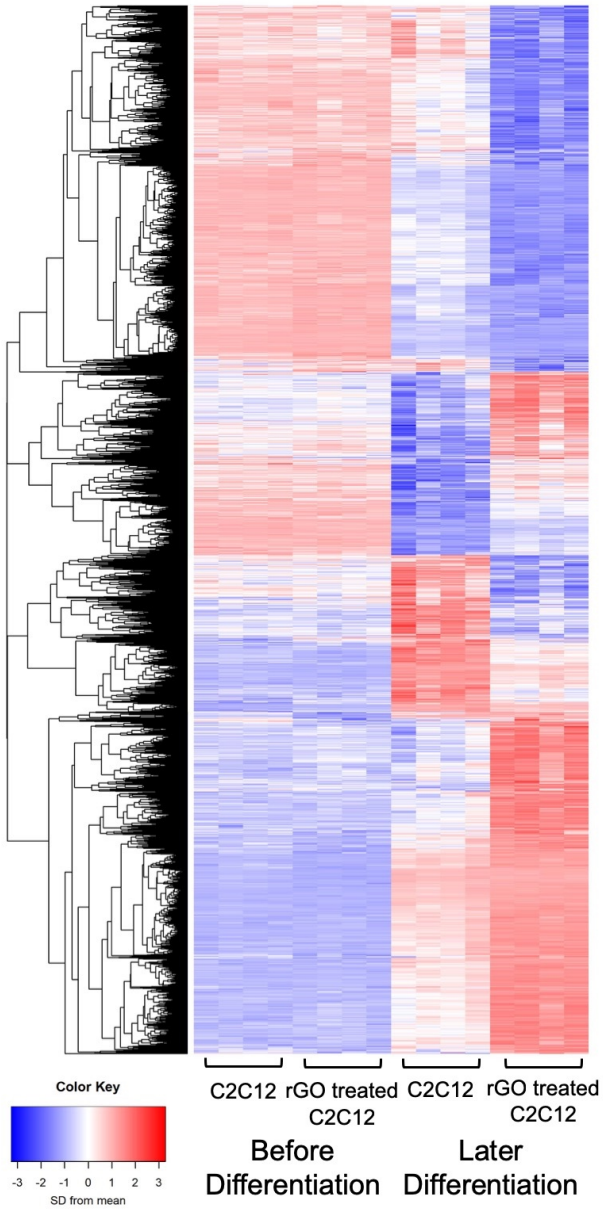

Figure 4.9 Changes in gene expression analyzed by RNA sequencing. Heat map showing the differentially expressed genes (total 7474 genes, p-value<0.05, n=4). The color key indicates the gene expression level; red indicating increased expression and blue indicating decreased expression level.

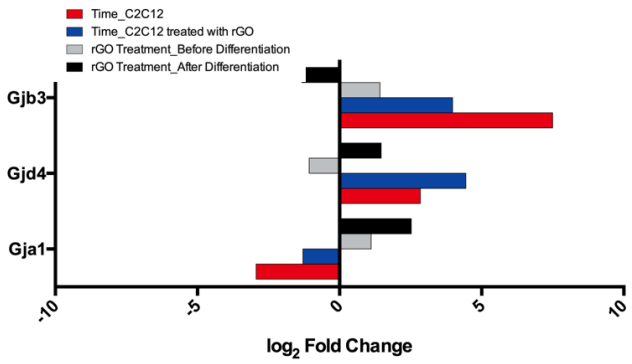

Figure 4.10 Gap junction related gene expression change in C2C12 and C2C12 treated with rGO. The effect of time and rGO treatment were plotted separately (FDR p-value<0.05).

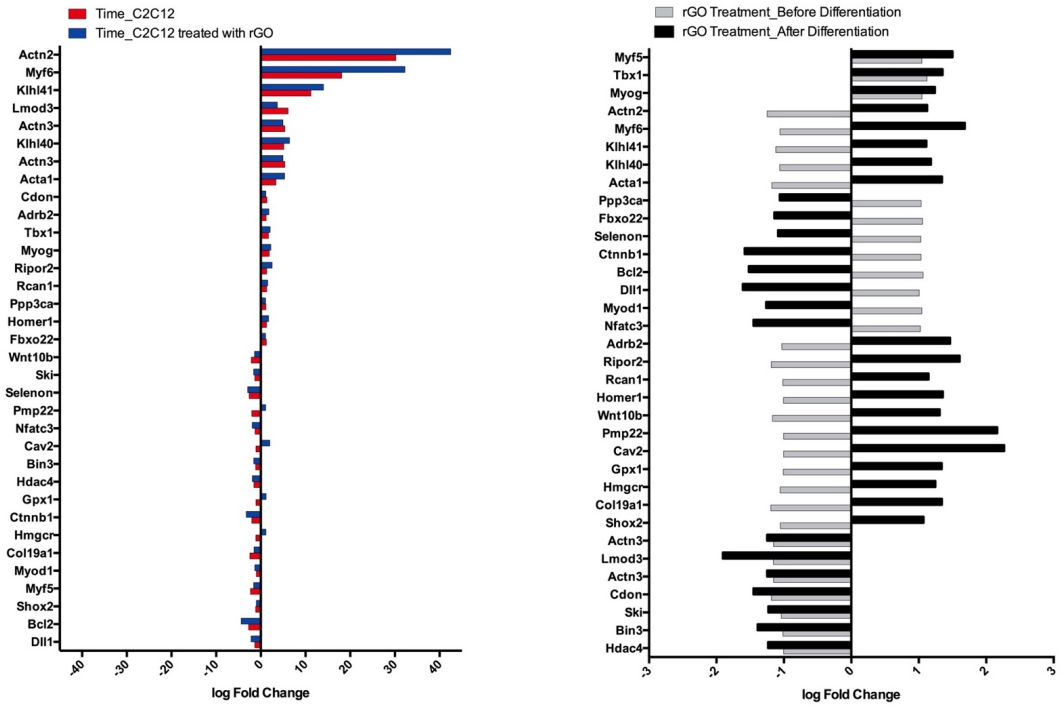

Figure 4.11 Genes that positively regulates myogenesis, myogenic differentiation, and muscle regeneration. (A) was plotted with respect to time and (B) was plotted with respect to presence of rGO (FDR p-value<0.05).

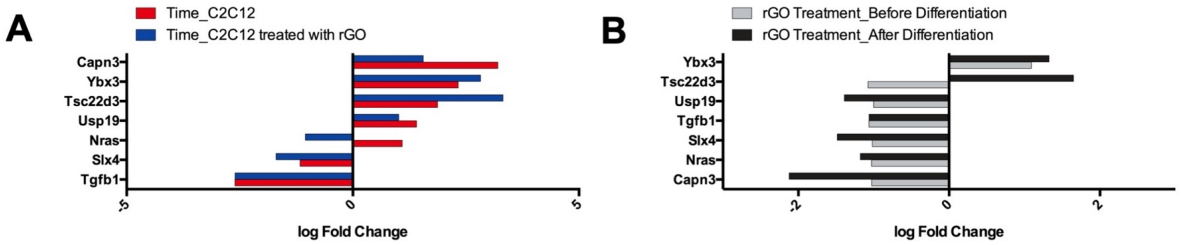

Figure 4.12 Genes that negatively regulates myogenesis, myogenic differentiation, and muscle regeneration. (A) was plotted with respect to time and (B) was plotted with respect to presence of rGO (FDR p-value<0.05).

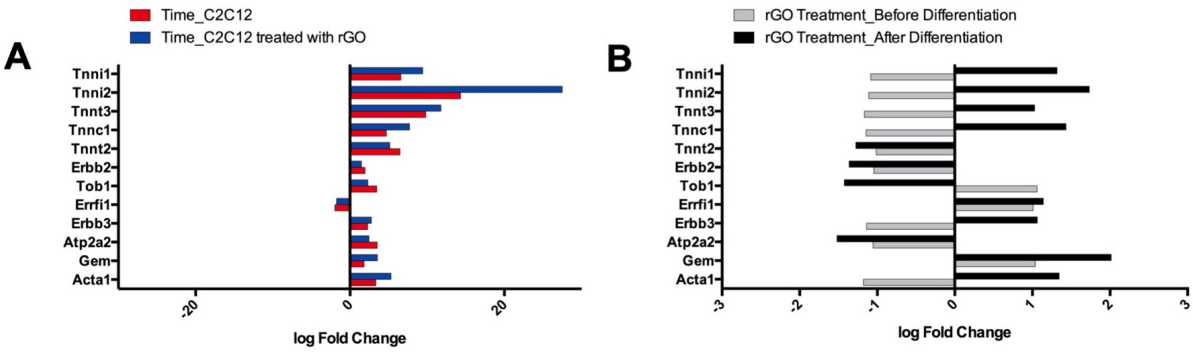

Figure 4.13 Genes that contribute to muscle development and function, but indirectly related to myogenesis, myogenic differentiation, or muscle regeneration. (A) was plotted with respect to time and (B) was plotted with respect to presence of rGO (FDR p-value<0.05).

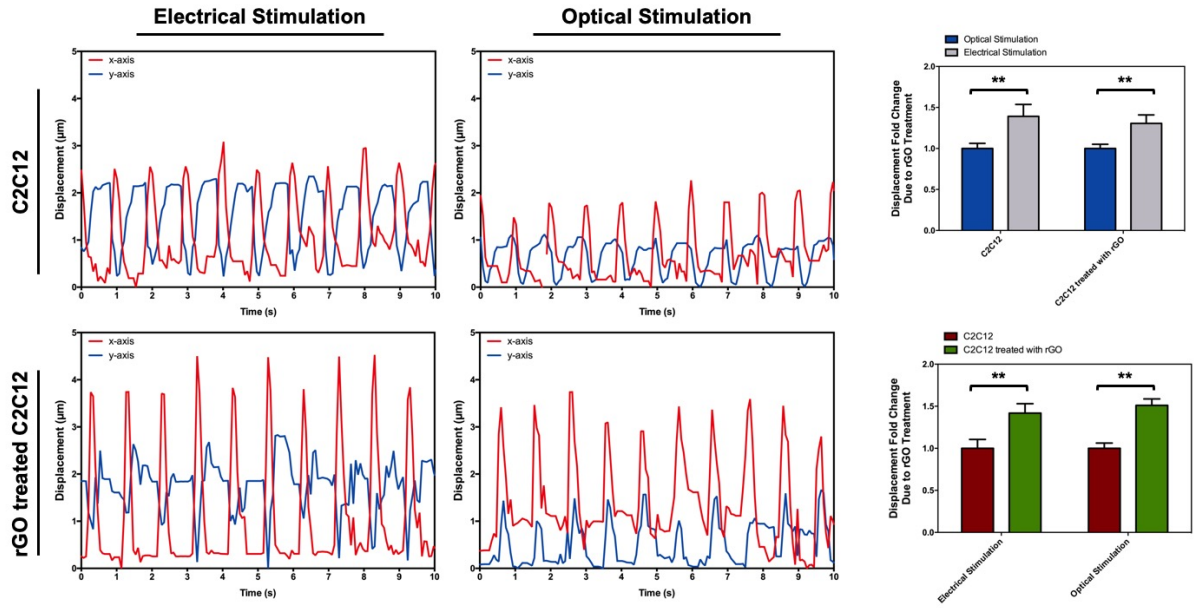

Figure 4.14 Displacement graph to show the effect of rGO. Channel rhodopsin transfected C2C12 cells were used to decouple the effect of conductivity from enhancement of connexin 43 resulted from rGO. The displacement of myotubes were recorded and plotted on a displacement vs time graph.

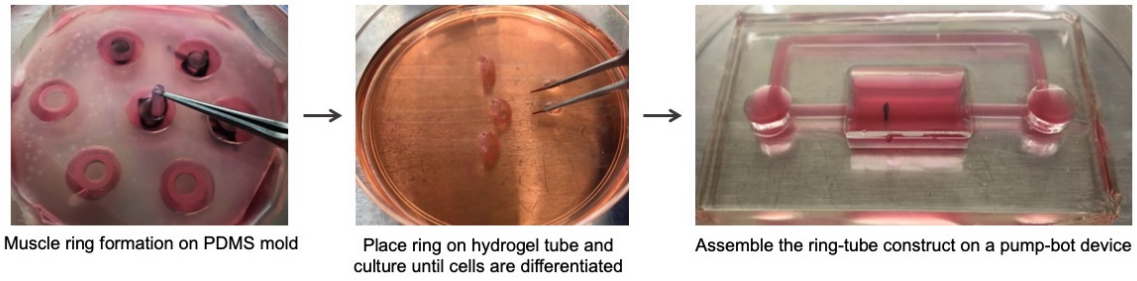

Figure 4.15 Procedure of Pump-bot assembly. Once the C2C12 myoblasts compact on the PDMS ring mold, the muscle ring was removed and placed on the polyacrylamide hydrogel tube. The ring-tube construct was assembled with the Pump-bot device to measure the fluid flow.

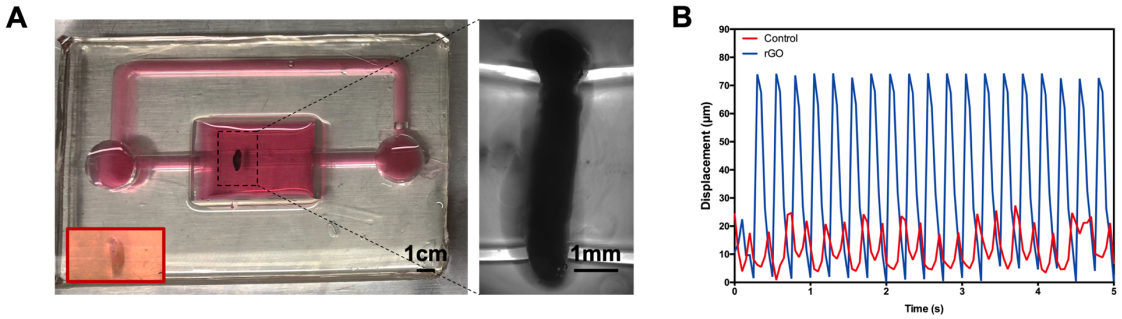

Figure 4.16 Displacement of the muscle ring in a Pump-bot device. (A) Image of the Pump-bot device assembled with rGO treated muscle ring. Image in the red box shows muscle ring formed with C2C12 without rGO treatment. (B)Representative deformation graph of the hydrogel tube.

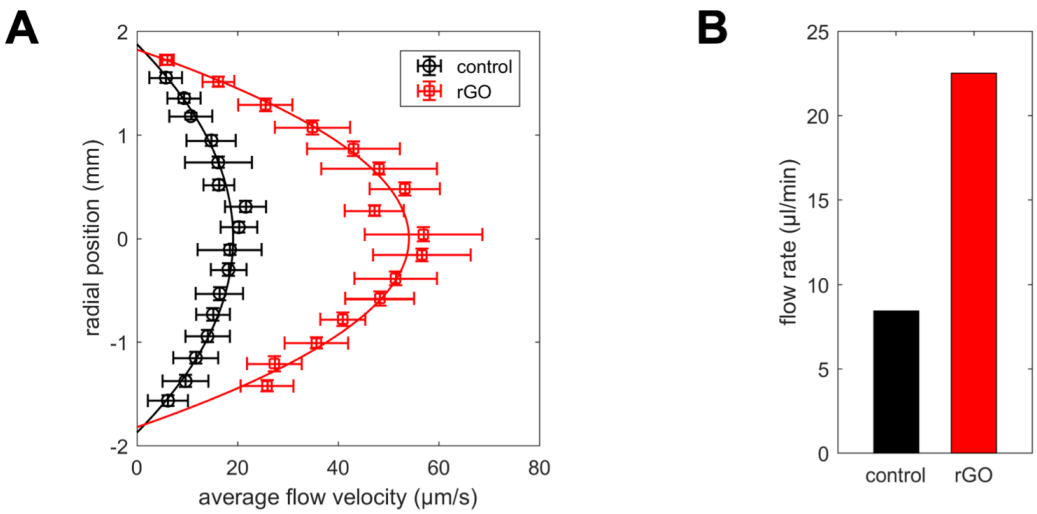

Figure 4.17 Analysis of the fluid flow caused by muscle contraction. (A) Fluid flow profile plotted on graph. Each point represents the flow velocity at each position. (B) Representative net fluid flow rate plotted on a bar graph.

	rGO Effect (C2C12 vs rGO treated C2C12)		Time Effect (Before Differentiation vs Late Differentiation)		Interaction
	Before Differentiation	Late Differentiation	C2C12	rGO treated C2C12	
Down Regulated	132	4769	5440	5887	3734
Up Regulated	28	4683	5393	5887	3740
Not Significant	13870	4578	3197	2256	6556

Table 4.1 The number of differentially expressed genes with FDR p-value < 0.05. The effect of rGO treatment and time were analyzed.

4.6. References

1. Janssen, I.; Heymsfield, S. B.; Wang, Z.; Ross, R., Skeletal Muscle Mass and Distribution in 468 Men and Women Aged 18–88 Yr. *Journal of applied physiology* **2000,** *89* (1), 81-88.

2. Kalantar-Zadeh, K.; Rhee, C.; Sim, J. J.; Stenvinkel, P.; Anker, S. D.; Kovesdy, C. P., Why Cachexia Kills: Examining the Causality of Poor Outcomes in Wasting Conditions. *Journal of cachexia, sarcopenia and muscle* **2013,** *4* (2), 89-94.

3. Zebracki, K.; Drotar, D., Pain and Activity Limitations in Children with Duchenne or Becker Muscular Dystrophy. *Developmental Medicine & Child Neurology* **2008,** *50* (7), 546-552.

4. Vandenburgh, H., High-Content Drug Screening with Engineered Musculoskeletal Tissues. *Tissue Engineering Part B: Reviews* **2009,** *16* (1), 55-64.

5. Zhao, Y.; Zeng, H.; Nam, J.; Agarwal, S., Fabrication of Skeletal Muscle Constructs by Topographic Activation of Cell Alignment. *Biotechnology and bioengineering* **2009,** *102* (2), 624-631.

6. Ko, E.; Yu, S. J.; Pagan-Diaz, G. J.; Mahmassani, Z.; Boppart, M. D.; Im, S. G.; Bashir, R.; Kong, H., Matrix Topography Regulates Synaptic Transmission at the Neuromuscular Junction. *Advanced Science* **2018**, 1801521.

7. Cvetkovic, C.; Raman, R.; Chan, V.; Williams, B. J.; Tolish, M.; Bajaj, P.; Sakar, M. S.; Asada, H. H.; Saif, M. T. A.; Bashir, R., Three-Dimensionally Printed Biological Machines Powered by Skeletal Muscle. *Proceedings of the National Academy of Sciences* **2014,** *111* (28), 10125-10130.

8. Morimoto, Y.; Kato-Negishi, M.; Onoe, H.; Takeuchi, S., Three-Dimensional Neuron–Muscle Constructs with Neuromuscular Junctions. *Biomaterials* **2013,** *34* (37), 9413-9419.

9. Pagan-Diaz, G. J.; Zhang, X.; Grant, L.; Kim, Y.; Aydin, O.; Cvetkovic, C.; Ko, E.; Solomon, E.; Hollis, J.; Kong, H., Simulation and Fabrication of Stronger, Larger, and Faster Walking Biohybrid Machines. *Advanced Functional Materials* **2018,** *28* (23), 1801145.

10. Raman, R.; Cvetkovic, C.; Uzel, S. G.; Platt, R. J.; Sengupta, P.; Kamm, R. D.; Bashir, R., Optogenetic Skeletal Muscle-Powered Adaptive Biological Machines. *Proceedings of the National Academy of Sciences* **2016,** *113* (13), 3497-3502.

11. Fuoco, C.; Rizzi, R.; Biondo, A.; Longa, E.; Mascaro, A.; Shapira-Schweitzer, K.; Kossovar, O.; Benedetti, S.; Salvatori, M. L.; Santoleri, S., In Vivo Generation of a Mature and Functional Artificial Skeletal Muscle. *EMBO molecular medicine* **2015,** *7* (4), 411-422.

12. Kumar, N. M.; Gilula, N. B., The Gap Junction Communication Channel. *Cell* **1996,** *84* (3), 381-388.

13. Meşe, G.; Richard, G.; White, T. W., Gap Junctions: Basic Structure and Function. *Journal of Investigative Dermatology* **2007,** *127* (11), 2516-2524.

14. Esseltine, J. L.; Shao, Q.; Brooks, C.; Sampson, J.; Betts, D. H.; Séguin, C. A.; Laird, D. W., Connexin43 Mutant Patient-Derived Induced Pluripotent Stem Cells Exhibit Altered Differentiation Potential. *Journal of Bone and Mineral Research* **2017,** *32* (6), 1368-1385.

15. Hervé, J.-C.; Derangeon, M., Gap-Junction-Mediated Cell-to-Cell Communication. *Cell and tissue research* **2013,** *352* (1), 21-31.

16. LeBeau, F. E.; Traub, R. D.; Monyer, H.; Whittington, M. A.; Buhl, E. H., The Role of Electrical Signaling Via Gap Junctions in the Generation of Fast Network Oscillations. *Brain research bulletin* **2003,** *62* (1), 3-13.

17. Merrifield, P. A.; Laird, D. W. In *Connexins in Skeletal Muscle Development and Disease*, Seminars in cell & developmental biology, Elsevier: 2016; pp 67-73.

18. Van der Velden, H. M.; Jongsma, H. J., Cardiac Gap Junctions and Connexins: Their Role in Atrial Fibrillation and Potential as Therapeutic Targets. *Cardiovascular research* **2002,** *54* (2), 270-279.

19. Von Maltzahn, J.; Wulf, V.; Willecke, K., Spatiotemporal Expression of Connexin 39 and−43 During Myoblast Differentiation in Cultured Cells and in the Mouse Embryo. *Cell communication & adhesion* **2006,** *13* (1-2), 55-60.

20. Araya, R.; Eckardt, D.; Riquelme, M. A.; Willecke, K.; Sáez, J. C., Presence and Importance of Connexin43 During Myogenesis. *Cell communication & adhesion* **2003,** *10* (4-6), 451-456.

21. Proulx, A.; Merrifield, P. A.; Naus, C. C., Blocking Gap Junctional Intercellular Communication in Myoblasts Inhibits Myogenin and Mrf4 Expression. *Developmental genetics* **1997,** *20* (2), 133-144.

22. Suzuki, K.; Brand, N. J.; Allen, S.; Khan, M. A.; Farrell, A. O.; Murtuza, B.; El Oakley, R.; Yacoub, M. H., Overexpression of Connexin 43 in Skeletal Myoblasts: Relevance to Cell Transplantation to the Heart. *The Journal of thoracic and cardiovascular surgery* **2001,** *122* (4), 759-766.

23. Proulx, A. A.; Lin, Z. X.; Naus, C., Transfection of Rhabdomyosarcoma Cells with Connexin43 Induces Myogenic Differentiation. *Cell growth & differentiation: the molecular biology journal of the American Association for Cancer Research* **1997,** *8* (5), 533-540.

24. Shen, H.; Grimston, S.; Civitelli, R.; Thomopoulos, S., Deletion of Connexin43 in Osteoblasts/Osteocytes Leads to Impaired Muscle Formation in Mice. *Journal of Bone and Mineral Research* **2015,** *30* (4), 596-605.

25. Li, Z.; Seo, Y.; Aydin, O.; Elhebeary, M.; Kamm, R. D.; Kong, H.; Saif, M. T. A., Biohybrid Valveless Pump-Bot Powered by Engineered Skeletal Muscle. *Proceedings of the National Academy of Sciences* **2019,** *116* (5), 1543-1548.

26. Park, J.; Kim, Y. S.; Ryu, S.; Kang, W. S.; Park, S.; Han, J.; Jeong, H. C.; Hong, B. H.; Ahn, Y.; Kim, B. S., Graphene Potentiates the Myocardial Repair Efficacy of Mesenchymal Stem Cells by Stimulating the Expression of Angiogenic Growth Factors and Gap Junction Protein. *Advanced Functional Materials* **2015,** *25* (17), 2590-2600.

27. Mu, Q.; Su, G.; Li, L.; Gilbertson, B. O.; Yu, L. H.; Zhang, Q.; Sun, Y.-P.; Yan, B., Size-Dependent Cell Uptake of Protein-Coated Graphene Oxide Nanosheets. *ACS applied materials & interfaces* **2012,** *4* (4), 2259-2266.

28. You, J.-O.; Rafat, M.; Ye, G. J.; Auguste, D. T., Nanoengineering the Heart: Conductive Scaffolds Enhance Connexin 43 Expression. *Nano letters* **2011,** *11* (9), 3643-3648.

29. Wei, X.-Q.; Hao, L.-Y.; Shao, X.-R.; Zhang, Q.; Jia, X.-Q.; Zhang, Z.-R.; Lin, Y.-F.; Peng, Q., Insight into the Interaction of Graphene Oxide with Serum Proteins and the Impact of the Degree of Reduction and Concentration. *ACS applied materials & interfaces* **2015,** *7* (24), 13367-13374.

30. Shi, X.; Chang, H.; Chen, S.; Lai, C.; Khademhosseini, A.; Wu, H., Regulating Cellular Behavior on Few-Layer Reduced Graphene Oxide Films with Well-Controlled Reduction States. *Advanced Functional Materials* **2012,** *22* (4), 751-759.

31. Heher, P.; Maleiner, B.; Prüller, J.; Teuschl, A. H.; Kollmitzer, J.; Monforte, X.; Wolbank, S.; Redl, H.; Rünzler, D.; Fuchs, C., A Novel Bioreactor for the Generation of Highly Aligned 3d Skeletal Muscle-Like Constructs through Orientation of Fibrin Via Application of Static Strain. *Acta biomaterialia* **2015,** *24*, 251-265.

32. Araya, R.; Eckardt, D.; Maxeiner, S.; Krüger, O.; Theis, M.; Willecke, K.; Sáez, J. C., Expression of Connexins During Differentiation and Regeneration of Skeletal Muscle: Functional Relevance of Connexin43. *J Cell Sci* **2005,** *118* (1), 27-37.

33. Trovato-Salinaro, A.; Belluardo, N.; Frinchi, M.; von Maltzahn, J.; Willecke, K.; Condorelli, D. F.; Mudo, G., Regulation of Connexin Gene Expression During Skeletal Muscle Regeneration in the Adult Rat. *American Journal of Physiology-Cell Physiology* **2009,** *296* (3), C593-C606.

34. Mok, B. W.; Yeung, W. S.; Luk, J. M., Differential Expression of Gap-Junction Gene Connexin 31 in Seminiferous Epithelium of Rat Testes. *FEBS letters* **1999,** *453* (3), 243-248.

35. Hindi, S. M.; Tajrishi, M. M.; Kumar, A., Signaling Mechanisms in Mammalian Myoblast Fusion. *Sci. Signal.* **2013,** *6* (272), re2-re2.

36. Blais, A.; Tsikitis, M.; Acosta-Alvear, D.; Sharan, R.; Kluger, Y.; Dynlacht, B. D., An Initial Blueprint for Myogenic Differentiation. *Genes & development* **2005,** *19* (5), 553-569.

37. Chal, J.; Pourquie, O., Making Muscle: Skeletal Myogenesis in Vivo and in Vitro. *Development* **2017,** *144* (12), 2104-2122.

38. Raman, R.; Grant, L.; Seo, Y.; Cvetkovic, C.; Gapinske, M.; Palasz, A.; Dabbous, H.; Kong, H.; Pinera, P. P.; Bashir, R., Damage, Healing, and Remodeling in Optogenetic Skeletal Muscle Bioactuators. *Advanced healthcare materials* **2017,** *6* (12), 1700030.

39. Gomes, A. V.; Potter, J. D.; Szczesna-Cordary, D., The Role of Troponins in Muscle Contraction. *IUBMB life* **2002,** *54* (6), 323-333.

40. Yang, Z.; Yamazaki, M.; Shen, Q. W.; Swartz, D. R., Differences between Cardiac and Skeletal Troponin Interaction with the Thin Filament Probed by Troponin Exchange in Skeletal Myofibrils. *Biophysical journal* **2009,** *97* (1), 183-194.

CHAPTER 5: THE ROLE OF CONNEXIN IN MYOGENIC DIFFERENTIATION OF SKELETAL MYOBLASTS

Acknowledgments

The work in this chapter was conducted through collaborative efforts. I especially would like to thank Lauren Grant for her great help in performing qPCR and the functional analyses. I would like to thank Dr. Juanita Matthews in TUFTS University for providing the C2C12 cell lines. I would also like to thank Jiaojiao Wang, Gelson J. Pagan-diaz, Yongdeok Kim for their help.

5.1 Introduction

Gap junction is a cluster of an intercellular protein called connexin. This gap junction channel forms when the two hemichannels of the adjacent cells interact. By this direct communication between the cells, the cells can mediate exchange of molecules, metabolites, waste products, and electrical signals.[1] Different types of connexin proteins exist and each protein is named after the molecular weight of the connexin. During skeletal muscle development, the myoblasts proliferate and fuse together to form multinucleated myotubes. Usually, the gap junctions play crucial role during this stage. Balogh et al., have reported that the connexin 43 protein expression was upregulated in myoblasts but the expression level decreased after myotube formation.[2] In addition, when gap junctions were blocked, myoblast fusion was inhibited and the myotubes were not formed properly.[3, 4] Thus, the results have suggested that the presence of gap junctions is essential during myogenesis. Furthermore, Suzuki et al., showed in their paper that myoblasts that overexpressed connexin 43 differentiated into myotubes better.[5] Previous studies have shown that skeletal myoblasts naturally express connexin 39, 40, 43, and 45 during myogenesis.[6-8] The connexin 43 and connexin 45 particularly facilitate myogenic differentiation

induced by extracellular ATP.[9] Furthermore, connexin 43 and 45 are found in skeletal muscle of the adult mice during regeneration. The connexin 39 and 40 proteins are expressed in embryos but disappear in adult mice muscle. The role of the gap junction proteins, however, are still not well understood.

Gene transfection is a powerful tool to investigate functions of genes and observe the cellular products that results from that genetic activity. With this technology, desired nucleic acids including DNA and RNA can be introduced to the cell. The main goal of transfection is to control the gene expression in cells, either by enhancement or inhibition, and produce recombinant proteins.[10] Since the role of connexin in skeletal muscle is still unclear, transfection has been used in muscle myogenesis studies to investigate the role of connexin in skeletal muscle. Suzuki et al., have reported that overexpression of connexin 43 in skeletal myoblasts enhances myogenic differentiation and intercellular communication between adjacent cells.[5] In another study, the C2C12 cells were transfected to express connexin 43 after the myotubes are formed.[11] When the myotubes expressing connexin 43 was grafted into the nude mouse hearts, the myotubes and host cardiomyocytes formed connexin 43 positive junctions.

Here, we hypothesize that expression of the gap junction protein during myogenic differentiation facilitates differentiation of the skeletal myoblasts, thereby, promotes mature myotubes to form. In this study, we genetically modified the skeletal myoblasts to express connexin once myogenic differentiation initiates. We delivered connexin 37, 40, and 43 using a commercially available vector, lipofectamine 3000. Connexin 37 and 40 populates in endothelial cells and form gap junctions between arteriolar endothelial cells, but this is not expressed in skeletal muscle.[12] Reports have shown connexin 37 generates new blood vessels around the skeletal muscle and contributes to angiogenesis of the skeletal muscle during regeneration.[12, 13]

Connexin 40 is also found in cardiomyocytes and developing myoblasts and myotubes. [6] However, it is only expressed in early stage of the myogenic differentiation particularly at the outer side where myoblasts fuse to form myotubes. Connexin 43 are known to be involved in skeletal muscle fusion and differentiation.[5, 13, 14] We differentiated C2C12 myoblasts without transfection (C2C12) and C2C12 myoblasts transfected with connexin 37 (C2C12-Cx37), connexin 40 (C2C12-Cx40), and connexin 43 (C2C12-Cx43) to explore how different connexin proteins influence myogenic differentiation. To examine this, we compared the morphology, creatine kinase activity, proliferation, and myogenic differentiation. We selected 3 different time points; day 2(before differentiation), day 4, (early differentiation) and day 8 (terminal differentiation) (Figure 1).

5.2 Results and Discussion

5.2.1 Connexin Expression in Undifferentiated Myoblasts and Differentiated Myotubes

We investigated if the presence of connexin protein is retained after myogenic differentiation in the transfected cells by qRT-PCR and immunofluorescence imaging (Figure 2-4). We performed qRT-PCR at different time points to examine the time when connexin was expressed in the C2C12 cells, and to confirm that each transfected cell line expressed the delivered gene after differentiation was initiated (Figure 2). From day 2, difference was observable between groups (Figure 2A). Compared to the control group, C2C12-Cx37 expressed higher level of connexin 37. Similar result was observed with C2C12-Cx40 and C2C12-Cx43. It is also interesting to note that C2C12-Cx43 group showed elevated connexin 40 expression. On day 4, at early differentiation stage, relative gene expression was similar to day 2 (Figure 2B). Connexin 37 expression level was elevated 120.64-fold compared to C2C12, C2C12-Cx40 and C2C12-Cx43 groups. Similar result was observed with connexin 40 which showed 395.02-fold change compared

to the C2C12. Connexin 43 gene was expressed 3-fold higher in C2C12-Cx43 cells. In addition, the result was similar on day 8 (Figure 2C). Connexin 37 gene was expressed 197.324-fold higher in C2C12-Cx37 compared to C2C12, C2C12-Cx40, and C2C12-Cx43 cells. The expression of connexin 40 and connexin 43 was similar. Connexin 40 was expressed 226.86-fold higher in C2C12-Cx40 compared to the other three groups, and connexin 43 was expressed 2-fold higher in C2C12-Cx43 cells. Then, all samples were normalized to the same group in day 2 to track the expression change occurred within the same group (Figure 3A-D). In C2C12 group, all connexin expression levels were downregulated as differentiation occurred (Figure 3A). The transfected C2C12 myoblasts showed different result. The connexin 40 and connexin 43 expression level decreased in C2C12-Cx37 group on day 4 and day 8 (Figure 3B). The expression level of connexin 37, however, was elevated on day 4, after myoblasts started fusion. Similarly, C2C12-Cx40 group showed elevated expression level of connexin 40 after differentiation (Figure 3C). The other connexin expression levels were downregulated compared to day 2. Lastly, C2C12-Cx43 group showed increased connexin 43 expression level while expression of connexin 37 and 40 were decreased compared to day 2 (Figure 3D). These results were confirmed with immunofluorescence images (Figure 4). When C2C12-Cx37 and C2C12-Cx40 were stained for connexin 40 on day 2, only C2C12-Cx40 cells showed fluorescence (Figure 4A). Connexin 43, however, were visible both in C2C12-Cx37 and C2C12-Cx40 groups on day 4 (Figure 4B). To investigate the expression of connexin 43 at different stages, we compared C2C12 with C2C12-Cx43 at different time points (Figure 4C). Connexin 43 expression was visible in both groups on day 2 and day 4. The expression level was higher on C2C12-Cx43 groups, as confirmed with qRT-PCR result. On day 8, connexin 43 expression was only visible in C2C12-Cx43 group.

The gap junction proteins are known to be downregulated after mature myotubes are formed. From the result, we could observe that wild type C2C12 cells showed decreased connexin 37, 40 and 43 expression level from day 4. Furthermore, C2C12 group did not express connexins on day 8, when mature myotubes developed. It is interesting to note that the experimental groups showed upregulated connexin expression levels in myotubes. According to the results, we expected that the cells may be express different levels of myogenic factors at different time points.

5.2.2 Effect of the Presence of Connexin in Myogenic Differentiation

First, we confirmed that the myotubes formed on day 8 were mature myotubes. We fluorescently imaged the differentiated myotubes by labeling the myotubes with alpha actinin (α-actinin), myosin heavy chain (MHC), and the nuclei (Figure 5A). The myotubes formed with C2C12, C2C12-Cx37, C2C12-Cx40, and C2C12-Cx43 cells were all striated and expressed myosin heavy chain on day 8. We also performed a morphometric analysis to compare the width and length of the myotubes (Figure 5B). The width of the myotubes formed with all 4 groups in the immunofluorescence images did not show much difference between the groups. The C2C12-Cx43 group formed the myotubes with the greatest width (25.26 μm), followed by C2C12 (21.85μm), C2C12-Cx40 (20.08 μm), and C2C12-Cx37 (19.99 μm). The length of the myotubes showed different tendency. The longest myotubes were formed with C2C12-Cx37 (1028.26 μm) followed by the myotubes formed by C2C12-Cx40 (1026.56 μm), C2C12-Cx43 (924.64 μm), and C2C12 (685.40 μm).

Then, we further examined the extent of the myogenic differentiation at different time points (Figure 6). First, we determined the viability of the myotubes formed at different time points and measured the creatine kinase activity (Figure 6A). The myotubes formed with C2C12-Cx37,

C2C12-Cx40, and C2C12-Cx43 cells showed no relative change in viability compared to the control group. The muscle creatine kinase (MCK) activity, which shows the degree of myogenesis, was also measured on day 2, 4, and 8 (Figure 6B). Before Differentiation, the relative MCK activity decreased in C2C12-Cx37, C2C12-Cx40, and C2C12-Cx43 cells compared to the C2C12 cells. Once the myoblasts committed to differentiation, the relative fold change in the transfected cells increased. After day 8, the relative fold change remained high in C2C12-Cx37, and C2C12-Cx40 groups. In C2C12-Cx43 group, the fold change decreased compared to the control group.

To investigate the maturity of the myotubes, we performed qRT-PCR and compared the myogenic markers expressed at different time points (Figure 7, 8). We used 8 different markers for the experiment: desmin (DES), myostatin (MSTN), myogenic factor 5 (MYF5), myogenic factor 6 (MYF6), myosin heavy chain 1 (MYH1), MyoD, myobenin (MYOG), and troponin 1 (TNN1). First, we normalized the relative mRNA expression of the myogenic markers expressed in the experimental group to C2C12 myoblasts on day 2, 4, and 8 (Figure 7). On day 2, C2C12-Cx43 myoblasts showed the greatest number of myogenic markers increased compared to the C2C12 myoblasts (Figure 7A). Interestingly, MSTN, an inhibitory factor that blocks muscle growth and differentiation, was down regulated in all the experimental groups at all time points compared to the C2C12 group.[15]

On day 4, the difference between the control group and the experimental group became more dramatic. The myoblasts modified with connexin genes showed significant increase in early-stage myogenic differentiation markers which includes DES, MYF5, and MYOD (Figure 7B). Additionally, MYOG, a mid-stage myogenic marker and terminal myogenic marker, MYF6 and TNN1, were significantly increased. Furthermore, MSTN expression was decreased in all the experimental groups. The expression of MSTN remained low in all the experimental groups. On

day 8, the myotubes in the experimental groups showed similar expression levels of the myogenic markers compared to the control group (Figure 7C). However, C2C12-Cx37 and C2C12-Cx43 still showed 1.46-fold and 1.32-fold increase in MYH1 expression level. In C2C12-Cx37, MYOG and TNN1 expression levels were also relatively higher than C2C12.

We further investigated the expression change within the group (Figure 8). Here, we normalized each group to the same group in day 2. On day 4, all of the experimental groups showed significant increase in MSTN, MYH1, MYOG, and TNN1 (Figure 8A). Interestingly, the early stage markers were increased in only the experimental groups. There was also a great increase in MYOG and TNN1 in C2C12-Cx40 group, showing 117.03-fold and 248.51-fold increase in expression levels. The difference in relative RNA expression levels were much greater on day 8 (Figure 8B). The early-stage markers MYF5 and MYOD were decreased compared to day 2 in all groups. The expression of DES showed slight increase. The mid-stage and terminal stage markers were greatly increased in all groups. MYOG, was expressed 245-folds higher in C2C12-Cx40 group on day 8 compared to day 2. The C2C12-Cx40 group also showed 871.88-fold increase in TNN1 expression level.

As reported, connexin 40 and connexin 43 facilitates myogenic differentiation and myogenesis of the myoblasts and the expression is downregulated after mature myotubes are formed.[6-8] Thus, during early differentiation, the overexpression of connexin 40 and connexin 43 in the myoblasts may have aided myogenic differentiation to occur faster. Furthermore, the inhibitory factor MSTN remained low in all the experimental groups compared to the control group at all 3 timepoints. This indicates that presence of connexin in differentiating myoblasts, regardless of the type, suppresses the myogenesis inhibitory protein. Moreover, MSTN was downregulated in dramatically in C2C12-Cx40 and C2C12-Cx43 groups. This suggests that the presence of

connexin related to myogenic differentiation can suppress the inhibitory protein further. The MYOG being

The C2C12-Cx37 cells also showed significant increase in myogenic markers and decrease in the inhibitory marker on day 4. Furthermore, myosin heavy chain 1 (MYH1), the protein that forms the muscle contractile unit to convert chemical energy to mechanical energy, and myogenin (MYOG), which helps muscle growth and regeneration, showed the greatest increase in fold change. Thus, this indicates that the presence of connexin, although not expressed in natural skeletal muscle, aids myogenic differentiation of the myoblasts.

5.3 Conclusion

This study sought to discover the role of connexin 37, connexin 40, and connexin 43 during myogenic differentiation. The C2C12 myoblasts were genetically modified to express connexin 37, connexin 40, and connexin 43 after differentiation initiated. In general, myoblasts naturally express connexin 40 and 43 during differentiation but the expression is downregulated once myotubes are formed. In contrary, connexin 37 is not expressed in skeletal muscle but are present in endothelial cells. In our results, the overexpression of connexin proteins, regardless of the type, facilitated myogenic differentiation. This event was noticeable particularly on early-stage differentiation, on day 4. All myogenic marker expression levels were increased, and the inhibitory marker expression level was decreased in C2C12-Cx37, C2C12-Cx40, and C2C12-Cx43 groups compared to the control C2C12 group. The increase in expression level compared to day 2 was the greatest in C2C12-Cx40 group on day 4 and day 8. Altogether, results of this study reveal the importance of the presence of connexin proteins during muscle development. For future study, the role of connexin in myotubes during muscle contraction can be further explored. These findings

could be useful to improve the function of the engineered muscle tissue used for drug screening or assembling a muscle-powered bio-actuators.

5.4 Materials and Methods

5.4.1 Transfection of C2C12 Myoblasts

The C2C12 cell lines were made using a hyperactive piggyBac transposase-based, helper-independent and self-inactivating delivery system, pmhyGENIE-3 containing a neomycin resistance gene for selection. The Cx43, Cx40, and Cx37 sequences were cloned downstream of the mouse MCK promoter cut from the pBS MCK promoter plasmid (Addgene plasmid # 12528; RRID:Addgene_12528). Constructed intermediate pENTR1A plasmid with a multiple cloning site followed by an IRES FusionRed from the plasmid FusionRed-pBAD (Addgene plasmid # 54677; RRID:Addgene_54677). The full MCK promoter +39nt (3389bp) was infused upstream of the MCS in pENTR1A MCS IRES FusionRed. Rat Cx37, Cx40, and Cx43 were infused afterwards. The resulting plasmids pENTR1A MCK Cx37 IRES FusionRed, pENTR1A MCK Cx40 IRES FusionRed, and pENTR1A MCK Cx43 IRES FusionRed were all LR recombined with the pmhyGENIE-3 containing a neomycin resistance gene in the backbone. Chief mCitrate from pcDNA3_1HChIEFmcit was added to pENTR1A intermediate clones by infusion upstream of MCK promoter. All final plasmids along with a FusionRed only control and a ChIEF mCitrate control were transfected into C2C12 mouse myoblasts using lipofectamine 3000. Cells were then selected with 1mg/mL G418 and stable lines of mixed lineages were used for subsequent experiments.

5.4.2 Cell Culture

C2C12 myoblasts were cultured in a cell culture flask in growth medium consisting of Dulbecco's modified Eagle medium (DMEM, Corning) supplemented with 10% (v/v) fetal bovine serum (FBS, VWR), 1% (v/v) L-glutamine (Corning) and 1% (v/v) penicillin-streptomycin (PS, Corning). The cells were maintained in 37°C with 5% CO_2. The cells were proliferated until they reach 70% confluency then collected for the experiments. After the cells were plated on a well plate for further analysis, the growth medium was replaced with differentiation medium on day 2 to induce myogenic differentiation. The differentiation medium was composed of DMEM supplemented with 10% (v/v) heat inactivated horse serum (Gibco), 1% (v/v) L-glutamine (Corning), 1% (v/v) PS (Corning), 50 ng/ml insulin-like growth factor-1 (IGF-1, Sigma Aldrich), and 1mg/mL aminocaproic acid (ACA, Sigma).

5.4.3 Viability Assays

Viability of the C2C12 myoblasts was quantified using a CellTiter 96 Aqueous One Solution (MTS, Promega) following the protocol provided by the manufacturer. The solution was mixed with DMEM without phenol red (LifeTechnologies) at a 5:1 (v/v) ratio. The cells were incubated in the mixture for 4 hours at 37°C and protected from light. Then, the absorbance was measured at 490nm using a plate reader (Synergy HT, BioTek). A blank solution without cells was subtracted from the value to read only the absorbance of the cells. The results were normalized to the control C2C12 cells.

5.4.4 Muscle Creatine Kinase Assay

The creatine kinase activity was determined by using a Liquid Creatine Kinase Reagent Set (Pointe Scientific) following the manufacturer's instructions. First, the cells were trypsinized and collected. After removing all the supernatant, radioimmunoprecipitation assay (RIPA) buffer was added to the cell pellet. the samples were vortexed and rocked at 4°C for 30 min. The samples were, then, sonicated for 10 sec and centrifuged for 15 min at 14000 G. Lastly, 50 µl of the supernatant in the sample tube was mixed with 1 ml of working solution and transferred to a 96 well plate. The absorbance of the samples was measured at 340 nm with a plate reader.

5.4.5 Immunofluorescence Staining

All samples used for immunofluorescence staining were fixed in 4% (v/v) paraformaldehyde (Sigma) for 20 min, permeablized with 0.1% (v/v) Triton X-100 (Sigma) for 5 min and blocked with 2% (v/v) normal goat serum (Sigma) for 1 hour. Between each step, phosphate buffer saline (PBS) washing was performed 2 times. All procedures were conducted at room temperature. Then, the samples were treated with primary antibodies. To test correct expression of connexin 40 and connexin 43 in mature myoblasts, the cells were labeled with anti-connexin 40 (Thermo Fisher), and anti-connexin43 (1:1000) (GJA1 antibody, Abcam). To analyze the myogenic differentiation, the samples were incubated with MF-20 anti-MHC (1:400) (iT FX, Developmental Studies Hybridoma Bank, The University of Iowa Department of Biology), anti-sarcomeric α-actinin (1:400, Abcam) overnight at 4 °C. On the next day, the samples were rinsed with PBS 2 times and incubated with the secondary antibodies. Connexin 43 was labeled with Alexa Fluor-488 donkey anti-rabbit IgG (1:500; Invitrogen). MF-20 were labeled with Alexa Fluor-594 goat anti-mouse IgG (1:500; Invitrogen) and sarcomeric α-actinin antibody was treated with Alexa Fluor-594

donkey anti-rabbit IgG (1:500; Invitrogen). The samples treated with MF-20 antibody was also stained with fluorescein (FITC)-conjugated Phalloidin. After 1hour incubation at room temperature, the nuclei were labeled with 4',6-Diamidino-2-Phenylindole (DAPI, Sigma). The fluorescence images were obtained with a multiphoton confocal microscope (LSM 710, Carl Zeiss).

5.4.6 Morphometric Analysis

The morphometric analysis was performed by measuring the width, length, and fusion index based on the immunofluorescence images. Total number of 100 myotubes positively stained for MF-20 was selected for the analysis.

5.4.7 Statistical Analysis

The statistical analyses in this study were performed based on unpaired Student's t-test using a Graph Pad Prism 6.0 (Graph Pad Software Inc.) software. Results were considered significant when p value was less than 0.05 and statistically significant when the value was smaller than 0.01.

5.5 Figures

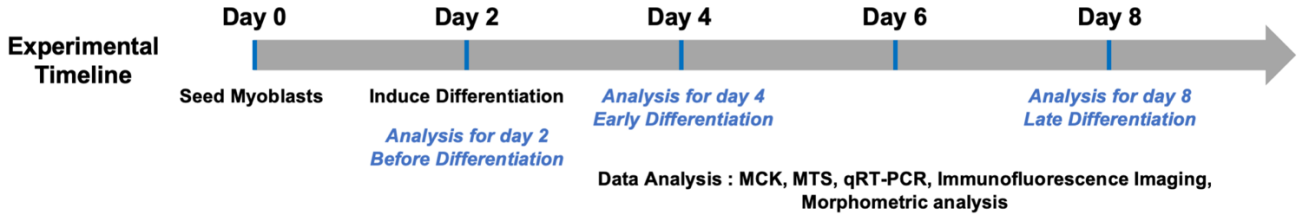

Figure 5.1 Timeline for the experimental procedure. The experimental procedure plotted on a timeline. Cells before differentiation was analyzed on day 2. Growth medium was exchanged with differentiation medium on day 2 and analyzed on day 4 to examine early-stage differentiation. The cells cultured for 6 days in differentiation medium was analyzed for terminal differentiation.

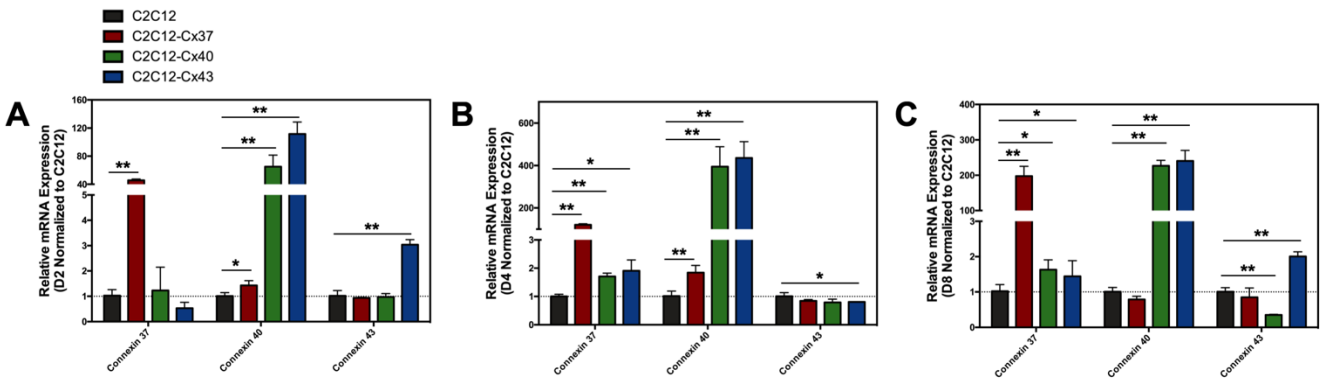

Figure 5.2 qRT-PCR performed to examine the relative connexin expression at different time points. Connexin 37, connexin 40, and connexin 43 expression levels were examined on day 2 (A), day 4 (B), and day 8 (C). All samples were normalized to C2C12 on the same day (n=3, *$p < 0.01$ vs C2C12, **$p < 0.05$ vs C2C12). The dashed line indicates 1 in the y-axis. The values below 1 show relatively lower expression and the values above 1 show relatively higher expression of connexin 37, 40, and 43 compared to C2C12.

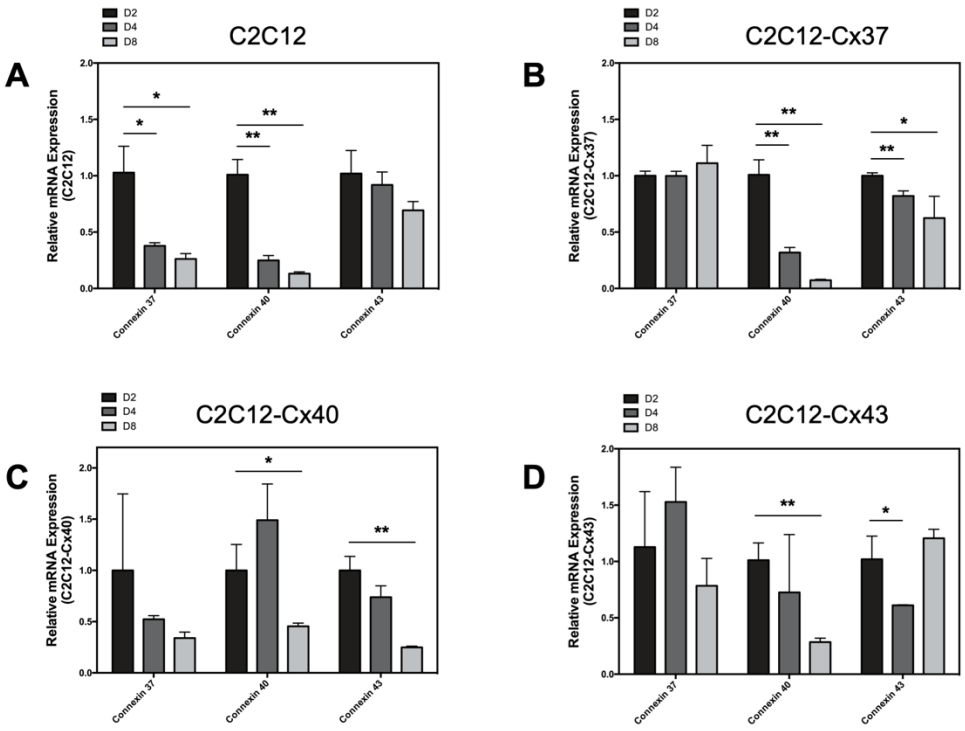

Figure 5.3 qRT-PCR result showing the change in connexin expression on day 4 and day 8 compared to day 2. The samples on day 4 (A) and day 8 (B) were normalized to the same group on day 2 (n=3, *$p < 0.01$ vs same group on day 2, **$p < 0.05$ vs same group on day 2). The dashed line indicates 1 in the y-axis. The values below 1 show relatively lower expression and the values above 1 show relatively higher expression of connexin 37, 40, and 43 compared to the same group on day 2.

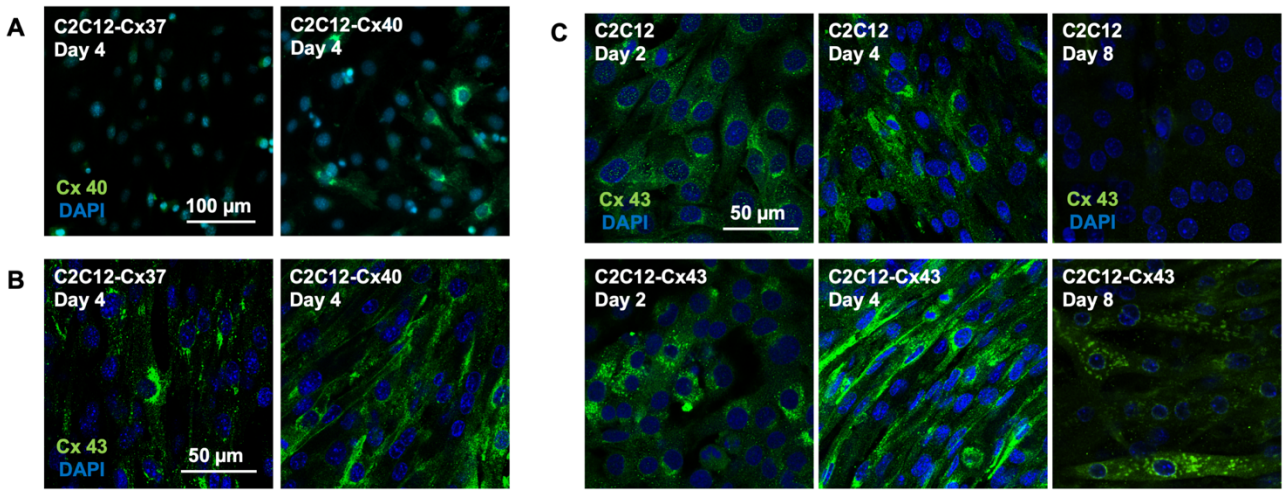

Figure 5.4 Immunofluorescence images of the myoblasts and myotubes stained for connexin 40 and connexin 43. (A) C2C12-Cx37 and C2C12-Cx40 on day 4 (in early-stage differentiation) were stained for connexin 40 (Cx40, green) and nuclei (DAPI, blue). (B) C2C12-Cx37 and C2C12-Cx40 on day 4 (in early-stage differentiation) stained for connexin 43 (Cx43, green), and nuclei (DAPI, blue). (C) C2C12 and C2C12-Cx43 on day 2, 4, and 8 stained for connexin 43 (Cx43, green), and nuclei (DAPI, blue).

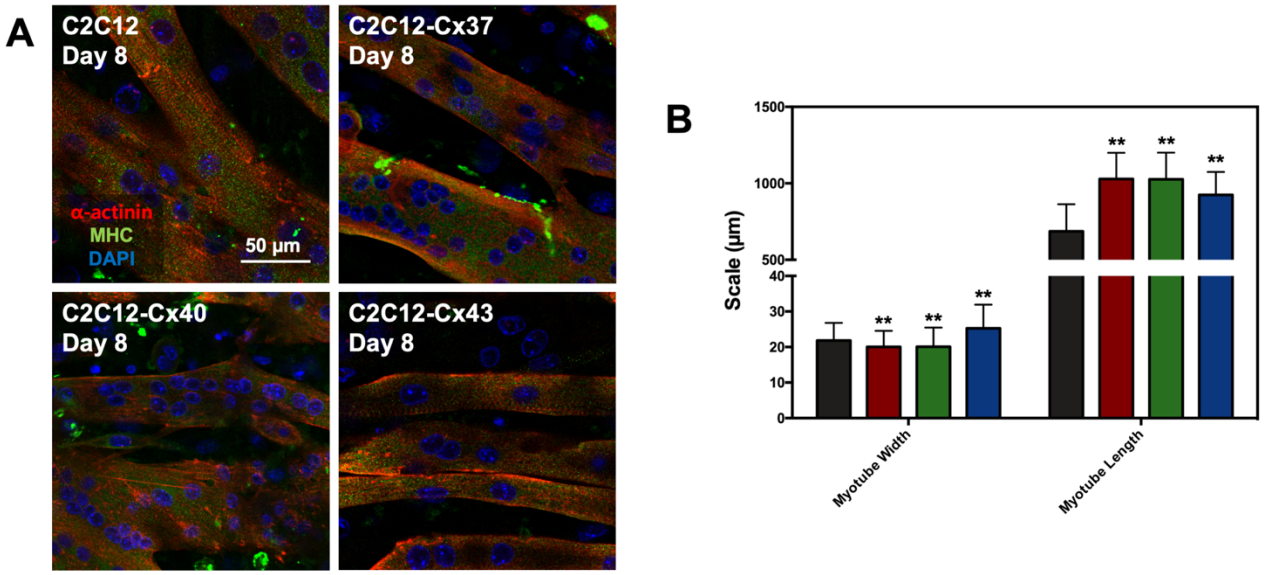

Figure 5.5 Differentiated myotubes analyzed with immunofluorescence imaging and morphometric analysis on day 8. (A) Myotubes differentiated with C2C12, C2C12-Cx37, C2C12-Cx40, and C2C12-Cx43 stained for α-actinin (red), myosin heavy chain (MHC, green), and nuclei (DAPI, blue). (B) Differentiated myotube width and myotube length on day 8 (n=100, **$p < 0.01$ vs C2C12).

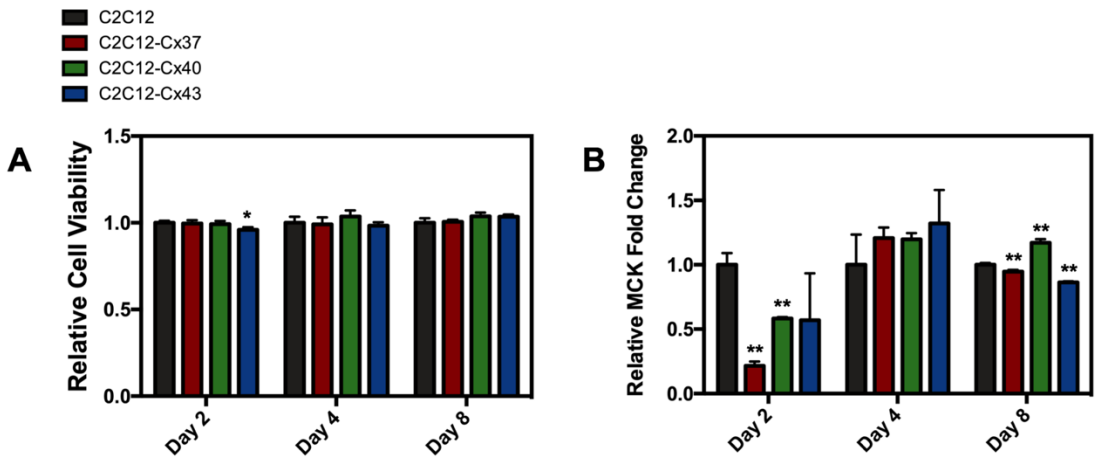

Figure 5.6 Cellular viability and muscle creatine kinase analyses performed on day 2, day 4, and day 8. (A) Relative metabolic activity of C2C12, C2C12-Cx37, C2C12-Cx40, and C2C12-Cx43 at different time points (n=4, *$p < 0.05$ vs C2C12). The samples were normalized to C2C12 sample on the same day. (B) Muscle creatine kinase fold change occurred in C2C12, C2C12-Cx37, C2C12-Cx40, and C2C12-Cx43 at different time points (n=4, **$p < 0.01$ vs C2C12, *$p < 0.05$ vs C2C12). The samples were normalized to C2C12 sample on the same day.

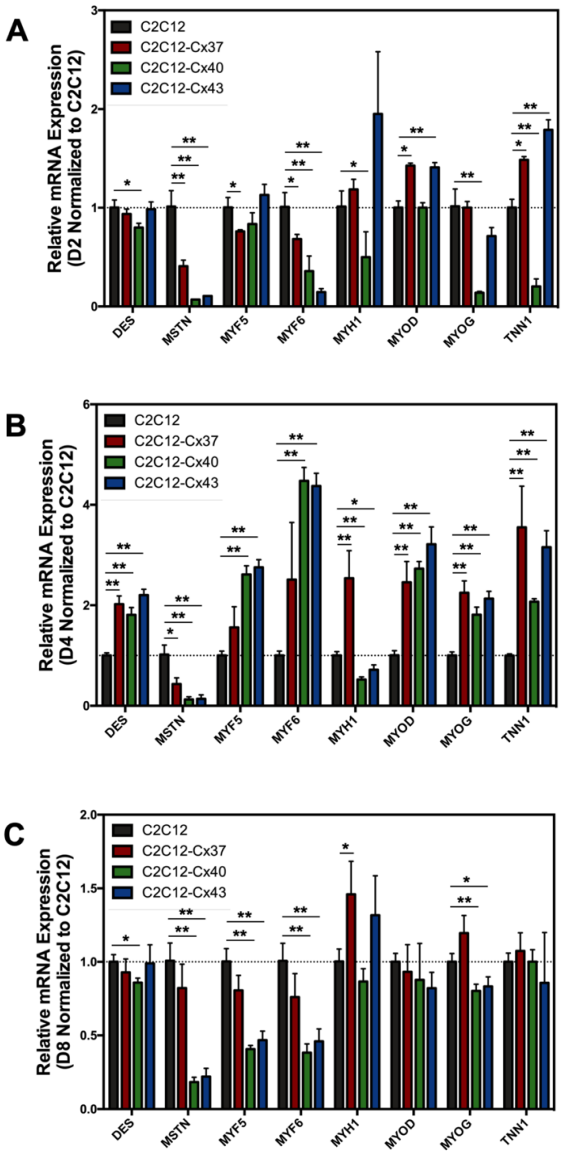

Figure 5.7 qRT-PCR performed to examine the relative myogenic markers at different time points normalized to C2C12. Early-stage markers (DES, MYF5, MYOD), mid-stage marker (MYOG), terminal stage markers (MYF6, MYH1, TNN1), and an inhibitory marker (MSTN1) expression levels were examined on day 2 (A), day 4 (B), and day 8 (C). All samples were normalized to C2C12 on the same day (n=3, *$p < 0.01$ vs C2C12, **$p < 0.05$ vs C2C12). The dashed line indicates 1 in the y-axis. The values below 1 show relatively lower expression and the values above 1 show relatively higher expression of the myogenic markers compared to C2C12.

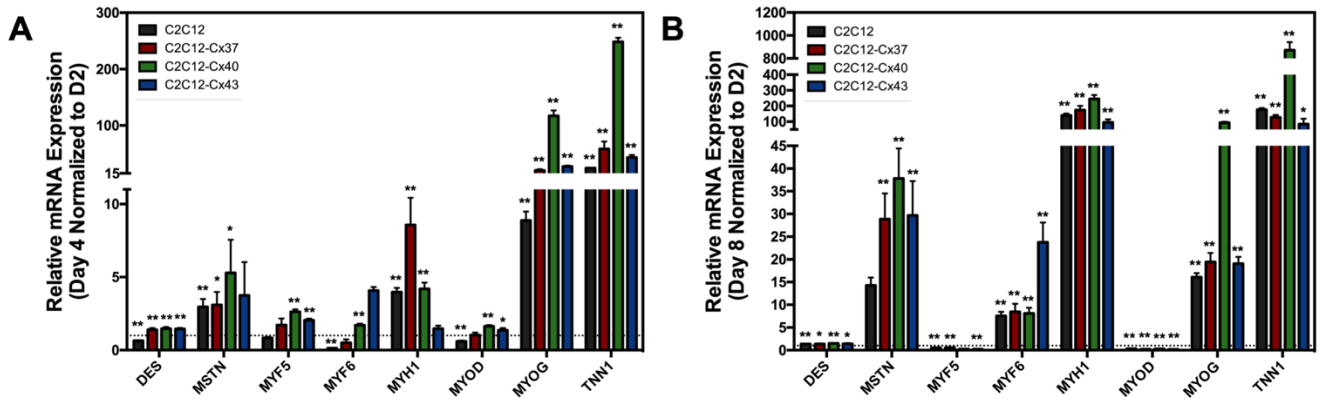

Figure 5.8 qRT-PCR performed to examine the relative myogenic markers on day 4 and day 8 compared to day 2. The samples on day 4 (A) and day 8 (B) were normalized to the same group on day 2 (n=3, *$p < 0.01$ vs same group on day 2, **$p < 0.05$ vs same group on day 2). The dashed line indicates 1 in the y-axis. The values below 1 show relatively lower expression and the values above 1 show relatively higher expression of the myogenic markers compared to the same group on day 2.

5.6. References

1. Goodenough, D. A.; Paul, D. L., Beyond the Gap: Functions of Unpaired Connexon Channels. *Nature reviews Molecular cell biology* **2003,** *4* (4), 285.

2. Jalil, J. E.; Doering, C. W.; Janicki, J. S.; Pick, R.; Shroff, S. G.; Weber, K. T., Fibrillar Collagen and Myocardial Stiffness in the Intact Hypertrophied Rat Left Ventricle. *Circul. Res.* **1989,** *64* (6), 1041-1050.

3. Proulx, A.; Merrifield, P. A.; Naus, C. C., Blocking Gap Junctional Intercellular Communication in Myoblasts Inhibits Myogenin and Mrf4 Expression. *Dev. Genet.* **1997,** *20* (2), 133-144.

4. Mège, R. M.; Goudou, D.; Giaume, C.; Nicolet, M.; Rieger, F., Is Intercellular Communication Via Gap Junctions Required for Myoblast Fusion? *Cell Adhes. Commun.* **1994,** *2* (4), 329-343.

5. Suzuki, K.; Brand, N. J.; Allen, S.; Khan, M. A.; Farrell, A. O.; Murtuza, B.; El Oakley, R.; Yacoub, M. H., Overexpression of Connexin 43 in Skeletal Myoblasts: Relevance to Cell Transplantation to the Heart. *The Journal of thoracic and cardiovascular surgery* **2001,** *122* (4), 759-766.

6. Dahl, E.; Winterhager, E.; Traub, O.; Willecke, K., Expression of Gap Junction Genes, Connexin40 and Connexin43, During Fetal Mouse Development. *Anat. Embryol. (Berl.)* **1995,** *191* (3), 267-278.

7. Araya, R.; Eckardt, D.; Maxeiner, S.; Krüger, O.; Theis, M.; Willecke, K.; Sáez, J. C., Expression of Connexins During Differentiation and Regeneration of Skeletal Muscle: Functional Relevance of Connexin43. *J. Cell Sci.* **2005,** *118* (1), 27-37.

8. von Maltzahn, J.; Euwens, C.; Willecke, K.; Söhl, G., The Novel Mouse Connexin39 Gene Is Expressed in Developing Striated Muscle Fibers. *J. Cell Sci.* **2004,** *117* (22), 5381-5392.

9. Araya, R.; Riquelme, M. A.; Brandan, E.; Sáez, J. C., The Formation of Skeletal Muscle Myotubes Requires Functional Membrane Receptors Activated by Extracellular Atp. *Brain Res. Rev.* **2004,** *47* (1-3), 174-188.

10. Kim, T. K.; Eberwine, J. H., Mammalian Cell Transfection: The Present and the Future. *Anal. Bioanal. Chem.* **2010,** *397* (8), 3173-3178.

11. Reinecke, H.; Minami, E.; Virag, J. I.; Murry, C. E., Gene Transfer of Connexin43 into Skeletal Muscle. *Hum. Gene Ther.* **2004,** *15* (7), 627-636.

12. Looft-Wilson, R. C.; Payne, G. W.; Segal, S. S., Connexin Expression and Conducted Vasodilation Along Arteriolar Endothelium in Mouse Skeletal Muscle. *J. Appl. Physiol.* **2004**.

13. Trovato-Salinaro, A.; Belluardo, N.; Frinchi, M.; von Maltzahn, J.; Willecke, K.; Condorelli, D. F.; Mudo, G., Regulation of Connexin Gene Expression During Skeletal Muscle Regeneration in the Adult Rat. *American Journal of Physiology-Cell Physiology* **2009,** *296* (3), C593-C606.

14. Merrifield, P. A.; Laird, D. W. In *Connexins in Skeletal Muscle Development and Disease*, Semin. Cell Dev. Biol., Elsevier: 2016; pp 67-73.

15. Charge, S. B.; Rudnicki, M. A., Cellular and Molecular Regulation of Muscle Regeneration. *Physiol. Rev.* **2004,** *84* (1), 209-238.

CHAPTER 6: CONCLUSION

6.1 Summary

This thesis has described several approaches to improve the quality of engineered skeletal muscle *in vitro*. We recapitulated the optimal microenvironment for skeletal muscle development using physical, chemical and biological approaches. To recapitulate the physical characteristics of the skeletal muscle, a grooved topography that resembles the diameter of a myofibril was introduced to a polymer substrate. The linear topography anisotropically aligned the myotubes and promoted mature myotube formation. This also aided the co-cultured neural stem cells to differentiate into motor neuron progenitor cells and innervate into the myotubes to form a greater number of neuromuscular junctions. The engineered neuromuscular interface with mature myotubes showed active response to glutamate and curare. Also, the skeletal myoblasts were stimulated chemically by rGO treatment to enhance connexin 43 expression at early stage of differentiation and retain the expression level of connexin 43 at later stage of differentiation. The expression of connexin 43 proteins promoted myogenic differentiation both in gene and protein level. Furthermore, when rGO treated skeletal muscles were assembled into a pump-bot, the force generation and fluid flow through the device became greater compared the skeletal muscle tissue engineered with myoblasts without chemical stimulation. Lastly, myoblasts were genetically modified to express connexin proteins after differentiation was initiated. The differentiated myotubes engineered with genetically modified myoblasts as well as control myoblasts both showed mature and striated myotubes on terminal differentiation stage. However, the speed of differentiation was faster, and relative expression level of myogenic markers at terminal differentiation stage compared to the time before differentiation was significantly higher with the experimental group. The presence of connexin protein 37, 40, and 43 promoted the cells to express

myogenic markers at early-stage differentiation. Regardless of the type, the connexin protein facilitated this process. In addition, the myogenic differentiation gene expression level was significantly elevated in mid- and terminal stage when the myoblasts were genetically modified with connexin genes.

6.2 Future Directions

The current work on engineering skeletal muscle tissue mainly focused on engineering skeletal muscle *in vitro* to present the possibility of engineering matured and functional tissue. Further work would need to focus on testing the engineered tissue as a potentially transplantable unit in an in *vivo* model or assembling a drug testing device with the functional tissue. The work on this thesis focused on the neural innervation to engineer a functional skeletal muscle tissue. In the natural skeletal muscle, the surrounding vasculature is also another significant factor that retains the health and function of the tissue. Future work should focus on investigating how to develop a co-culture system for endothelial cells and skeletal myoblasts for recapitulating the vascularization. In addition, uncovering the role of connexin protein in skeletal muscle function and force production would be needed.